Doctorate Program in Molecular Oncology and Endocrinology
Doctorate School in Molecular Medicine

XXIV cycle - 2008–2011
Coordinator: Prof. Massimo Santoro

"NCOA4 depletion leads to replication stress and premature senescence"

Roberto Bellelli

University of Naples Federico II
Dipartimento di Biologia e Patologia Cellulare e Molecolare
"L. Califano"

Administrative Location

Dipartimento di Biologia e Patologia Cellulare e Molecolare “L. Califano”
Università degli Studi di Napoli Federico II

Partner Institutions

Italian Institutions
Università degli Studi di Napoli “Federico II”, Naples, Italy
Istituto di Endocrinologia ed Oncologia Sperimentale “G. Salvatore”, CNR, Naples, Italy
Seconda Università di Napoli, Naples, Italy
Università degli Studi di Napoli “Parthenope”, Naples, Italy
Università degli Studi del Sannio, Benevento, Italy
Università degli Studi di Genova, Genova, Italy
Università degli Studi di Padova, Padova, Italy
Università degli Studi “Magna Graecia”, Catanzaro, Italy
Università degli Studi di Udine, Udine, Italy

Foreign Institutions
Université Libre de Bruxelles, Bruxelles, Belgium
Universidade Federal de Sao Paulo, Brazil
University of Turku, Turku, Finland
Université Paris Sud XI, Paris, France
University of Madras, Chennai, India
University Pavol Jozef Šafàrik, Kosice, Slovakia
Universidad Autonoma de Madrid, Centro de Investigaciones Oncologicas (CNIO), Spain
Johns Hopkins School of Medicine, Baltimore, MD, USA
Johns Hopkins Krieger School of Arts and Sciences, Baltimore, MD, USA
National Institutes of Health, Bethesda, MD, USA
Ohio State University, Columbus, OH, USA
Albert Einstein College of Medicine of Yeshiwa University, N.Y., USA

Supporting Institutions
Dipartimento di Biologia e Patologia Cellulare e Molecolare “L. Califano”, Università degli Studi di Napoli “Federico II”, Naples, Italy
Istituto di Endocrinologia ed Oncologia Sperimentale “G. Salvatore”, CNR, Naples, Italy
Istituto Superiore di Oncologia, Italy

Italian Faculty

Salvatore Maria Aloj
Francesco Saverio Ambesi Impiombato
Francesco Beguinot
Maria Teresa Berlingieri
Bernadette Biondi
Francesca Carlomagno
Gabriella Castoria
Maria Domenica Castellone
Angela Celetti
Lorenzo Chiariotti
Vincenzo Ciminale
Annamaria Cirafici
Annamaria Colao
Sabino De Placido
Gabriella De Vita
Monica Fedele
Pietro Formisano
Alfredo Fusco
Domenico Grieco
Michele Grieco
Maddalena Illario
Massimo Imbriaco
Paolo Laccetti
Antonio Leonardi
Paolo Emidio Macchia
Barbara Majello
Rosa Marina Melillo
Claudia Miele
Nunzia Montuori
Roberto Pacelli
Giuseppe Palumbo
Silvio Parodi
Nicola Perrotti
Maria Giovanna Pierantoni
Rosario Pivonello
Giuseppe Portella
Giorgio Punzo
Maria Fiammetta Romano
Antonio Rosato
Giuliana Salvatore
Massimo Santoro
Giampaolo Tortora
Donatella Tramontano
Giancarlo Troncone
Giancarlo Vecchio,
Giuseppe Viglietto
Mario Vitale

“NCOA4 depletion leads to replication stress and premature senescence”

TABLE OF CONTENTS

LIST OF ORIGINAL PUBLICATIONS

This dissertation is based on the following publications:

I. Bellelli R et al. Ncoa4 depletion leads to replication stress and premature senescence. Manuscript in preparation (main body of the Dissertation)

II. Bellelli R, et al. Foxm1 is a molecular determinant of the mitogenic and invasive phenotype of anaplastic thyroid carcinoma. Manuscript in preparation (attached at the end of Dissertation)

III. Castellone MD, Cantisani MC, Perala M, Vidal F, Sadelberg N, Bellelli R, Laukkanen MO, Kallioniemi OP, Santoro M Identification of EPHRs as new mediators of thyroid carcinogenesis through an RNA interference screening. Manuscript in preparation (attached at the end of Dissertation)

IV. Castellone MD, De Falco V, Rao DM, Bellelli R, Muthu M, Basolo F, Fusco A, Gutkind JS, Santoro M. The beta-catenin axis integrates multiple signals downstream from RET/papillary thyroid carcinoma leading to cell proliferation. Cancer Res. 2009 Mar 1;69(5):1867-76 (attached at the end of Dissertation)

V. Faraonio R, Salerno P, Passaro F, Sedia C, Iaccio A, Bellelli R, Nappi TC, Comegna M, Romano F, Salvatore G, Santoro M, Cimino F. "A set of MiRNA partecipate to the cellular senescence program in human diploid fibroblasts" Cell Death Diff, 2011 (attached at the end of Dissertation)

List of abbreviations

53BP1	p53-binding protein 1
AR	androgen receptor
ATC	anaplastic thyroid carcinoma
ATM	ataxia-teleangectasia mutated
ATR	ataxia-teleangectasia and Rad 3 related
CCDC6	coiled-coil domain-containing protein 6
CldU	5-Chloro-2'-Deoxyuridine
DDR	DNA damage response
DSB	double strands break
ER	estrogen receptor
FTC	follicular thyroid carcinoma
GDNF	glial-cell line-derived neurotrophic factor
HT	heterozygous
IdU	5-Iodo-2'-Deoxyuridine
IOD	inter-origin distance
IR	ionizing radiation
KO	knock-out
MAPK	mitogen-activated protein kinases
MCM	mini-chromosome maintenance
MDC1	mediator of the DNA damage checkpoint 1
MEF	mouse embryo fibroblast
MEN2	multiple endocrine neoplasia type 2
MTC	medullary thyroid carcinoma
NCOA4	nuclear receptor coactivator 4
NTRK1	neurotrophic receptor-tyrosine kinase 1
OIS	oncogene-induced senescence
PDL	population doubling level
PDTC	poorly differentiated thyroid carcinoma
PFGE	pulsed field gel electrophoresis
PPARγ	peroxisome-proliferator activated receptor γ
PTC	papillary thyroid carcinoma
RET	rearranged during transfection
RET/PTC	RET/papillary thyroid carcinoma
ROS	reactive oxygen species
SAβ-gal	senescence-associated β-galactosidase
WDTC	well differentiated thyroid carcinoma
WT	wild type
γH2AX	gamma-histone 2A variant X

Abstract

The Nuclear Receptor Coactivator 4 (NCOA4) gene (also known as RFG/ELE1/ARA70) is frequently targeted by chromosomal rearrangements in papillary thyroid carcinoma (PTC). These events join the N-ter (exons 1-5, encoding amino acids 1-238) of the NCOA4 gene to the DNA sequence encoding the tyrosine kinase (TK) domain of the receptor tyrosine kinase RET, generating the RET/PTC3 chimeric gene, whose protein product displays oncogenic activity. The NCOA4 N-ter mediates homodimerization of the RET TK domain, followed by RET kinase activation and, in turn, gain of transforming activity. Disruption of NCOA4 gene might contribute to the neoplastic phenotype as well, however to date no cellular phenotype has been associated with NCOA4 deficiency. To gain insight into the physiological function of NCOA4, we disrupted NCOA4 in mice. NCOA4-deficient mice did not exhibit any apparent phenotypic alteration. However, when grown at 20% O_2, NCOA4-/- mouse embryonic fibroblasts (MEFs) undergo premature senescence, characterized by block of cell proliferation and BrdU incorporation, as well as SA(senescence-associated)-β-galactosidase positive staining. This phenotype is associated with accumulation of DNA damage and activation of a DNA damage response (DDR). Using a fiber stretching assay, that monitors DNA replication fork progression, we show that NCOA4-depleted cells accumulate replication fork stalling lesions and feature increased DNA replication origin activation. In addition, NCOA4-/- MEFs, grown at 3% O_2 concentration, feature increased sensitivity to genotoxic stress, particularly that induced by S-phase specific DNA damaging agents. In conclusion, these findings highlight a novel role for NCOA4 in the prevention of replication stress, DNA damage, and premature senescence and, thus, in the maintenance of genome stability. Loss of such NCOA4 function may contribute to thyroid cancer formation.

1. Background

1.1 Thyroid cancer

Thyroid cancer is the most frequent endocrine malignancy and represents around 1% of newly diagnosed cancers (Hundahl et al. 1998; Gimm 2001), with an incidence stably increasing over the last decades (Jemal et al. 2010). It comprises a broad spectrum of neoplasms classified according to distinct clinical and pathological features (Kondo et al. 2006; DeLellis and Williams 2004; DeLellis 2006) (Table 1). The great majority of thyroid tumors (~ 95%) derive from follicular cells that synthesize and secrete thyroid hormones. The remainder derive from the parafollicular or C-cells that synthesize calcitonin. Thyroid follicular cell-derived carcinomas are classified into: well differentiated thyroid carcinoma (WDTC), [which comprises papillary (PTC) and follicular (FTC) thyroid carcinoma], poorly differentiated (PDTC), and anaplastic (ATC) thyroid carcinoma. Medullary thyroid carcinoma (MTC) derives from parafollicular cells and represents a rare thyroid malignancy (3-5%).

PTC comprises 80-85% of all thyroid carcinomas and is characterized by a branching (papillary) architecture and specific nuclear features. Several PTC variants are recognized, including solid-follicular, follicular, tall-cell and hurthle cell with different pathological and clinical features (DeLellis 2006). PTC generally has an indolent behaviour, metastasizes prevalently at the local lymph nodal stations and has a survival rate greater than 90% (Schlumberger 1998; Sherman 2003). However, some PTC cases lose the ability to concentrate iodine and become resistant to radio-iodine mediated ablation.

FTC is defined as a tumor with follicular cell differentiation in the absence of the nuclear diagnostic features of PTC (DeLellis 2006). ATC is the rarest tumor of the thyroid gland (2-3%). Despite this, ATC represents the first cause of death for thyroid cancer. Morphologically, it is defined as a malignant tumor composed entirely or partially of undifferentiated cells (DeLellis 2006). PDTC is defined as a neoplasm of follicular origin, with limited evidence of follicular cell differentiation (DeLellis 2006); PDTC is considered, morphologically and clinically, as an intermediate lesion between WDTC and ATC. MTC comprises both sporadic (~ 75%) and familial (~ 25%) cases in the context of the autosomal dominant MEN2 syndromes (Marx, 2005).

Table 1: Classification of thyroid carcinomas (modified from Kondo et al. 2006)

Tumor type	Prevalence	Sex ratio (female:male)	Age (years)	Lymphnode metastasis	Distant metastasis	Survival rate (5 years)
Papillary thyroid carcinoma	85-90%	2:1 - 4:1	20-50	<50%	5-7%	>90%
Follicular thyroid carcinoma	<10%	2:1 - 3:1	40-60	<5%	20%	>90%
Poorly differentiated thyroid carcinoma	rare-7%	0.4:1 - 2.1:1	50-60	30-80%	30-80%	50%
Undifferentiated thyroid carcinoma	2%	1.5:1	60-80	40%	20-50%	1-17%
Medullary thyroid carcinoma	3%	1.1-1.2:1	30-60	50%	155	80%

1.2 Genetic alterations in thyroid carcinoma

In the last two decades, some genetic lesions that underlie thyroid follicular cell transformation have been unveiled, including genetic alterations that initiate WDTC and those responsible for the progression to PDTC and ATC (Table 2). Around 70% of PTC is associated with two kind of genetic lesions: oncogenic rearrangements involving RET (REarranged during Transfection) and NTRK1 (Neurotrophic Receptor-Tyrosine Kinase 1) and point mutations in BRAF gene (Table 2). Importantly these genetic lesions are mutually exclusive and activate a common signal transduction pathway, the MAPK (Mitogen-Activated Protein Kinases) one, that leads to cellular proliferation, survival and motility (Melillo et al. 2005). NTRK1 is a tyrosine kinase receptor that binds NGF (Nerve Growth Factor); in PTC, NTRK1 undergoes chromosomal rearrangements leading to its oncogenic activation (Greco et al. 2010). Such rearrangements involve principally three fusion partners (TPR, TPM3 and TFG) (Greco et al. 1993; Greco et al. 1995; Greco et al. 1997). BRAF is a serine-threonine kinase that transduces regulatory signals through the MAPK pathway. In PTC, BRAF can be activated by point mutations within the kinase domain, the most frequent being a transversion from thymine to adenine at nucleotide 1799 (T1779A), resulting in the substitution of a glutamic acid for a valine at position 600 (V600E). BRAF mutations are found in 29-69% of PTCs

(Ugolini et al. 2007). Transgenic mice expressing BRAFV600E develop thyroid carcinomas that closely recapitulate PTC features in humans, showing an aggressive behaviour and progression to PDTCs (Knauf et al. 2011). Thus, BRAF mutations correlate with tumor recurrence, reduced radioiodine concentration and decreased overall survival (Lupi et al. 2007; Elisei et al. 2008; Xing 2010).

FTC develops through two main different pathways, involving either RAS or PPARγ (Peroxisome Proliferator-Activated Receptor gamma) (Table 2). RAS family members are small GTP-ases activating the MAPK pathway and are frequently mutated in cancer. RAS point mutations in codons 12, 13 and 61 are found in FTCs, in the follicular variant of PTC (Zhu et al. 2003; Kondo et al. 2006) and in PDTC and ATC suggesting a role for RAS mutations in thyroid tumor progression (Garcia-Rostan et al. 2003; Volante et al. 2009). PPARγ is a member of the nuclear-hormone-receptor superfamily and forms heterodimers with the retinoid X receptor. Some FTC harbour a rearrangement (PPFP: PAX8-PPARγ) mediated by a translocation between PAX8, a thyroid specific transcription factor, and PPARγ (Eberhardt et al. 2010). In PPFP, the DNA binding domain of PAX8 is fused to the A-F domains of PPARγ. The resulting chimeric protein acts as a dominant negative PPARγ and displays oncogenic properties (Kroll et al. 2000; Castro et al. 2006). PI3KCA mutation or gene amplification have been also reported in some FTCs (Garcia-Rostan et al. 2005; Liu et al. 2008).

PDTC and ATC share genetic lesions with WDTC, consistent with the hypothesis of a multi-step carcinogenesis model for thyroid cancer. Some PDTC and ATC present BRAF mutations, particularly samples with morphological evidence of pre-existing PTC (Nikiforova et al. 2003; Soares et al. 2004; Begum et al. 2004). In PDTC and ATC are also frequently detected point mutations of RAS (Garcia-Rostan et al. 2003; Volante et al. 2009) as well as amplifications or point mutations of PI3KCA (Garcia-Rostan et al. 2005; Liu et al. 2008). However, differently from WDTC, around 70% of ATC and a significant fraction of PDTC shows point mutation of TP53 (Nikiforov 2004, Kondo et al. 2006) or p53 disfunction induced by other mechanisms, including upregulation of negative p53 regulators like HMGA1, ΔNp73 or HDM2 (Pierantoni et al. 2007; Malaguarnera et al. 2007). Furthermore, ATC and to a lesser extent PDTC are associated with point mutation in exon 3 of the CTNNB1 gene encoding β-catenin (Garcia-Rostan et al. 2001), suggesting a role for this gene in the loss of differentiation of thyroid tumors.

MTC, as previously mentioned, can be sporadic (75%) or familial in the context of the autosomal dominant cancer syndromes MEN2 (Multiple Endocrine Neoplasias 2) (MEN2A, MEN2B and FMTC) (Marx 2005). RET point mutations are associated to both sporadic (50%) and familial (virtually 100%) MTC cases (Elisei et al. 2008). In MEN2A, mutations target extracellular cysteine residues of

RET, while MEN2B is associated predominantly with the Met918Thr intracellular substitution involving the tyrosine kinase domain (Leboullex et al. 2004). Recently, RAS mutations have been described in RET-negative sporadic MTC (Moura et al. 2011).

Table 2: Genetic alterations in follicular cell-derived thyroid carcinomas (modified from Kondo et al. 2006)

Genetic alteration	Papillary thyroid carcinoma	Follicular thyroid carcinoma	Poorly differentiated thyroid carcinoma	Undifferentiated thyroid carcinoma
RET rearrangement	13-43%	0%	0-13%	0%
BRAF mutation	29-69%	0%	0-13%	10-35%
BRAF rearrangement	1%	Unknown	Unknown	Unknown
NTRK1 rearrangement	5-13%	Unknown	Unknown	Unknown
Ras mutation	0-21%	40-53%	18-27%	20-60%
PPARG rearrangement	0%	25-63%	0%	0%
CTNNB1 mutation	0%	0%	0-25%	66%
TP53 mutation	0-5%	0-9%	17-38%	67-88%

CTNNB1, β-catenin; NTRK1, neurotrophic tyrosine kinase receptor, type 1; PPARG, peroxisome-proliferator-activated-receptor-Y

1.3 RET/PTC rearrangements

The REarranged during Transfection (RET) gene was discovered in 1985 by Takahashi and coworkers as a proto-oncogene activated by DNA rearrangements (Takahashi et al. 1985). RET is located on the long arm of chromosome 10 (10q12.2) and encodes a transmembrane receptor tyrosine kinase that binds to growth factors of the glial-cell line-derived neurotrophic factor (GDNF) family (Manie' et al. 2001). RET protein is composed by 4 functional domains: an extracellular ligand-binding portion with four cadherin like and a juxtamembrane cysteine rich domain, a hydrophobic transmembrane segment, an intracellular tyrosine kinase domain and a COOH-terminal tail. Binding of the ligand induces

receptor dimerization, autophosphorylation of target tyrosine residues which function as binding sites for signalling molecules cointaining phosphotyrosine-binding motifs (SH2 or PTB), and the activation of several signalling pathways (Santoro et al. 2004). RET is normally expressed in the central and peripheral nervous system and is required for renal organogenesis, enteric neurogenesis and spermatogenesis (Schuchardt et al. 1994). RET is normally expressed at high levels in C-cells, but not in follicular cells (Santoro and Carlomagno 2006).

About 30% of PTC harbour oncogenic rearrangements, induced by chromosomal inversions or translocations, in which the tyrosine kinase domain of RET is fused in frame with the 5'-portion of several gene partners leading to the formation of the chimeric RET/PTC oncogenes (Fusco et al. 1987; Grieco et al. 1990). The presence in the gene partners of coiled-coil domains causes a constitutive dimerization and kinase activation of the rearranged RET/PTC oncoprotein. In addition, RET/PTC becomes ectopically expressed in thyrocytes, loses RET protein domains that negatively regulate its kinase activity (like the extracellular domain) and relocalizes to the cytoplasm. RET/PTC rearrangements are particularly common in PTC from patients exposed to ionizing radiation and in pediatric PTC (Nikiforov et al. 1997). More then ten different RET/PTC rearrangements have been reported differring in the RET fusion partner (Figure 1). RET/PTC1 and RET/PTC3 involving genes CCDC6, previously known as H4(D10S170) (Grieco et al. 1990), and NCOA4 (also known as RFG/ELE1/ARA70) (Santoro et al. 1994; Bongarzone et al. 1994) respectively, constitute more then 90% of the total.

RET/PTC3 is formed by the fusion of the tyrosine kinase domain of RET with the first 238 aminoacids of the NH2 portion of NCOA4. RET/PTC3 results from a paracentric inversion of the long arm of chromosome 10 and it has a high prevalence in post-Chernobyl pediatric PTC (Nikiforov et al. 1997). Furthermore, RET/PTC3 is associated with more aggressive PTC variants like the solid-follicular and tall-cell ones (Basolo et al. 2002).

Oncogenic activation of RET in RET/PTC rearrangements represents a major mechanism explaining the tumorigenic properties of this chimeric oncoprotein. However, it cannot be excluded that the genetic alteration of the partner genes might contribute to the transformation as well. For instance, in the case of RET/PTC2 rearrangement that involves the regulatory subunit type 1-α of the protein Kinase A (RIα) it is possible that loss-of-function of RIα is involved in tumorigenesis (Bongarzone et al. 1993). Indeed, RIα is a *bona fide* tumor suppressor since its germline inactivating mutations are responsible for an inherited neoplastic syndrome, the Carney complex, featuring predisposition to develop several neoplasias comprising thyroid cancer (Bossis and Stratakis, 2004). Furthermore, RIα depletion in mice induces the formation of thyroid tumors (Griffin et al. 2004).

Along this line, multiple evidences suggest that other RET partner genes in RET/PTC rearrangements might play a role in tumorigenesis. In particular, CCDC6 (Coiled-coil domain-containing protein 6), which is involved in the formation of RET/PTC1, has been recognized as a target of the DNA Damage Response (DDR) kinase ATM and to function as a apoptosis mediator. ATM-mediated phosphorylation of CCDC6 in response to DNA damage, promotes its nuclear accumulation and leads to apoptosis. Its alteration in RET/PTC1 transformed cells may, therefore, contribute to PTC development by impairing apoptotic response to DNA damage (Merolla et al. 2007). Furthermore, CCDC6 has also been shown to interact with and repress the activity of the pro-proliferative transcription factor CREB1 by recruiting HDAC1 (Histone Deacetylase 1) and PP1 (Protein Phosphatase 1) at CRE (CREB responding elements) sites (Leone et al. 2010). Thus, CCDC6 disruption may contribute to thyroid cell transformation mediated by the RET/PTC1 oncogene. Finally, other genes less frequently involved in RET/PTC rearrangements have beeen suggested to play a role in cancer development like HTIF1 (also known as TRIM24) (Khetchoumian et al. 2007) and TRIM27 (Dho & Kwon 2003).

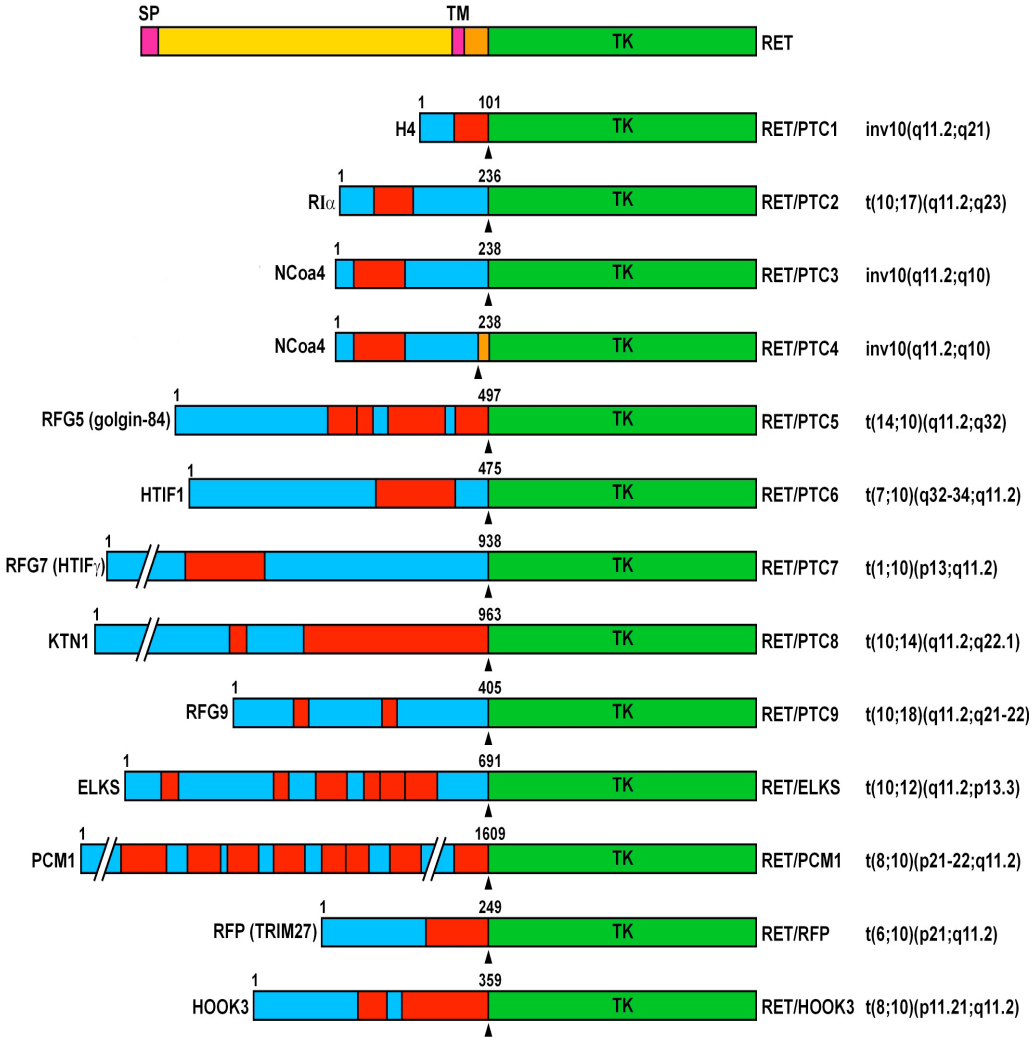

Figure 1: RET/PTC rearrangements in papillary thyroid carcinoma

1.4 The NCOA4 (RFG/ELE1/ARA70) gene

The NCOA4 gene encodes an ubiquitously expressed 70-KDa protein. Initially identified as a gene rearranged with the tyrosine kinase receptor RET in PTC (Santoro et al. 1994; Bongarzone et al. 1994) and named RFG (Ret-fused gene) or Ele1, it was subsequently discovered as a co-activator of the androgen receptor (Yeh et al. 1996). NCOA4 is able to interact and promote the transcriptional activity of other nuclear receptors: the LXXLL motif (aa 92-96) and the FXXLF motif (aa 328-332) mediate its interaction with the peroxisome-proliferator activated receptor γ (PPARγ) (Heinlein et al. 1999) and the androgen receptor (AR) (Hu et al. 2004) and estrogen receptor (ER) (Lanzino et al. 2005), respectively (Figure 2). Several evidences suggest a role for NCOA4 in tumorigenesis. NCOA4 expression is reduced in prostate cancer as well as in prostate cancer cell lines and its adoptive overexpression in prostate cancer cells reduces cellular proliferation and colony formation (Li et al. 2002; Tekur et al. 2001). Moreover, its expression is also reduced in a subset of breast carcinomas, particularly in HER2+ samples (Kollara et al. 2001). Finally, genome mapping association studies linked the presence of SNPs at the 10q11 locus, harbouring NCOA4, with an increased susceptibility to prostate cancer (Chang et al. 2009; Pomerantz et al. 2010).

The NCOA4 protein contains a coiled-coil domain (aa 17-125) that mediates protein oligomerization (Monaco et al. 2001). Thus, one functional consequence of NCOA4-RET fusion (RET/PTC3) is NCOA4 mediated homodimerization of the RET tyrosine kinase domain followed by constitutive autophosphorylation and oncogenic activation. This is probably a major mechanism of the tumorigenic role of RET/PTC3 rearrangement in thyroid cancer (Monaco et al. 2001).

However, disruption of the NCOA4 gene, as well as its inhibition by a dominant negative effect of RET/PTC3 oncoprotein may have a role in RET/PTC3-mediated tumorigenesis. To study NCOA4 function in our laboratory a yeast-two-hybrid screening was performed to identify new NCOA4 protein interactors. Using as a bait the N-terminal 238 aa of NCOA4, corresponding to the portion fused to RET gene in the RET/PTC3 rearrangement, two clones encoding the C-terminal portion of the MCM7 gene were isolated (Carlomagno et al. personal communication).

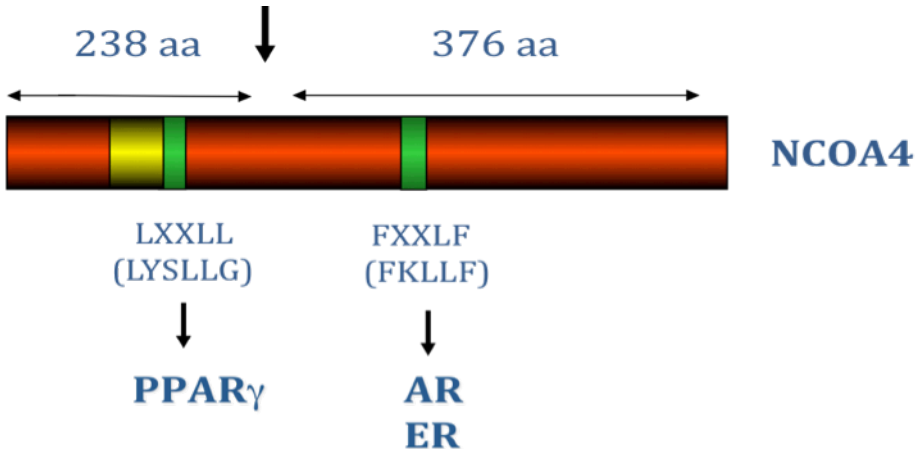

Figure 2: Structure of NCOA4 protein; domains mediating interaction with PPARγ (peroxisome-proliferator activated receptor γ), AR (androgen receptor) and ER (estrogen receptor) are shown. A vertical arrow indicates the breakpoint site in RET/PTC3 rearrangement.

1.5 DNA replication

DNA replication is a complex multistep process whose accuracy is essential for the maintenance of genome stability (Bell and Dutta 2002; Branzei and Foiani 2010) (Figure 3). DNA replication involves the stepwise formation of several protein complexes. Initially, the Pre-Replication Complex (Pre-RC) is assembled at replication origins in early G1 to license them (Chong et al. 1995; Kubota et al. 1995; Tanaka et al. 1997; Yan et al. 1993). The pre-RC assembly starts with the binding of the six-subunit complex ORC (origin recognition complex) that allows the sequential binding of the licensing factors Cdc6 and Cdt1, necessary for the recruitment of the MCM2-7 complex and its stable loading onto chromatin as double hexamers (Remus et al. 2009). At this point, chromatin is "licensed" to be replicated (Chevalier and Blow 1996). Several mechanisms restrain these events to the G1 phase of the cell cycle, inhibiting MCM2-7 loading onto chromatin in S and G2 phases to avoid re-replication (Blow and Dutta 2005; Arias and Walter 2007). The principal one involves the activity of Geminin which inhibits Cdt1 by directly binding to it, protecting it from degradation and leaving it in an inactive form unable to further promote licensing (Wohlschlegel et al. 2000). Replication initiation depends on activation of the helicase function of MCM2-7 by phosphorylation of several components of the Pre-RC by Cyclin E/A-CDK2 (cyclin dependent kinase 2) and Cdc7/DDK (Dbf4 and Drf1 dependent kinase) during G1

to S phase transition (Pasero and Schwob 2000; Sclafani 2000). This event is referred to as "origin firing". Cdc6 is then phosphorylated, released from chromatin and extruded from nucleus (Delmolino et al. 2001) while Cdt1 is subsequently degraded by a PCNA-coupled degradation pathway involving the Cul4-Cdt2 ubiquitin ligase (Arias & Walter 2005; Jin et al. 2006) and by a Skp2-containing SCF complex after CDK-dependent phosphorylation (Li et al. 2003). Other replication factors, such as CDC45 and the GINS complex [Go(5)-Ichi(1)-Ni(2)-San(3); tetrameric complex composed of Sld5, Psf1, Psf2, Psf3], bind to licensed origins to form the so called Pre-IC (Pre-initiation complex) or CMG (Cdc45-MCM2-7-GINS) complex that represents the processive helicase that unwinds double strand DNA during replication. Subsequently, the CMG complex opens the replication bubble, allowing loading of the single-strand binding protein RPA, that stabilizes the single strand DNA and promotes the binding of DNA polα-Primase. In turn, DNA polα produces a short RNA/DNA primer recognized by the clamp loader, RFC. Finally, RFC recruits PCNA, the processivity factor of DNA polymerases. PCNA is a homotrimeric ring protein that encircles double strand DNA with a 3' free end allowing polymerase activation. DNA polα is replaced by DNA polδ and DNA polε, which display greater processivity and possess a 3'-5' proofreading exonuclease activity (Ritzi and Knippers 2000). At each replication bubble, the replication starts and proceeds bidirectionally, with helicase moving onto leading strand (Fu et al. 2011) to generate single strand and DNA polymerases elongating the nascent strand in 5'-3'direction. The MCM2-7 proteins gradually dissociate from chromatin as S-phase proceeds (Krude et al. 1996) and replication forks merge, consistent with their predicted function as a DNA helicase (Ishimi 1997).

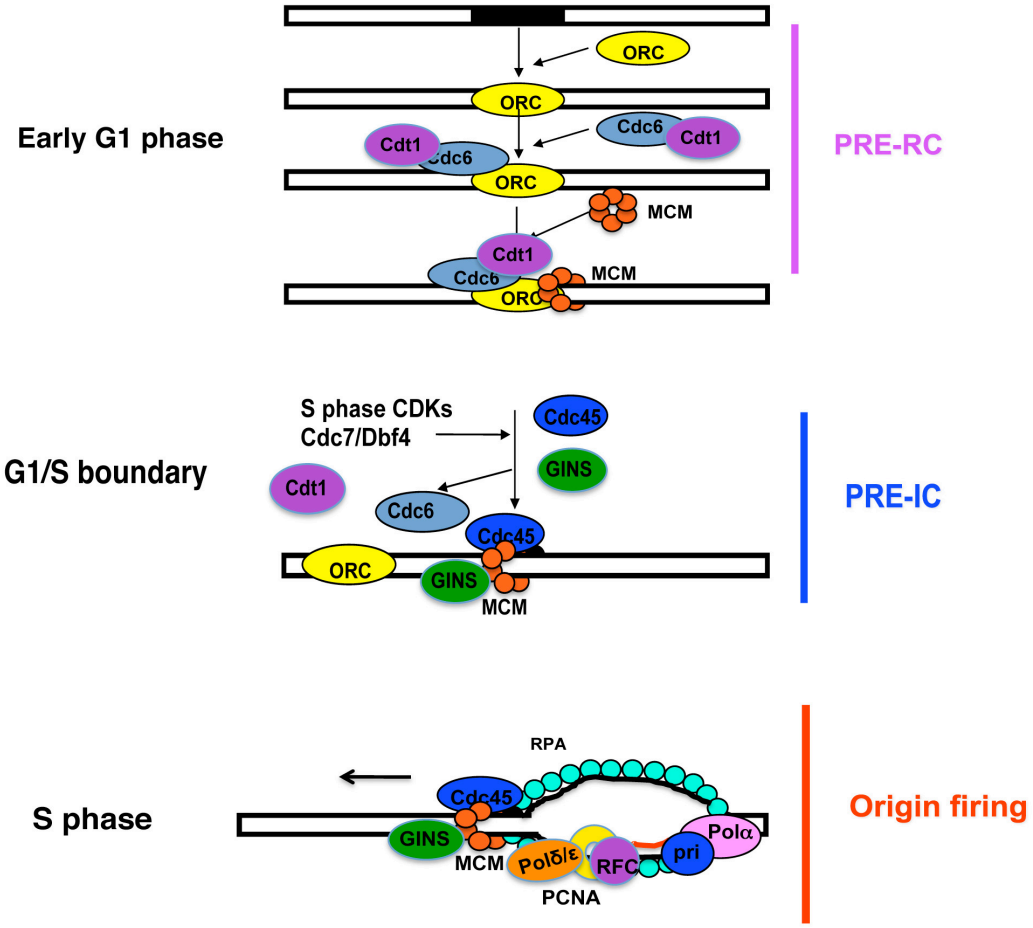

Figure 3 : A schematic representation of the main steps of DNA replication

1.6 DNA damage, genome instability and cellular senescence

The primary objective for every life form is to deliver its genetic material, intact and unchanged, to the next generation (Jackson & Bartek 2010). Eukaryotes have to deal constantly with endogenous and exogenous sources of DNA damage that can affect genome integrity. An evolutionary conserved pathway senses DNA damage and relays this information by activating a signal transduction pathway, known as DNA damage response (DDR) (Figure 4). DDR halts cell cycle

progression to prevent the transmission of altered genetic material and coordinates cellular efforts to repair DNA and maintain genome integrity. DDR is robustly activated by double strand breaks (DSBs) or by RPA-coated single-stranded DNA.

DSBs are sensed by the Mre11-Rad50-Nbs1 (MRN) complex which recruits, through the C-terminus of Nbs1, the Ataxia-Teleangectasia mutated (ATM) kinase leading to its autophosphorylation and activation (Falck et al. 2005). Activated ATM phosphorylates the histone variant H2AX on Ser 139 (also known as γH2AX) at sites of damage to help recruitment of additional checkpoint proteins including MDC1 (Mediator of the DNA damage Checkpoint 1), which directly binds to phosporylated H2AX (Stucki et al. 2005), and 53BP1 (p53 Binding Protein 1). MDC1 binds to and help recruitment of further MRN complexes that by spreading onto chromatin induce a positive loop that fosters DDR. Furthermore, MDC1 and 53BP1 induce the transient loading of the checkpoint kinase Chk2 which is phosphorylated by ATM and then rapidly released from chromatin to activate the checkpoint.

On the other hand, RPA-coated single-stranded DNA leads to the recruitment of the ATR (ATM-related)-ATRIP (ATR-Interacting Protein) dimer (Zou and Elledge 2003), whose activity is boosted by the loading of the RAD9-HUS1-RAD1 and Rad17-RFC complexes onto replication stalling lesions. ATR activity is also stimulated by its own target TOBP1, while Claspin is necessary for ATR-mediated phosphorylation of Chk1, which is then released to activate the intra-S-phase checkpoint (Smits et al. 2006).

Chk2 and Chk1 represent the checkpoint proteins responsible for the spreading of the DDR signalling cascade into the nucleus far away from the initial DNA-damage site. Finally, p53 and Cdc25 phosphatases are the ultimate effectors of this pathway and connect DDR signalling to the cell cycle machinery. In particular, p53 activates transcription of the cell cycle inhibitor p21 which halts cell cycle progression by inhibiting CDKs (Cyclin Dependent Kinases). Cdc25 family phosphatases, which normally activate CDKs during cell cycle progression, are inactivated either by degradation or nuclear extrusion induced by DDR. This cell cycle arrest can be transient and upon DNA damage repair cells can resume proliferation. However, if DNA damage is particularly severe cells may undergo apoptosis or enter a protracted DDR-induced cell cycle arrest known as cellular senescence (d'Adda di Fagagna 2008).

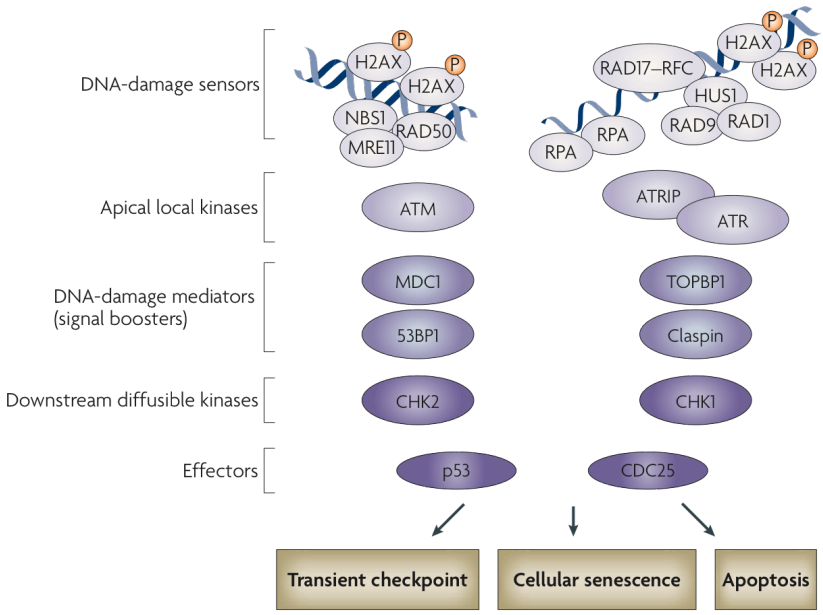

Figure 4: The DNA Damage Response (DDR). A schematic representation of the main players involved in the recognition of DNA damage and the transmission of the signal throghout the cell to activate effectors that halt cell cycle progression and favour DNA repair (modified from d'Adda di Fagagna 2008).

Senescent cells have been observed in vivo in mammals in association with normal ageing and with the first stages of tumorigenesis (Collado and Serrano 2010; Bartkova et al. 2005; Braig et al. 2005; Gorgoulis et al. 2005). Indeed, cellular senescence is induced (in vivo and in vitro) by oncogene activation (Serrano et al. 1997) because of the induction of a hyperproliferative stress associated with replication stalling lesions and DDR activation (Di Micco et al. 2006; Bartkova et al. 2006). Recently Kerem and colleagues suggested that oncogene-induced hyper-replication leads to a reduction in the nuclear nucleotides pool that causes replication failure inducing genetic instability (Bester et al. 2011). Whatever the mechanism, the so called oncogene-induced senescence (OIS) represents one of the principal barriers that restrain cancer development in vivo (Bartkova et al. 2006; Halazonetis et al. 2008). It has been suggested that breaches to this barrier, arising from mutational or epigenetic inactivation of DDR components, are subsequently selected for during tumor development, thus allowing malignant progression. This model for the DDR as an anti-cancer barrier helps explaining the high frequency of DDR defects in human cancer (Halazonetis

et al. 2008). Furthermore, oncogene-induced hyper-replication and DNA damage could explain the main hallmark of human cancer: e.g. genetic instability (Negrini et al. 2010) (Figure 5).

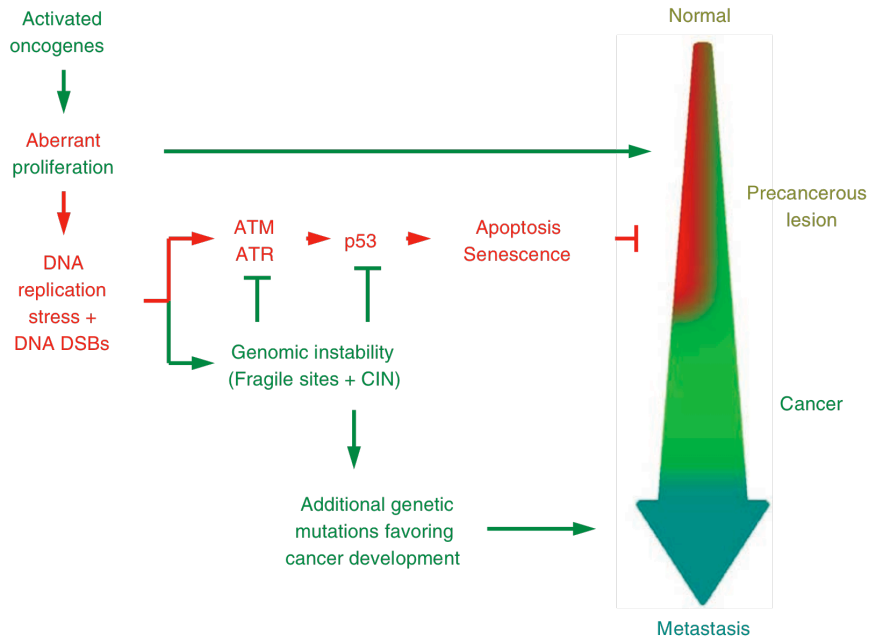

Figure 5: An oncogene-induced DNA damage model for cancer development. Oncogene-induced replication stress causes DNA damage and DDR activation to restrain tumor development. However, by favouring genetic instability, it promotes a selective pressure for p53 inactivation and further tumor progression (modified from Halazonetis et al. 2008).

2. Aim of the study

In papillary thyroid carcinoma (PTC), RET TK domain is fused to heterologous genes to form the RET/PTC oncogenes. RET/PTC3, one of the most common variant, is generated by a chromosomal inversion leading to the fusion of the NCOA4 gene 5' portion to the 3'-ter of the RET gene, coding for the tyrosine kinase domain. NCOA4 drives RET/PTC3 expression in thyroid follicular cells and induces its constitutive dimerization, switching on RET kinase activity. However, inactivation of NCOA4 function may contribute to tumorigenesis as well. Aim of this study has been to verify this hypothesis by characterizing the physiological function of mammalian NCOA4. To this aim, we:

1. generated a NCOA4 gene knock-out mouse and analysed its phenotype;

2. generated Mouse Embryo Fibroblasts (MEFs) from E13.5 embryos wild type (WT), heterozygous (HT) and knock-out (KO) for NCOA4 and analysed their proliferation rate;

3. studied replication properties and DNA damage accumulation of NCOA4-/- cells by different molecular approaches.

Additional aims of this study were to address:

- the role exerted by the beta-catenin mitogenic pathway in thyroid cancer;
- FOXM1-mediated control of cell cycle progression in ATC

These further studies are described in the manuscripts attached at the end of Dissertation.

3. Materials and methods

3.1 Murine NCOA4 gene targeting

Several overlapping genomic clones were isolated from a λϕIXII phage library of a 129SVJ mouse strain (Stratagene) using standard procedures. Exons II-VII of the murine NCOA4 gene were replaced by a neomycin-resistant (neo) cassette. The targeting construct was transfected by electroporation into embryonic stem (ES) AB2.1 cells. Genomic DNA from each G418-resistant clone was digested with StuI and hybridized by southern blot to an external 3' genomic sequence that detects 9 Kbp and 4 Kbp fragments corresponding to the wild-type (WT) and knock-out (KO) alleles, respectively. Two correctly targeted ES cell lines were injected into C57BL/6 blastocysts at BIOGEM facility (Ariano Irpino, Italy). Both gave rise to germ line chimeras that were backcrossed to C57BL/6 females to obtain heterozygous NCOA4-KO offsprings. Heterozygous NCOA4-KO mice were inter-crossed with each other to yield homozygous NCOA4-KO animals. Mice were maintained under specific pathogen-free condition in our laboratory animal facility and all studies were conducted with respect to the Italian regulation for experimentations on animals.

3.2 Preparation of MEFs and cell culture conditions

NCOA4+/- mice of C57BL/6 genetic background were mated. Pregnant females at 13.5 d of gestation were sacrificed under anesthesia, followed by uterine dissection to isolate individual embryos. Each embryo was washed in PBS (pH 7.2), followed by removal of head (used for embryo genotyping) and internal organs (hearth and liver). The embryo body was minced and then forced through a 5ml syringe with a 18-gauge needle. Cell suspension was incubated in a 10 cm plate (now considered passage 0) and cultured in Dulbecco's modified Eagle's medium (DMEM) supplemented with 10% FBS (HyClone), 50μg/ml penicillin-streptomycin, 2mM L-glutamine. Once cells became subconfluent, we followed a 3T3 subculture schedule by counting the total number of cells using a hemocytometer and plating $5x10^5$ per 100-mm dish. Every 3 days, cells were trypsinized and counted to determine the numer of population doublings, and then plated onto a new dish. The accumulation of population doubling level (PDL) was calculated by using the formula $\Delta PDL=\log(n_h/n_i)/\log 2$, where n_i was the initial number of cells and n_h is the final number of cells at each passage.

3.3 Protein studies

Protein extractions and immunoblotting experiments were performed according to standard procedures. Briefly, cells were harvested in lysis buffer (50 mM HEPES, pH7.5, 150 mM NaCl, 10% glycerol, 1% Triton X-100, 1 mM EGTA, 1.5 mM MgCl2, 10 mM NaF, 10 mM sodium pyrophosphate, 1 mM Na3VO4, 10 μg of aprotinin/ml, 10 μg of leupeptin/ml) and clarified by centrifugation at 10,000 x g for 30 min. Protein concentration was estimated with a modified Bradford assay (Bio-Rad, Munich, Germany). Immune complexes were detected with the enhanced chemiluminescence kit (ECL, Amersham). Anti-human-NCOA4 antibody is a rabbit polyclonal antibody raised against the last 376 C-terminal residues of human RFG (Monaco et al. 2001). Secondary anti-mouse and anti-rabbit antibodies coupled to horseradish peroxidase were from Bio-Rad.

3.4 Senescence-associated β-galactosidase (SAβ-gal) staining

SAβ-gal stain was performed according to Dimri et al. (1995). Briefly, cells were washed twice with PBS, fixed with 2% formaldehyde and 0.2% glutaraldehyde in PBS, and washed twice with PBS. Then, cells were stained overnight in X-gal staining solution (1mg/ml X-gal, 40 mM citric acid/sodium phosphate (pH 6.0), 5mM potassium ferricyanide, 5 mM potassium ferrocyanide, 150 mM NaCl, 2 mM MgCl2). Photographs were taken using a Canon CCD camera mounted on a Zeiss phase contrast microscope.

3.5 Immunofluorescence staining

For indirect immunofluorescence, cells were fixed in 4% paraformaldehyde and permeabilized with Triton 0.2% X-100 (5 minutes on ice), and then incubated with α-H2AX phosphorylated on Ser139 (γH2AX) (R&D Systems) or α-53BP1 (Cell Signalling) for 1h at room temperature. Coverslips were washed and incubated with an Alexa-488 goat anti-rabbit antibody (Invitrogen) for 30 minutes at room temperature. After 5 minutes of Hoechst counterstaining, coverslips were mounted in Glycerol/PBS (1:1) and observed with a Zeiss LSM 510 META confocal microscope (Carl Zeiss). At least 300 cells were counted in triplicate.

3.6 DNA fiber analysis

MEF cells were pulse-labeled with 10 μM CldU for 20 min, washed once with medium and subsequently pulse-labeled with 150 μM IdU for 20 min. Labelled cells were harvested, resuspended in PBS (10^6 cells/ml) and 2.5 μl were spotted onto the top of cleaned glass slides and lysed with 7.5 μl of 0.5% SDS in 200 mM Tris-HCL, pH 7.4, 50 mM EDTA (10 min, 20°C). Slides were tilted (15° to horizontal), allowing a stream of DNA to run slowly down the slide, air dried and then fixed in methanol/acetic acid (3:1). CldU was detected by incubating acid-treated fiber spreads with rat anti-BrdU monoclonal antibody (1:1000; AbD Serotec) O.N. at +4°C. IdU was detected using a mouse anti-BrdU monoclonal antibody (1:500; Becton Dickinson) for 1h at R.T. Slides were finally incubated with a mix of secondary antibodies cointaining AlexaFluor 594-coniugated goat anti rat IgG (1:500; Molecular probes) and AlexaFluor 488-coniugated goat anti mouse IgG (1:500; Molecular Probes) for 30 min at R.T. Fibers were examined using a Zeiss microscope with 60x oil immersion objective. For quantification of replication structures at least 200 structures were counted per experiments. The lengh of red (AF 594) or green (AF 488) labeled patches were measured using the ImageJ software (National Insitute of health; http://rsbweb.nih.gov/ij/) and arbitrary lenght values were converted into micrometers using the scale bars created by the microscope. Kb values were finally obtained by multiplying micrometers for 2.5, a constant stretching factor.

3.7 Alkaline sucrose gradient sedimentation.

Cells were labeled in MEF medium containing 5 μCi/mL of ^{3}H-thymidine for 15 min at 37°C, harvested and resuspended in PBS at 5 x 10^6/mL. A 1 ml syringe was cut at the top and 300 μl of alkaline lysis solution (0.5M NaOH, 0.02M EDTA, pH 12.5, 0.1% NP-40) was added to the bottom. Subsequently, 50 μl of the cell suspension cointaining 2.5 x 10^5 cells was gently layered onto the lysis solution. The syringe was sealed to prevent evaporation and incubated at room temperature for 3h. Then, the cell lysate (350 μl) was layered on the top of a 5-20% alkaline sucrose gradient by inverting the cut syringe and slowly moving the piston while touching the top of the gradient. Sealed buckets were placed into the swing out rotor (SW40 TI-rotor) and centrifuged at 26,100 rpm for 90 min at 20°C using low acceleration setting and allowing the rotor to stop without brakes. After centrifugation, gradients were fractionated in 1-mL fractions starting from the top and collected into 1.5 ml eppendorf tubes. Each fraction was then spotted onto a piece of GF/C glass microfiber filter. After 3 washing in 10% TCA and deionized

water, filters were allowed to dry and transferred into scintillation vials. Two ml of 0.5 M NaOH was added to each vial and allowed to incubate at 60°C for 12 h. After the addition of 2ml of 0.5 M HCL to neutralize NaOH, 10 ml of scintillation fluid was added to each vial, vortexed vigorously and ^{3}H-activity was counted using a liquid scintillation counter. To obtain a sedimentation profile, the cpm values were plotted as percent of total ^{3}H-thymidine activity per fraction starting from the top fraction containing the shorter DNA fragments to the bottom containing the longer ones.

3.8 Pulsed field gel electrophoresis

Subconfluent cultures of KO and WT MEFs were irradiated with 40 Gy of Rx. Cells were harvested by trypsinization at different time points after irradiation, and agarose plugs of 10^{6} cells were prepared with a CHEF disposable plug mold (BioRad). Plugs were incubated in lysis buffer (100 mM EDTA, 1% (w/v) sodium laurylsarcosyne, 0.2% (w/v) sodium deoxycholate, 1 mg ml^{-1} proteinase K) at 37°C for 48 h and then washed four times in TE buffer (10 mM Tris-HCl (pH 8.0), 100 mM EDTA) before loading onto an agarose gel. Electrophoresis was performed for 23 h at 13°C in 0.9% (w/v) agarose containing 250 mM Tris-Borate with EDTA (TBE) using a CHEF MAPPER apparatus (BioRad) with the following parameters: voltage 180-120 V log; angle from 120° to 110° linear; interval 30 s to 5 s log. In these conditions, high molecular weight genomic DNA (more then 20 million base pairs (Mbp)) remains into the well, whereas low molecular weight DNA fragments (10 Mbp to 500 kbp) migrate into the gel as a compact single band. The gel was stained with Ethidium bromide and analysed using a Typhoon 9200 scanner (Amersham). Band intensities were quantified using the ImageJ software (National Insitute of health; http://rsbweb.nih.gov/ij/). The amount of broken DNA was calculated as the intensity of the DNA in the migrated fraction over the intensity of DNA in the well plus the migrated fraction (total DNA intensity).

3.9 Statistical analysis

The two-tailed unpaired Student's t test was used for statistical analysis. All P values were two sided and differences were significant when P was less then 0.05. All statistical analysis were carried out using the GraphPad Instat software program (version 3.06.3).

4. Results

4.1 Generation of a Knock-out mouse for the NCOA4 gene.

To examine the *in vivo* role of NCOA4, we used a gene targeting technique in ES cells to generate a null mutation at the murine NCOA4 genomic locus (Figure 6A). Heterozygous progeny of chimeric animals was identified by Southern Blot analysis of StuI-digested tail DNA and matings were established to produce mice heterozygous or homozygous for the NCOA4-null allele (Figure 6B). The knock-out allele was transmitted in a mendelian fashion and both heterozygous and homozygous mice were viable and fertile. Immunoprecipitation of cell lysates from mouse embryonic fibroblasts (MEFs) with an anti-NCOA4 antibody followed by Western blot for NCOA4 confirmed that homozygous mouse cells did not express the NCOA4 protein (Figure 6C). We followed mice growth and performed macroscopic and microscopic analysis of the principal mouse organs and tissues and no significant differences were detected between knock-out (KO) and wild-type (WT) mice (data not shown).

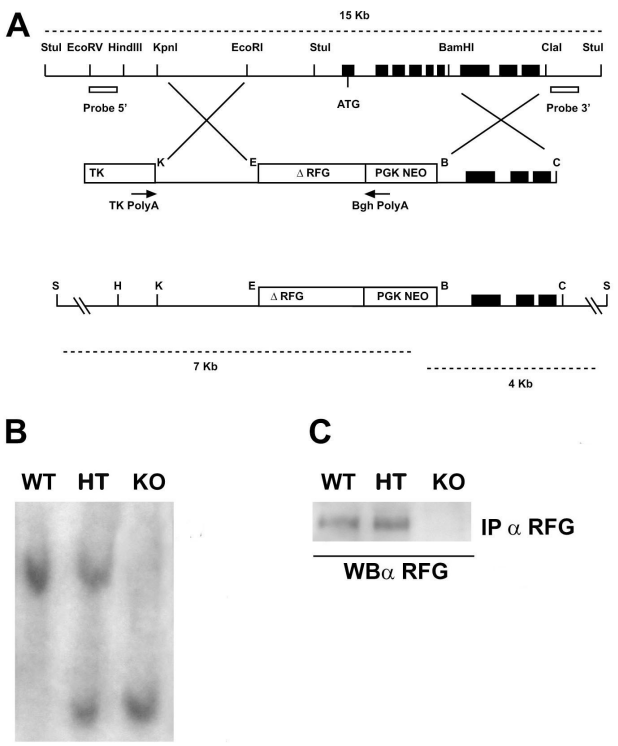

Figure 6: Targeted disruption of the murine NCOA4 gene. (A) Schematic representation of the genomic locus surrounding the targeted NCOA4 exons, the targeting vector and locus. (B) Southern blot analysis of tail DNA from wild type (WT), heterozygous (HT) and knock-out (KO) mice. Genomic DNA was digested with StuI and hybridized to a 3' external probe as shown in A. The wild type band is ~ 9 Kb while the disrupted allele generates a ~ 4 Kb band. (C) Protein extracts from wild type (WT), heterozygous (HT) and knock-out (KO) MEFs were imuunoprecipitated with anti-NCOA4 antibody, run on SDS PAGE and incubated with anti-NCOA4 antibody.

4.2 MEF homozygous for NCOA4 deletion show reduced growth rate

To determine whether NCOA4 is important for cell cycle progression in mice, mouse embryo fibroblasts (MEFs) from NCOA4 wild-type (WT), heterozygous (HT) and knock-out (KO) animals were cultured according to a standard 3T3 protocol. Cells seeded at a fixed density were cultured for 3 days, counted and then re-seeded at the same initial density. Cell confluence was

avoided by seeding cells at a relatively low confluence (500,000 cells/10 cm plate). The number of population doublings was calculated as described in Materials and Methods.

As shown in Figure 7, NCOA4-/- cells showed a decreased accumulation of population doublings compared to the WT cells. Heterozygous cells showed an intermediate phenotype. In particular, after 3 to 4 population doublings NCOA4 -/- cells accumulated into the plates with a flattened and enlarged morphology and no increase in cell number was obtained despite serial passaging.

We rarely succeeded in establishing spontaneously immortalized cell lines from NCOA4-/- embryos (data not shown). However, after prolonged passages in culture (more then 2 months) we could isolate from 20-30% of KO embryos a few proliferating cell clones. In contrast, 100% of WT and HT embryos gave rise to immortalized cells. Such immortalized NCOA4-/- MEFs displayed a slow proliferation rate compared to both HT and WT immortalized cells lines (data not shown) suggesting that the proliferative defect seen in primary cells is conserved also in immortalized cell lines.

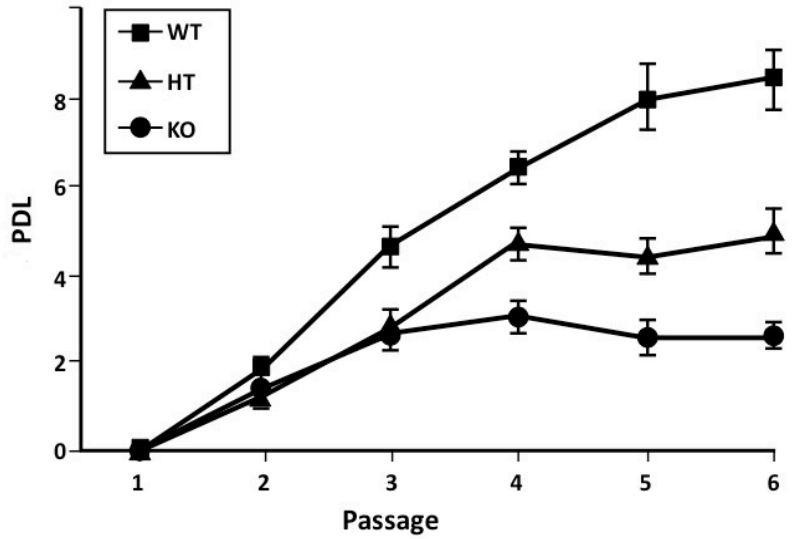

Figure 7: NCOA4-/- cells show impaired cell proliferation. Growth of NCOA4 WT, HT and KO MEFs was examined by using a 3T3 protocol. The data are presented as the accumulated population doublings (PDL) during six passages in culture. The bars represent standard deviation of triplicate experiments.

4.3 NCOA4 depleted cells undergo premature senescence as a consequence of DNA damage accumulation

In response to genomic stress, murine primary cells undergo a cellular response known as DDR (see Introduction) that restrains cellular proliferation leading to a permanent cell cycle arrest known as cellular senescence. Despite being alive, senescent cells are unable to re-enter cell cycle in the presence of serum and display a typical morphology and gene expression pattern. After 3-4 population doublings, NCOA4-/- cells stopped growing and acquired an enlarged and flattened morphology suggesting premature senescence. To address this possibility, we performed a senescence associated β-galactosidase assay (SAβ-gal assay). As shown in Figure 8, compared to WT cells, a greater number of NCOA4-/- cells stained positively for β-gal both at passage 3 and 4, with more then 50% of cells being positive in the latter.

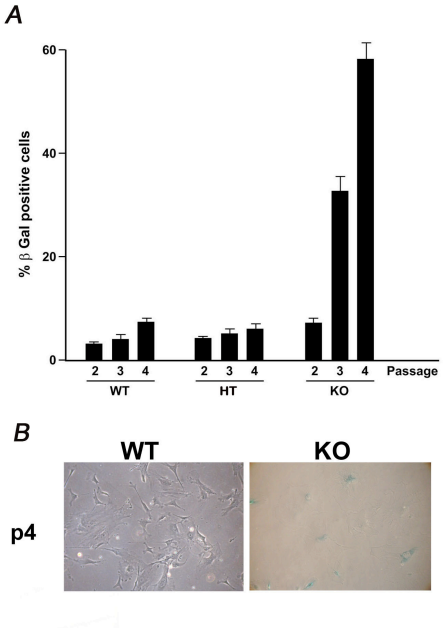

Figure 8: Senescent phenotype of NCOA4-/- cells. (A) Bar-graphs showing the percentage of senescent cells in WT, HT and KO MEFs at the described passages ± SD (standard deviation). (B) Representative images of passage 4 WT and KO cells stained for the β-galactosidase.

Primary cells undergo cellular senescence as a consequence of DNA damage accumulation. This event impedes the transmission of altered genetic information and represents a fundamental mechanism to prevent genetic instability and cancer development (D'adda di Fagagna 2008). To address the hypothesis that NCOA4-/- cells undergo premature senescence as a consequence of DNA damage accumulation, we looked for markers of DDR activation at single cell level by immunofluorescence. Cells rapidly recognize DNA damage and activate a signalling pathway that restrains cell cycle progression and activates DNA repair. One of the first event in this cascade is the phosphorylation of the histone variant H2AX on Serine 139 (known as γH2AX). This event is fundamental to allow the sequential recruitment of checkpoint and repair proteins, like 53BP1 and MDC1, and to activate the Chk2 kinase to spread the signal into the nucleus and activate the checkpoint response. We performed a confocal immunofluorescence analysis of NCOA4 WT and KO cells using an antibody that specifically recognizes γH2AX. As shown in Figure 9, we found a statistically significant ($p < 0.0001$) increased number of cells positive for the presence of γH2AX foci in NCOA4-/- MEFs compared to wild type controls.

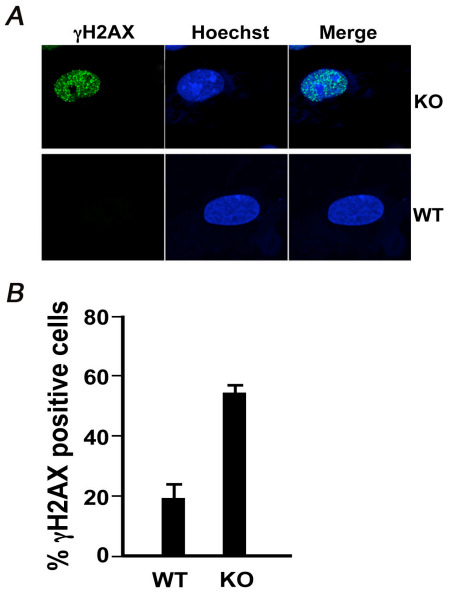

Figure 9: NCOA4-/- cells accumulate γH2AX foci. (A) Representative immunofluorescence staining for γH2AX in KO and WT cells (B) Bar-graphs showing the percentage of γH2AX positive WT and KO cells ± SD (standard deviation).

4.4 NCOA4 depleted cells display a normal DSBs repair ability

The accumulation of DNA damage in NCOA4-/- cells could be the consequence of a defect in the repair of DNA damage induced by the exposure to a stressfull environment (in particular high O_2 concentration). To verify whether NCOA4 exerts a role in DNA damage repair, we studied the efficiency of DNA repair after double strand breaks (DSBs) induction in WT and KO MEFs. Cells where subjected to 40 Gy Rx to induce cell cycle independent DSBs and DNA repair was followed by Pulsed field gel electrophoresis (PFGE). Cells where harvested at different time points after the irradiation, included in agarose plugs and processed for PFGE to detect broken DNA. Broken to intact DNA ratio was calculated by analysing bands intensity using the Image J software. As shown in Figure 10, NCOA4-/- MEFs showed a DSBs recovery curve overlapping to the wild type one. These data strongly suggest that NCOA4 is not involved in DSBs repair and exclude the possibility that DDR activation in KO cells is due to the inability to repair endogenous DNA DSBs.

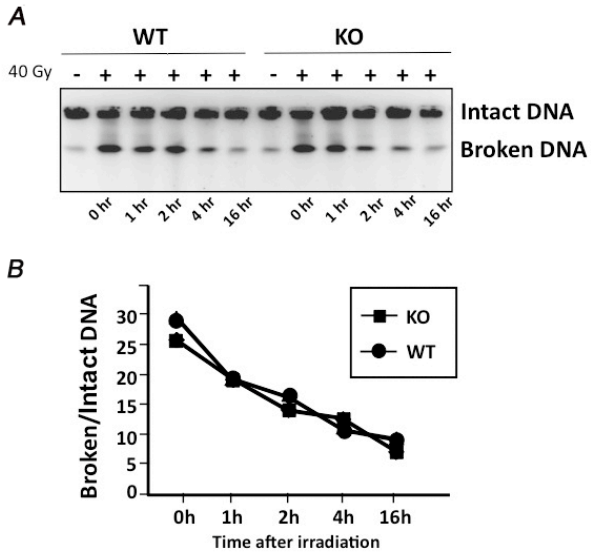

Figure 10: PFGE analysis of DSBs recovery after IR. (A) Cells irradiated with 40 Gy Rx were harvested at different time points and included into agarose plugs. PFGE was performed and gel stained with Etidium Bromide to detect intact DNA and double stranded molecules (fragmented DNA). (B) Quantification of recovery from DSBs formation in NCOA4 WT and KO MEFs shown as percentage of broken to intact DNA.

4.5 NCOA4-/- cells undergo replication stress

DNA damage accumulation in NCOA4-/- MEFs could be explained by replication stress due to unscheduled DNA synthesis. DNA replication represents the most challenging phase of cell cycle, since native single strand DNA is particularly fragile. Furthermore, primary cells show a peculiar sensitivity to high proliferation rate induced by high serum concentration. This suggests that serum-induced hyper-replication could promote genetic instability (Di Micco et al. 2008; Woo et al. 2004). Similarly, oncogene activation in primary cells induce senescence due to unscheduled DNA synthesis and replication stress (Di Micco et al. 2006).

Recently different research groups established the role of a mediator of the DNA damage checkpoint, 53BP1, in marking sites of DNA damage arising from replication stress (Lukas et al. 2011; Harrigan et al. 2011). Thus, following an immunofluorescence-based approach, we looked for evidence of 53BP1 nuclear bodies accumulation in NCOA4 WT and KO cells. As shown in Figure 11, we found an incresead number of 53BP1-foci positive cells as well as an increased number of foci/cell in NCOA4-/- MEFs. These data suggest that increased DDR activation in NCOA4-/- cells could be the consequence of a replication stress.

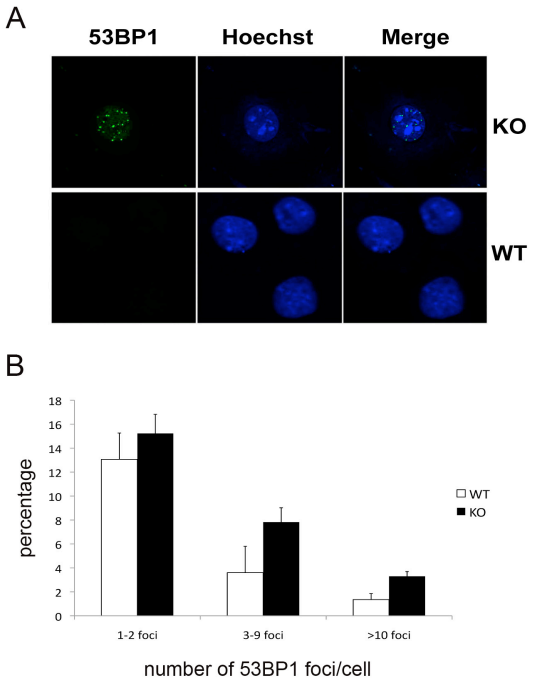

Figure 11: 53BP1 nuclear bodies accumulation in NCOA4-/- cells. (A) Representative immunofluorescence staining of NCOA4-/- and +/+ for 53BP1. (B) Bar-graphs showing the percentage of WT and KO cells with 1-2 ; 3-9 and >10 53BP1 foci/cell ± SD (standard deviation).

Replication stress is not only the consequence of hyper-replication induced by oncogene activation or high serum concentration but can also be caused by agents that perturb the activity of the MCM2-7 helicase complex (cisplatin and mitomycin C) or the processive polymerases (UV irradiation). To investigate the hypothesis that replication stress in NCOA4-/- cells is the consequence of unscheduled origin activation or replication fork dynamics we studied replication forks progression in NCOA4 WT and KO MEFs. First, we studied the sedimentation profile of newly synthesized DNA molecules labelled with ^{3}H-Thimidine. As shown in Figure 12, through an alkaline sucrose gradient assay, we discovered that NCOA4-/- cells accumulate shorter radiolabelled DNA fragments compared to WT cells. The accumulation of shorter replicons in KO cells suggests the presence of fork stalling and increased origin firing.

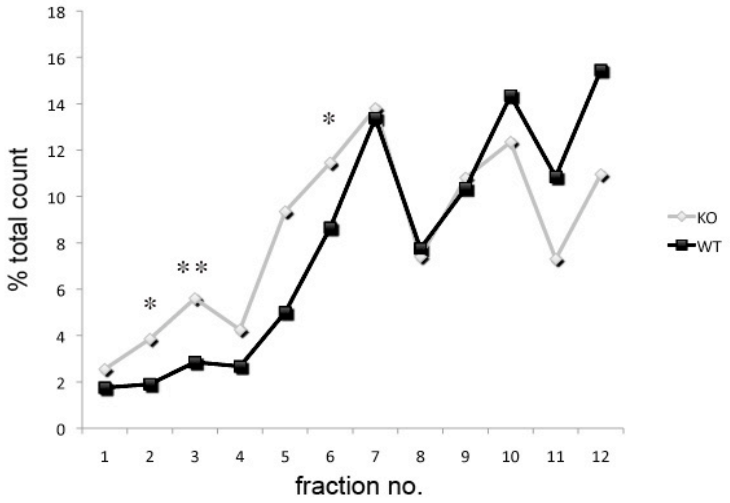

Figure 12: Alkaline sucrose gradient profiles of NCOA4 WT and KO MEFs. (* p< 0.05; ** p< 0.001)

To confirm these data, we took advantage of an immunofluorescence-based approach known as fiber stretching or DNA fiber assay that allows the study of replication fork progression. A detailed explanation of the experimental procedure is described in materials and methods, while a representation of replication fork patterns and the measurable variables is represented in Figure 13.

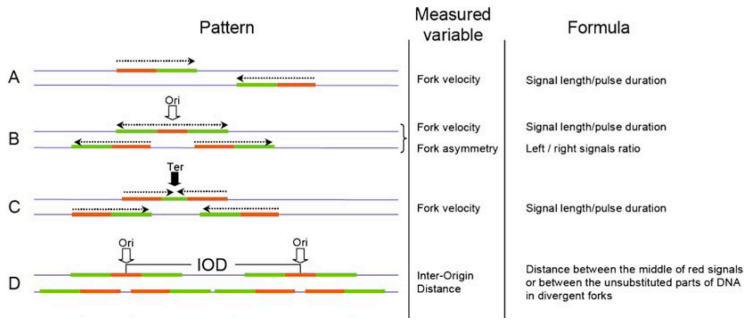

Figure 13: Fiber stretching assay. A representative picture of DNA replication patterns recognized through fiber assay and of the measurable DNA replication parameters.

Briefly, NCOA4 WT and KO cells were pulse-labelled sequentially with CldU and IdU and nucleotides incorporation was followed on DNA fibers by using specific primary and secondary antibodies that allow the detection of CldU and IdU as red and green tracks respectively. Through this approach, we could study the execution of DNA replication and its abnormalities in NCOA4 WT and KO cells. First, to confirm the data obtained with the alkaline sucrose gradient we studied the lenght of newly synthesized DNA. We evaluated more then 200 replication tracks from NCOA4 WT and KO cells and to obtain the fork velocity (a parameter directly dependent on the lenght of the tracks) we divided double tracks (red+green) for pulse duration (40 minutes) to have a distribution of fork velocities in those groups. As show in Figure 14, the distribution of fork velocities between NCOA4-/- and +/+ cells was highly divergent with the first group accumulating slower (and therefore shorter) tracks ($p < 0.0001$).

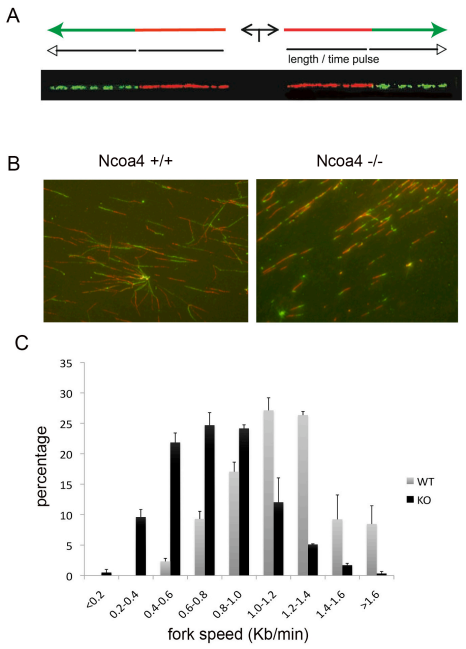

Figure 14: Reduced fork speed in NCOA4-/- cells. (A) Representative image of a replicon observed on a stained DNA fiber after a consecutive pulse labelling with CldU and IdU, detected as red and green tracks respectively. (B) Representative images of replication tracks of NCOA4+/+ and NCOA4-/- MEFs. (C) Bar-graphs showing replication fork speed distribution in NCOA4-/- and NCOA4+/+ cells. The bars represent standard deviations deriving from experiments performed in triplicate.

From each origin, replication forks normally proceed bi-directionally in a symmetric way. Oncogene activation as well as fork perturbation induced by stalling agents (UV, cisplatin) are associated with replication fork asymmetry which is directly correlated with fork stalling. Using the fiber stretching assay we studied the symmetry of anti-directional replicated traits from newly firing DNA replication origins in NCOA4+/+ and -/- MEFs. This can be obtained by the calculation of the ratio between the two arms that move away from the open replication bubble (the green tracks in Figure 15A). As shown in Figure 15 B-C, NCOA4-/- cells accumulate an increased amount of asymmetric replication forks compared to WT cells, suggesting that the absence of NCOA4 induces extensive fork stalling.

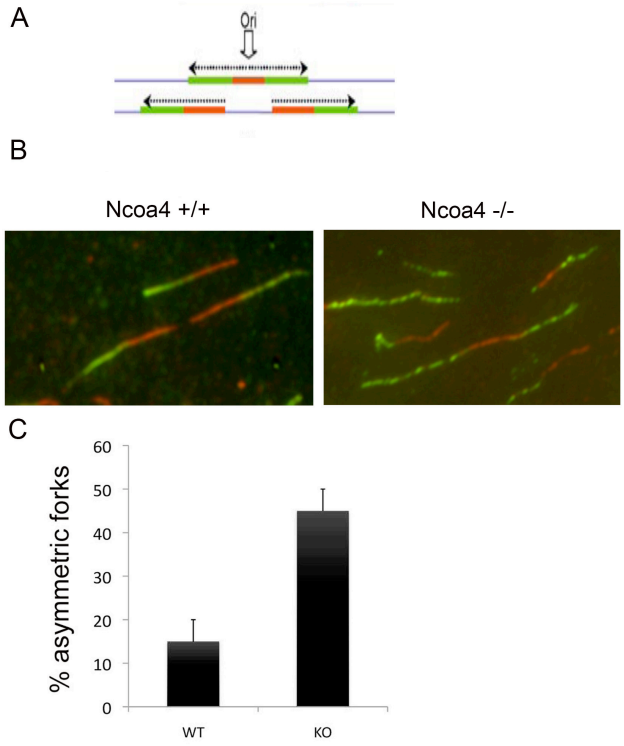

Figure 15: NCOA4 depleted cells accumulate replication fork stalling lesions. (A) Representative images of DNA replication tracks upon pulse labelling with CldU (red) and IdU (green). (B) Representative images of newly firing replication origins in wild type and knock-out cells. (C) Bar-graphs showing the percentages of asymmetric replication forks in NCOA4-/- and +/+ MEFs. The numbers of asymmetrical replication bubbles was divided by the total number of replication bubbles ± SD (standard deviation).

Oncogene activation induces replication stress by activating simultaneously an excessive number of replication origins and therefore inducing fork stalling because of nucleotide depletion. This has been suggested to be a primary source of genomic instability during the initial phases of cancer development (Bester et al. 2011). Furthermore, the stalling of a replication fork prompts the activation of dormant origins to prevent the transmission of unreplicated genomic regions. Therefore, increased origin density and consequently reduced inter-origin distance (IOD) are bona fide indicators of replication stress. By measuring the distance between newly firing origins (IOD), we could detect the density of activated origins in WT and KO cells (Figure 16). We found a reduced IOD in NCOA4 KO compared to WT cells suggesting extensive origin activation in NCOA4 depleted cells ($p < 0.0001$). These data could be explained by an increased activity of replication origin induced by a reduced inhibition of MCM2-7 activity as well as by an increased use of dormant origins activated by fork stalling.

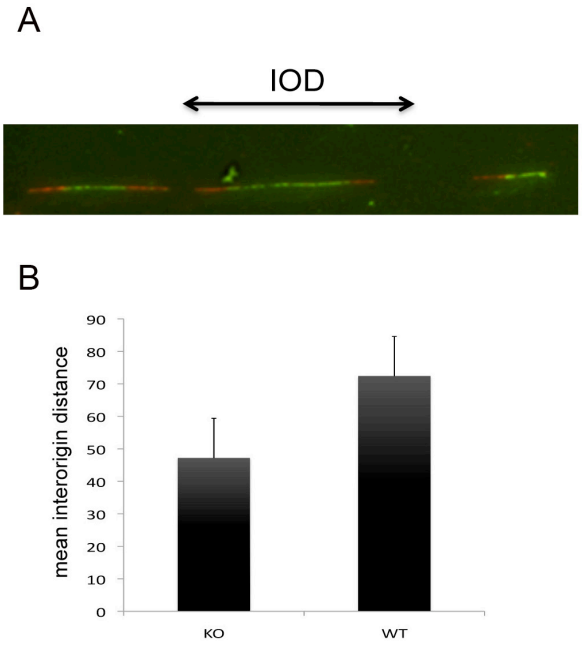

Figure 16: Reduced inter-origin distance in NCOA4-/- cells. (A) Representative image of two adiacent replicons observed on individual DNA fibers. Cldu is detected in red and IdU in green. The distance between the two origins (double arrow) correspond to the interorigin distance. (B) Bar-graphs showing average IOD (inter-origin distance) values in NCOA4 KO and WT MEF ± SD (standard deviation).

All together, these data indicate the failure of NCOA4-/- cells to maintain a normal replication rate.

4.6 NCOA4-/- cells cultured in 3% O_2 concentration are hypersensitive to agents inducing replication stress

Campisi's group recently showed that primary murine cells are highly susceptible to culture stress induced by elevated oxygen concentrations. In particular, MEFs cultured in 3% O_2 do not show evidence of cellular senescence and undergo spontaneous immortalization (Parrinello et al. 2003). However, murine cells grown in the absence of serum are resistant to senescence even if cultured in 20% O_2 concentrations (Loo et al. 1987; Woo & Poon 2004). One of the mechanism responsible for DDR-dependent oncogene-induced senescence (OIS) in primary cells is linked to an increased production of ROS (Reactive oxygen species) (Di Micco et al. 2006). This suggests that growth factors (in high O_2 concentrations) and oncogenes (by increasing ROS production) induce a replication stress that impairs faithful transmission of the genome. The exact contribution exerted by ROS in this process is still unclear. ROS could accelerate replication rate as well as directly damage DNA, increasing the activity of repair systems working in the context of the intra-S-phase checkpoint.

When cultured at 3% O_2 concentrations, NCOA4-/- cells showed a growth rate similiar to WT cells at least for the initial 8-9 passages (data not shown). This discrepancy in the growth rate of NCOA4-/- MEFs when kept at 3% or 20% oxygen concentration could be explained by the efficiency of the cellular DNA repair machineries. One possibility is that DNA repair mechanisms could be sufficient to counteract low levels of DNA damage at low oxygen concentration but not high levels of DNA damage induced by high oxygen concentration. To address this hypothesis, we mimicked a replication stress at 3% O_2, by treating WT and KO cells with agents able to perturb replication fork progression. To this aim, we treated WT and KO cells, grown at 3% O_2, with increasing doses of different DNA damaging agents. To address specifically a role for NCOA4 in preventing replication stress, we used agents known to induce DNA lesions that alter replication fork progression and activate the intra-S-phase checkpoint, such as cisplatin and UV. The former induces the formation of intra-strand and inter-strand crosslinks that alter the progression of the replicative helicase during the unwinding phase of DNA replication, while the latter causes the formation of pyrimidine dimers inducing polymerases to stall. As shown in Figure 17, KO cells showed an increased sensitivity to both

agents compared to WT cells. As a control, we used ionizing radiations that are known to induce prevalently DSBs in a cell cycle-independent manner. NCOA4-/- cells displayed only a moderately increase of sensitivity to IR compared to WT cells. This is not surprising since IR have been shown to induce the formation of replication stalling lesions (Harper et al. 2010). These data suggest that NCOA4 ablation is normally tolerated in the absence of an exogenous stress because of the activation of an intra-S-phase checkpoint that allows the execution of a normal replication program. The addition of a O_2 induced stress, probably by saturating DNA repair machineries, increases the sensitivity of cells to the stress induced by NCOA4 ablation. These data can also be reconciled with the apparent normal phenotype of NCOA4-/- mice, because they show that a genotoxic stress is required to unveil the DNA damage accumulation in cells lacking NCOA4.

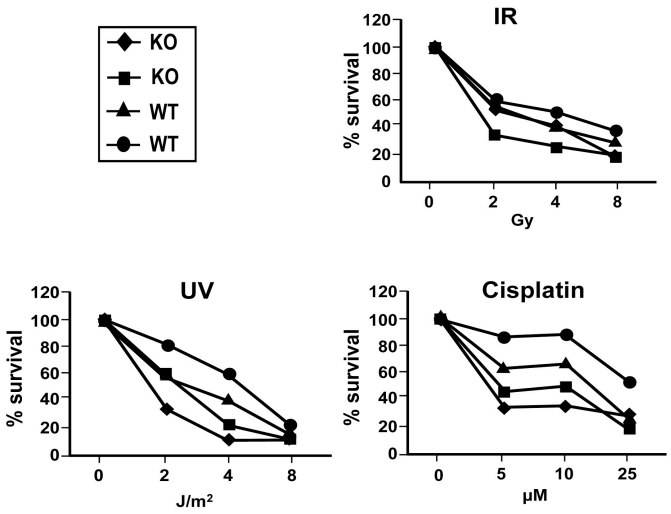

Figure 17: Increased sensitivity of NCOA4-/- cells to S-phase damaging agents. Two WT and KO MEF cell lines where treated with increasing doses of IR, UV or Cisplatin and their survival rate was measured after 48 hours.

5. Discussion

5.1 NCOA4 ablation leads to replication stress and premature senescence in cultured cells.

Maintenance of genome integrity is a primary objective for mammals to allow the transmission of a correct genetic information to progeny and to restrain genetic instability and cancer formation. Several conserved mechanisms have adapted during evolution to deal with damaging forces that affect faithful genome duplication. During replication, DNA is particularly vulnerable because of the generation of unprotected single strand DNA. Thus, DNA replication and oncogene-associated genome instability allows cancer cells to continously rearrange their genome favouring cancer progression, and providing the chance to escape anticancer barriers, such as senescence. Here, we show that NCOA4 is a novel player of the control of genome stability during replication. Indeed, we show that primary murine cells lacking the NCOA4 gene show genetic instability and premature senescence as a consequence of replication stress and DNA damage.

As far as the mechanism of NCOA4-mediated control of DNA replication, our group has recently shown that NCOA4 protein binds to MCM7 protein, a component of the MCM2-7 helicase complex involved in DNA unwinding during replication (Carlomagno et al, personal communication). Through the use of an in vitro model of DNA replication that recapitulates all the step of vertebrate DNA replication, the *Xenopus laevis* egg extracts, our group demonstrated that NCOA4 inhibits DNA replication by hindering the helicase activity of the whole MCM2-7 complex (Carlomagno et al, personal communication). Thus, NCOA4 may be normally required to keep under check MCM2-7 complex activity and NCOA4 ablation may release MCM2-7 control allowing unscheduled DNA replication and replication stress.

Our findings provide strong evidence of the key role played by the control of MCM2-7 activity to maintain genome stability during DNA replication. Accordingly, we show that NCOA4-/- cells accumulate replication stalling lesions that prompts DDR activation and cellular senescence. Two mechanisms, not mutually exclusive, may explain replication stress in NCOA4-/- cells.

On one hand, inappropiate origin firing due to unscheduled MCM2-7 activation may trigger replication stress. Nucleotide depletion induced by increased origin firing and DNA lesions generated by oxidative damage during replication may be the driving forces able to increase number of stalled lesions ultimately leading to a saturation of the intra-S-phase repair mechanisms, DNA damage accumulation and premature senescence.

On the other hand, unchecked MCM2-7 activity by increasing replication fork speed and single strand DNA exposure may lead to fork stalling and increased damage accumulation.

Whatever the mechanism, we show that lack of control of MCM2-7 activity leads to genome instability in mammalian cells. This findings could be important to understand the mechanisms that allow faithful DNA replication and maintenance of genome integrity.

5.2 NCOA4 gene is dispensable for mouse viability and development.

Despite its essential function in regulating MEFs proliferation, NCOA4 appears dispensable for mouse viability and development. It should be noted, however, that mouse targeting studies have shown that many genes that are important for cell cycle progression are dispensable for mice viability (Sherr and Roberts, 2004). Redundancy of mechanisms that control cell cycle progression and in particular DNA replication is a possible explanation for this observation. In the case of NCOA4, our data show that primary mouse cells (MEFs) accumulate DNA damage when grown under stressed conditions produced by a combination of high serum concentration and O_2 pressure (Sherr & DePinho 2000; Parrinello et al. 2003), both conditions absent in mouse tissues. Future work will be required to explore the viability of NCOA4 KO mice upon treatment with genotoxic agents. To this aim we plan to treat NCOA4 WT and KO mice with Ionizing radiation (IR) and increasing doses of cisplatin.

5.3 Role of NCOA4 in RET/PTC-induced tumorigenesis.

In RET/PTC oncogenes, the oncogenic activation of RET is fostered by the presence of coiled-coil domains in RET fusion genes mediating RET TK dimerization, kinase activation and signaling. It should be noted, however, that oncogenic rearrangements involving two genes, such as RET/PTC ones, may follow a "two-hits model" in which the activation of a proto-oncogene (RET) is coupled to the loss-of-function of a tumor suppressor gene (Figure 18). Data shown in this Dissertation, suggest that RET/PTC3 could follow such a two-hits model. Indeed, by leading to genome instability, NCOA4 disruption may determine the loss of a care-taker mechanism, thereby leading to release from genome stability control, DNA damage and genomic instability. We propose that loss of such NCOA4 function may be involved in RET/PTC3 driven oncogenesis in papillary thyroid carcinoma.

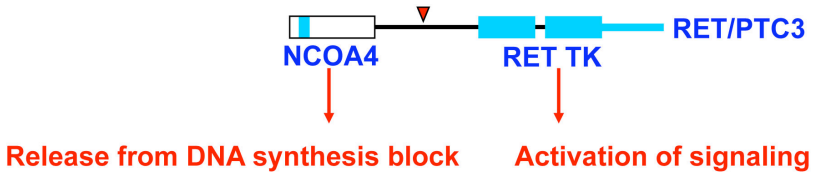

Figure 18: Two-hit model for RET/PTC3 mediated carcinogenesis

6. Conclusions

Here we show that NCOA4-/- cells are prone to accumulate DNA damage and undergo premature senescence as a consequence of the activation of a DNA damage response (DDR). Our previous findings suggested a role for NCOA4 in negatively regulating DNA replication by hindering the activity of the MCM2-7 helicase complex (Carlomagno et al, personal communication). Accordingly, here we show that NCOA4-/- mouse embryo fibroblasts (MEFs) fail to maintain normal replication fork progression, accumulate stalled forks and feature increased origin activation. All together these data suggest that NCOA4 depletion causes unscheduled activation of MCM2-7 function thereby leading to altered replication dynamics and genomic instability. We propose that NCOA4 might be a novel care-taker tumor suppressor involved in genome integrity maintenance. Loss of such funtion may contribute to RET/PTC induced oncogenesis in thyroid carcinoma.

7. Acknowledgements

My study has been carried out at the Dipartimento di Biologia e Patologia cellulare e molecolare "L. Califano", Università degli studi di Napoli "Federico II".
Firstly, I wish to thank Prof. Giancarlo Vecchio, who introduced me to Santoro's lab and always encouraged me in doing research.
I'm deeply grateful to my supervisor Prof. Massimo Santoro for giving me the opportunity to run a challenging and very much interesting project: I hope I've done a good job. His outstanding dedication to research has been a strong example for me during these years and his guidance of fundamental importance for my slow scientific growth.
I wish to thank Maria Domenica Castellone who developed the NCOA4 KO mouse and under whose supervision I started to work in the lab since I was a young medical student. I've been an "unconventional" PhD student but she always allowed me to freely follow my ideas and carry out my thesis experiments. Somehow, in this way she made me do my best.
I also have to thank Annamaria Cirafici for her precious help in organizing mouse work and all the other reaserchers and collegues of Santoro's lab: Drs Giuliana Salvatore, Valentina de Falco, Mikko Laukkanen, Magesh Muthu, Mara Cantisani and Gennaro Di Maro.
I'd like to sincerely thank Prof. Francesca Carlomagno for her support. Her enthusiasm for research and replication has led my last PhD year and her help has been fundamental for the talks I had and the writing of my thesis. Together with her, I thank Francesco Merolla for tecnical suggestions and discussions and all the people of "Lab 11". A special thank go to Salvatore Sequino who took care of my mice for all these years and to BIOGEM facility (Ariano Irpino) for help with the NCOA4 KO mouse generation.
I also wish to truly thank Prof. Anindya Dutta and all the members of his lab for the wonderful time I had in Charlottesville (VA, USA) working in his lab: I will never forget the enthusiasm of those days and the kindness of all of them.
Finally I have to thank my family and Mariacarla for their continous support during these years; without it I wouldn't have been able to go throughout them.

8. References

- Arias EE, Walter JC. PCNA functions as a molecular platform to trigger Cdt1 destruction and prevent re-replication. Nat Cell Biol. 2006 Jan;8(1):84-90.
- Arias EE, Walter JC. Strength in numbers: preventing rereplication via multiple mechanisms in eukaryotic cells. Genes Dev. 2007 Mar 1;21(5):497-518.
- Bartkova J, Horejsí Z, Koed K, Krämer A, Tort F, Zieger K, Guldberg P, Sehested M, Nesland JM, Lukas C, Ørntoft T, Lukas J, Bartek J. DNA damage response as a candidate anti-cancer barrier in early human tumorigenesis. Nature. 2005 Apr 14;434(7035):864-70.
- Bartkova J, Rezaei N, Liontos M, Karakaidos P, Kletsas D, Issaeva N, Vassiliou LV, Kolettas E, Niforou K, Zoumpourlis VC, Takaoka M, Nakagawa H, Tort F, Fugger K, Johansson F, Sehested M, Andersen CL, Dyrskjot L, Ørntoft T, Lukas J, Kittas C, Helleday T, Halazonetis TD, Bartek J, Gorgoulis VG. Oncogene-induced senescence is part of the tumorigenesis barrier imposed by DNA damage checkpoints. Nature. 2006 Nov 30;444(7119):633-7.
- Basolo F, Giannini R, Monaco C, Melillo RM, Carlomagno F, Pancrazi M, Salvatore G, Chiappetta G, Pacini F, Elisei R, Miccoli P, Pinchera A, Fusco A, Santoro M. Potent mitogenicity of the RET/PTC3 oncogene correlates with its prevalence in tall-cell variant of papillary thyroid carcinoma. Am J Pathol. 2002 Jan;160(1):247-54.
- Begum S, Rosenbaum E, Henrique R, Cohen Y, Sidransky D, Westra WH. BRAF mutations in anaplastic thyroid carcinoma: implications for tumor origin, diagnosis and treatment. Mod Pathol. 2004 Nov;17(11):1359-63.
- Bell SP, Dutta A. DNA replication in eukaryotic cells. Annu. Rev. Biochem. 2002; 71: 333-374.
- Bester AC, Roniger M, Oren YS, Im MM, Sarni D, Chaoat M, Bensimon A, Zamir G, Shewach DS, Kerem B. Nucleotide deficiency promotes genomic instability in early stages of cancer development. Cell. 2011 Apr 29;145(3):435-46.
- Blow JJ, Dutta A. Preventing re-replication of chromosomal DNA. Nat Rev Mol Cell Biol. 2005 Jun;6(6):476-86.
- Bongarzone I, Butti MG, Coronelli S, Borrello MG, Santoro M, Mondellini P, Pilotti S, Fusco A, Della Porta G, Pierotti MA. Frequent activation of ret protooncogene by fusion with a new activating gene in papillary thyroid carcinomas. Cancer Res. 1994 Jun 1;54(11):2979-85.
- Bongarzone I, Monzini N, Borrello MG, Carcano C, Ferraresi G, Arighi E, Mondellini P, Della Porta G, Pierotti MA. Molecular characterization of a thyroid tumor-specific transforming sequence formed by the fusion of ret

tyrosine kinase and the regulatory subunit RI alpha of cyclic AMP-dependent protein kinase A. Mol Cell Biol. 1993 Jan; 13(1):358-66.
- Bossis I, Stratakis CA. Minireview: PRKAR1A: normal and abnormal functions. Endocrinology 2004; 145(12):5452-8.
- Braig M, Lee S, Loddenkemper C, Rudolph C, Peters AH, Schlegelberger B, Stein H, Dörken B, Jenuwein T, Schmitt CA. Oncogene-induced senescence as an initial barrier in lymphoma development. Nature. 2005 Aug 4;436(7051):660-5.
- Branzei D, Foiani M. Maintaining genome stability at the replication fork. Nat Rev Mol Cell Biol. 2010 Mar;11(3):208-19.
- Castro P, Rebocho AP, Soares RJ, Magalhaes J, Roque L, Trovisco V, Viera de castro I, Cardoso-de-Oliveira M, Fonseca E, Soares P, Sobrinho-Simoes M. PAX8-PPARgamma rearrangement is frequently detected in the follicular variant of papillary thyroid carcinoma. J Clin Endocrinol Metab. 2006 Jan;91(1):213-20.
- Chang BL, Cramer SD, Wiklund F, Isaacs SD, Stevens VL, Sun J, Smith S, Pruett K, Romero LM, Wiley KE, Kim ST, Zhu Y, Zhang Z, Hsu FC, Turner AR, Adolfsson J, Liu W, Kim JW, Duggan D, Carpten J, Zheng SL, Rodriguez C, Isaacs WB, Grönberg H, Xu J. Fine mapping association study and functional analysis implicate a SNP in MSMB at 10q11 as a causal variant for prostate cancer risk. Hum Mol Genet. 2009 Apr 1;18(7):1368-75.
- Chevalier S, Blow JJ. Cell cycle control of replication initiation in eukaryotes. Curr Opin Cell Biol 1996; 8(6):815-21.
- Chong J, Mahbubani HM, Khoo CY and Blow JJ. Purification of an MCM-containing complex as a component of the DNA replication licensing system. Nature. 1995; 375: 418-421.
- Collado M, Serrano M. Senescence in tumours: evidence from mice and humans. Nat Rev Cancer. 2010 Jan;10(1):51-7.
- d'Adda di Fagagna F. Living on a break: cellular senescence as a DNA-damage response. Nat Rev Cancer. 2008 Jul;8(7):512-22.
- DeLellis RA, Williams ED. Thyroid and parathyroid tumors. In Tumors of Endocrine Organs, World Health Organization Classification of Tumors. DeLellis RA, Lloyd RV, Heitz PUU and Eng C. 2004 (eds), p. 51-56
- DeLellis RA. Pathology and genetics of thyroid carcinoma. J Surg Oncol. 2006 Dec 15;94(8):662-9.
- Delmolino LM, Saha P, Dutta A. Multiple mechanisms regulate subcellular localization of human CDC6. J Biol Chem. 2001 Jul 20;276(29):26947-54.
- Dho SH, Kwon KS. The Ret finger protein induces apoptosis via its RING finger-B box-coiled-coil motif. J Biol Chem. 2003 Aug 22;278(34):31902-8.
- Di Micco R, Cicalese A, Fumagalli M, Dobreva M, Verrecchia A, Pelicci PG, D' adda di Fagagna F. DNA damage response activation in mouse embryonic

fibroblast undergoing replicative senescence adn following spontaneous immortalization. Cell Cycle. 2008 Nov 15;7(22): 3601-6.

- Di Micco R, Fumagalli M, Cicalese A, Piccinin S, Gasparini P, Luise C, Schurra C, Garre' M, Nuciforo PG, Bensimon A, Maestro R, Pelicci PG, d'Adda di Fagagna F. Oncogene-induced senescence is a DNA damage response triggered by DNA hyper-replication. Nature. 2006 Nov 30;444(7119):638-42.
- Dimri GP, Lee X, Basile G, Acosta M, Scott G, Roskelley C, Medrano EE, Linskens M, Rubelj I, Pereira-Smith O, et al. A biomarker that identifies human cells in culture and in aging skin in vivo. Proc Natl Acad Sci USA. 1995 Sep 26;92(20):9363-7.
- Eberhardt NL, Grebe SK, McIver B, Reddi HV. The role of the PAX8/PPARgamma fusion oncogene in the pathogenesis of follicular thyroid cancer. Mol Cell Endocrinol. 2010 May 28;321(1):50-6.
- Elisei R, Ugolini C, Viola D, Lupi C, Biagini A, Giannini R, Romei C, Miccoli O, Pinchera A, Basolo F. BRAF(V600E) mutation and outcome of patients with papillary thyroid carcinoma: a 15-year median follow-up study. J Clin Endocrinol Metab. 2008 Oct;93(10):3943-9
- Elisei R, Cosci B, Romei C, Bottici V, Renzini G, Molinaro E, Agate L, Vivaldi A, Faviana P, Basolo F, Miccoli P, Berti P, Pacini F, Pinchera A. Prognostic significance of somatic RET oncogene mutations in sporadic medullary thyroid cancer: a 10-year follow-up study. J Clin Endocrinol Metab. 2008 Mar;93(3):682-7.
- Falck J, Coates J, Jackson SP. Conserved modes of recruitment of ATM, ATR and DNA-PKcs to sites of DNA damage. Nature. 2005 Mar 31;434(7033):605-11.
- Fu YV, Yardimci H, Long DT, Ho TV, Guainazzi A, Bermudez VP, Hurwitz J, van Oijen A, Schärer OD, Walter JC. Selective bypass of a lagging strand roadblock by the eukaryotic replicative DNA helicase. Cell. 2011 Sep 16;146(6):931-41.
- Fusco A, Grieco M, Santoro M, Berlingieri MT, Pilotti S, Pierotti MA, Della Porta G, Vecchio G. A new oncogene in human thyroid papillary carcinomas and their lymph-nodal metastases. Nature. 1987; 328(6126):170-2.
- García-Rostán G, Camp RL, Herrero A, Carcangiu ML, Rimm DL, Tallini G. Beta-catenin dysregulation in thyroid neoplasms: down-regulation, aberrant nuclear expression, and CTNNB1 exon 3 mutations are markers for aggressive tumor phenotypes and poor prognosis. Am J Pathol. 2001;158:987-96.
- García-Rostán G, Costa AM, Pereira-Castro I, Salvatore G, Hernandez R, Hermsem MJ, Herrero A, Fusco A, Cameselle-Teijeiro J, Santoro M. Mutation of the PIK3CA gene in anaplastic thyroid cancer. Cancer Res. 2005 Nov 15;65(22):10199-207.

- García-Rostán G, Zhao H, Camp RL, Pollan M, Herrero A, Pardo J, Wu R, Carcangiu ML, Costa J, Tallini G. Ras mutations are associated with aggressive tumor phenotypes and poor prognosis in thyroid cancer. J Clin Oncol. 2003 Sep 1;21(17):3226-35.
- Gimm O. Thyroid cancer. Cancer Lett. 2991 Feb 26;163(2):143-56.
- Gorgoulis VG, Vassiliou LV, Karakaidos P, Zacharatos P, Kotsinas A, Liloglou T, Venere M, Ditullio RA Jr, Kastrinakis NG, Levy B, Kletsas D, Yoneta A, Herlyn M, Kittas C, Halazonetis TD. Activation of the DNA damage checkpoint and genomic instability in human precancerous lesions. Nature. 2005 Apr 14;434(7035):907-13.
- Greco A, Mariani C, Miranda C, Lupas A, Pagliardini S, Pomati M, Pierotti MA. The DNA rearrangement that generates the TRK-T3 oncogene involves a novel gene on chromosome 3 whose product has a potential coiled-coil domain. Mol Cell Biol. 1995 Nov;15(11):6118-27.
- Greco A, Mariani C, Miranda C, Pagliardini S, Pierotti MA. Characterization of the NTRK1 genomic region involved in chromosomal rearrangements generating TRK oncogenes. Genomics. 1993 Nov;18(2):397-400.
- Greco A, Miranda C, Pagliardini S, Fusetti L, Bongarzone I, Pierotti MA. Chromosome 1 rearrangements involving the genes TPR and NTRK1 produce structurally different thyroid-specific TRK oncogenes. Genes Chromosomes Cancer. 1997 Jun;19(2):112-23.
- Greco A, Miranda C, Pierotti MA. Rearrangements of NTRK1 gene in papillary thyroid carcinoma. Mol Cell Endocrinol. 2010 May 28;321(1):44-9.
- Grieco M, Santoro M, Berlingieri MT, Melillo RM, Donghi R, Bongarzone I, Pierotti MA, Della Porta G, Fusco A, Vecchio G. PTC is a novel rearranged form of the ret proto-oncogene and is frequently detected in vivo in human thyroid papillary carcinomas. Cell. 1990; 60: 557-563.
- Griffin KJ, Kirschner LS, Matyakhina L, Stergiopoulos S, Robinson-White A, Lenherr S, Weinberg FD, Claflin E, Meoli E, Cho-Chung YS & Stratakis CA. Down-regulation of regulatory subunit type 1A of protein kinase A leads to endocrine and other tumors. Cancer Res. 2004 Dec 15; 64(24):8811–15.
- Halazonetis TD, Gorgoulis VG, Bartek J. An oncogene-induced DNA damage model for cancer development. Science. 2008 Mar 7;319(5868):1352-5.
- Harper JV, Anderson JA, O'Neill P. Radiation induced DNA DSBs: Contribution from stalled replication forks ? DNA Repair (Amst.). 2010 Aug 5;9(8):907-13.
- Harrigan JA, Belotserkovskaya R, Coates J, Dimitrova DS, Polo SE, Bradshaw CR, Fraser P, Jackson SP. Replication stress induces 53BP1-containing OPT domains in G1 cells. J Cell Biol. 2011 Apr 4;193(1):97-108.

- Heinlein CA, Ting HJ, Yeh S, Chang C. Identification of ARA70 as a ligand enhanced coactivator for the peroxisome proliferator-activated receptor gamma. J Biol Chem. 1999; 274: 16147-16152.
- Hu YC, Yeh S, Yeh SD, Sampson ER, Huang J, Li P, Hsu CL, Ting HJ, Lin HK, Wang L, Kim E, Ni J, Chang C. Functional domain and motif analyses of androgen receptor coregulator ARA70 and its differential expression in prostate cancer. J Biol Chem. 2004; 279(32):33438-46.
- Hundahl SA, Fleming ID, Fregen AM, Menck HR. A National Cancer Data Base Report on 53,856 cases of thyroid carcinoma treated in the U.S., 1985-1995. Cancer. 1998 Dec 15;83(12):2638-48.
- Ishimi Y. A DNA helicase activity is associated with an MCM4, -6, and -7 protein complex. J Biol Chem. 1997 Sep 26;272(39):24508-13.
- Jackson SP, Bartek J. The DNA-damage response in human biology and disease. Nature. 2009 Oct 22;461(7267):1071-8.
- Jemal A, Siegel R, Xu J, Ward E. Cancer statistics, 2010. CA Cancer J Clin. 2010 Sep-Oct;60(5):277-300.
- Jin J, Arias EE, Chen J, Harper JW, Walter JC. A family of diverse Cul4-Ddb1-interacting proteins includes Cdt2, which is required for S phase destruction of the replication factor Cdt1. Mol Cell. 2006 Sep 1;23(5):709-21.
- Khetchoumian K, Teletin M, Tisserand J, Mark M, Herquel B, Ignat M, Zucman-Rossi J, Cammas F, Lerouge T, Thibault C, Metzger D, Chambon P, Losson R. Loss of Trim24 (Tif1alpha) gene function confers oncogenic activity to retinoic acid receptor alpha. Nat Genet. 2007 Dec;39(12):1500-6.
- Knauf JA, Sartor MA, Medvedovic M, Lundsmith E, Ryder M, Salzano M, Nikiforov YE, Giordano TJ, Ghossein RA, Fagin JA. Progression of BRAF-induced thyroid cancer is associated with epithelial-mesenchymal transition requiring concomitant MAP kinase and TGF-beta signaling. Oncogene. 2011 Jul 14;30(28):3153-62.
- Kollara A, Kahn HJ, Marks A, Brown TJ. Loss of androgen receptor associated protein 70 (ARA70) expression in a subset of HER2-positive breast cancers.Breast Cancer Res Treat. 2001; 67: 245-53.
- Kondo T, Ezzat S, Asa SL. Pathogenetic mechanisms in thyroid follicular-cell neoplasia. Nat Rev Cancer. 2006;6:292-306.
- Kroll TG, Sarraf P, Pecciarini L, Chen CJ, Mueller E, Spiegelman BM, Fletcher JA. PAX8-PPARgamma1 fusion oncogene in human thyroid carcinoma. Science. 2000;289:1357-60.
- Krude T, Musahl C, Laskey RA, Knippers R. Human replication proteins hCdc21, hCdc46 and P1Mcm3 bind chromatin uniformly before S-phase and are displaced locally during DNA replication. J Cell Sci. 1996; 109 (Pt 2):309-18.
- Kubota Y, Mimura S, Nishimoto SL, Takisawa H and Nojima H. Identification

of the yeast MCM3-related protein as a component of Xenopus DNA replication licensing factor. Cell. 1995; 81: 601-610.
- Lanzino M, De Amicis F, MsPhaul MJ, Marsico S, Panno ML, Andò S. Endogenous coactivator ARA70 interacts with estrogen receptor alpha (ERalpha) and modulates the functional ERalpha/androgen receptor interplay in MCF-7 cells. J Biol Chem. 2005 May 27;280(21):20421-30.
- Leboullex S, Baudin E, Travagli JP, Schlumberger M. Medullary thyroid carcinoma. Clin Endocrinol (Oxf). 2004;61:299-310.
- Leone V, Mansueto G, Pierantoni GM, Tornincasa M, Merolla F, Cerrato A, Santoro M, Grieco M, Scaloni A, Celetti A, Fusco A. CCDC6 represses CREB1 activity by recruiting histone deacetylase 1 and protein phosphatase 1. Oncogene. 2010 Jul 29;29(30):4341-51.
- Li P, Yu X, Ge K, Melamed J, Roeder RG, Wang Z. Heterogeneous expression and functions of androgen receptor co-factors in primary prostate cancer. Am J Pathol. 2002 Oct;161(4):1467-74.
- Li X, Zhao Q, Liao R, Sun P, Wu X. The SCF(Skp2) ubiquitin ligase complex interacts with the human replication licensing factor Cdt1 and regulates Cdt1 degradation. J Biol Chem. 2003 Aug 15;278(33):30854-8.
- Liu Z, Hou P, Ji M, Guan H, Studeman K, Jensen K, Vasko V, El-Naggar AK, Xing M. Highly prevalent genetic alterations in receptor tyrosine kinases and phosphatidylinositol3-kinase/akt and mitogen-activated protein kinase pathways in anaplastic and follicular thyroid cancers. J Clin Endocrinol Metab. 2008 Aug;93(8):3106-16.
- Loo DT, Fuquay JI, Rawson CL, Barnes DW. Extended culture of mouse embryo cells without senescence: inhibition by serum: Science. 1987 Apr 10;236(4798):200-02.
- Lukas C, Savic V, Bekker-Jensen S, Doil C, Neumann B, Pedersen RS, Grøfte M, Chan KL, Hickson ID, Bartek J, Lukas J. 53BP1 nuclear bodies form around DNA lesions generated by mitotic transmission of chromosomes under replication stress. Nat Cell Biol. 2011 Mar;13(3):243-53.
- Lupi C, Giannini R, Ugolini C, Proietti A, Berti P, Minuto M, Materazzi G, Elisei R, Santoro M, Miccoli P, Basolo F. Association of BRAF V600E Mutation with Poor Clinicopathological Outcomes in 500 Consecutives Cases of Papillary Thyroid Carcinoma. J Clin Endocrinol Metab. 2007;92:4085-90.
- Malaguarnera R, Vella V, Vigneri R, Frasca F. p53 family proteins in thyroid cancer. Endocr Relat Cancer. 2007 Mar;14(1):43-60.
- Manie' S, Santoro M, Fusco A, Billaud M. The RET receptor: function in development and dysfuntion in congenital malformation. Trends Genet. 2001;17:580-9.
- Marx SJ. Molecular genetics of multiple endocrine neoplasia types 1 and 2. Nat Rev Cancer. 2005;5(5):367-75.

- Melillo RM, Castellone MD, Guarino V, De falco V, Cirafici AM, Salvatore G, Cauiazzo F, Basolo F, Giannini R, Kruhoffer M, Orntoft T, Fusco A, Santoro M. The RET/PTC-RAS-BRAF linear signalling cascade mediates the motile and mitogenic phenotype of thyroid cancer cells. J Clin Invest. 2005 Apr;115(4):1068-81.
- Merolla F, Pentimalli F, Pacelli R, Vecchio G, Fusco A, Grieco M, Celetti A. Involvement of H4(D10S170) protein in ATM-dependent response to DNA damage. Oncogene. 2007 Sep 13;26(42):6167-75.
- Monaco C, Visconti R, Barone MV, Pierantoni GM, Berlingieri MT, De Lorenzo C, Mineo A, Vecchio G, Fusco A, Santoro M. (2001) The RFG oligomerization domain mediates kinase activation and re-localization of the RET/PTC3 oncoprotein to the plasma membrane. Oncogene 2001; 20: 599-608.
- Moura MM, Cavaco BM, Pinto AE, Leite V. High prevalence of RAS mutations in RET-negative sporadic medullary thyroid carcinomas. J Clin Endocrinol Metab. 2011 May;96(5):E863-8.
- Negrini S, Gorgoulis VG, Halazonetis TD. Genomic instability--an evolving hallmark of cancer. Nat Rev Mol Cell Biol. 2010 Mar;11(3):220-8.
- Nikiforov YE, Rowland JM, Bove KE, Monforte-Munoz H, Fagin JA. Distinct pattern of ret oncogene rearrangements in morphological variants of radiation-induced and sporadic thyroid papillary carcinomas in children. Cancer Res. 1997 May 1;57(9):1690-4.
- Nikiforov YE. Genetic alterations involved in the transition from well-differentiated to poorly differentiated and anaplastic thyroid carcinomas. Endocr Pathol. 2004 Winter;15(4):319-27.
- Nikiforova MN, Kimura ET, Gandhi M, Biddinger PW, Knauf JA, Basolo F, Zhu Z, Giannini R, Salvatore G, Fusco A, Santoro M, Fagin JA, Nikiforov YE. BRAF mutations in thyroid tumors are restricted to papillary carcinomas and anaplastic or poorly differentiated carcinomas arising from papillary carcinomas. J Clin Endocrinol Metab. 2003 Nov;88(11):5399-404.
- Parrinello S, Samper E, Krtolica A, Goldstein J, Melov S, Campisi J. Oxygen sensitivity severely limits the replicative lifespan of murine fibroblasts. Nat Cell Biol. 2003 Aug;5(8):741-7.
- Pasero P, Schwob E. Think global, act local--how to regulate S phase from individual replication origins. Curr Opin Genet Dev. 2000; 10(2):178-86.
- Pierantoni GM, Rinaldo C, Mottolese M, Di Benedetto A, Esposito F, Soddu S, Fusco A. High-mobility group A1 inhibits p53 by cytoplasmic relocalization of its proapoptotic activator HIPK2. J Clin Invest. 2007 Mar;117(3):693-702.
- Pomerantz MM, Shrestha Y, Flavin RJ, Regan MM, Penney KL, Mucci LA, Stampfer MJ, Hunter DJ, Chanock SJ, Schafer EJ, Chan JA, Tabernero J, Baselga J, Richardson AL, Loda M, Oh WK, Kantoff PW, Hahn WC, Freedman

ML. Analysis of the 10q11 cancer risk locus implicates MSMB and NCOA4 in human prostate tumorigenesis. PLoS Genet. 2010 Nov 11;6(11)
- Remus D, Beuron F, Tolun G, Griffith JD, Morris EP, Diffley JF. Concerted loading of Mcm2-7 double hexamers around DNA during DNA replication origin licensing. Cell. 2009 Nov 13;139(4):719-30.
- Ritzi M, Knippers R. Initiation of genome replication: assembly and disassembly of replication-competent chromatin. Gene. 2000; 245(1):13-20.
- Santoro M, Carlomagno F. Drug insight: Small-molecule inhibitors of protein kinases in the treatment of thyroid cancer. Nat Clin Pract Endocrinol Metab. 2006 Jan;2(1):42-52.
- Santoro M, Dathan NA, Berlingieri MT, Bongarzone I, Paulin C, Grieco M, Pierotti MA, Vecchio G, Fusco A. Molecular characterization of RET/PTC3; a novel rearranged version of the RETproto-oncogene in a human thyroid papillary carcinoma. Oncogene. 1994 Feb;9(2):509-16.
- Santoro M, Melillo RM, Carlomagno F, Vecchio G, Fusco A. Minireview: RET: normal and abnormal functions. Endocrinology 2004;145:5448-51
- Schlumberger MJ. Papillary and follicular thyroid carcinoma. N Engl J Med. 1998;338:297-306.
- Schuchardt A, D'Agati V, Larsson-Blomberg L, Costantini F, Pachnis V. Defects in the kidney and enteric nervous system of mice lacking the tyrosine kinase receptor Ret. Nature. 1994; 367(6461): 380-3.
- Sclafani RA. Cdc7p-Dbf4p becomes famous in the cell cycle. J Cell Sci 2000;
- Serrano M, Lin AW, McCurrach ME, Beach D, Lowe SW. Oncogenic ras provokes premature cell senescence associated with accumulation of p53 and p16INK4a. Cell. 1997 Mar 7;88(5):593-602.
- Sherman SI. Thyroid carcinoma. Lancet. 2003;361:501-11.
- Sherr CJ, DePinho RA. Cellular senescence: mitotic clock or culture shock ? Cell. 2000 Aug 18;102(4):407-10.
- Sherr CJ, Roberts JM. Living with or without cyclins and cyclin-dependent kinases. Genes Dev. 2004 Nov 15;18(22):2699-711.
- Smits VA, Reaper PM, Jackson SP. Rapid PIKK-dependent release of Chk1 from chromatin promotes the DNA-damage checkpoint response. Curr Biol. 2006 Jan 24;16(2):150-9.
- Soares P, Trovisco V, Rocha AS, Feijão T, Rebocho AP, Fonseca E, Vieira de Castro I, Cameselle-Teijeiro J, Cardoso-Oliveira M, Sobrinho-Simões M. BRAF mutations typical of papillary thyroid carcinoma are more frequently detected in undifferentiated than in insular and insular-like poorly differentiated carcinomas. Virchows Arch. 2004 Jun;444(6):572-6.
- Stucki M, Clapperton JA, Mohammad D, Yaffe MB, Smerdon SJ, Jackson SP. MDC1 directly binds phosphorylated histone H2AX to regulate cellular

responses to DNA double-strand breaks. Cell. 2005 Dec 29;123(7):1213-26. Erratum in: Cell. 2008 May 2;133(3):549.
- Takahashi M, Ritz J, Cooper GM. Activation of a novel human transforming gene, ret, by DNA rearrangement. Cell. 1985;42:581-588.
- Tanaka T, Knapp D and Nasmyth K. Loading of an MCM protein onto DNA replication origins is regulated by Cdc6p and CDKs. Cell. 1997; 90:649-660.
- Tekur S, Lau KM, Long J, Burnstein K, Ho SM. Expression of RFG/ELE1alpha/ARA70 in normal and malignant prostatic epithelial cell cultures and lines: regulation by methylation and sex steroids. Mol Carcinog. 2001; 30(1):1-13.
- Ugolini C, Giannini R, Lupi C, Salvatore G, Miccoli P, Proietti A, Elisei R, Santoro M, Basolo F. Presence of BRAF V600E in very early stages of papillary thyroid carcinoma. Thyroid. 2007;17:381-8.
- Volante M, Rapa I, Gandhi M, Bussolati G, Giachino D, Papotti M, Nikiforov YE. RAS muations are the predominant molecular alteration in poorly differentiated thuroid carcinoma and bear prognostic impact. J Clin Endocrinol Metab. 2009 dec;94(12):4735-41.
- Wohlschlegel JA, Dwyer BT, Dhar SK, Cvetic C, Walter JC, Dutta A. Inhibition of eukaryotic DNA replication by geminin binding to Cdt1. Science. 2000 Dec 22;290(5500):2309-12.
- Woo RA, Poon RY. Activated oncogenes promote and cooperate with chromosomal instability for neoplastic transformation. Genes Dev. 2004 Jun 1;18(11):1317-30.
- Xing M. Prognostic utility of BRAF mutation in papillary thyroid cancer. Mol Cell Endocrinol. 2010 May 28;321(1):86-93.
- Yan H, Merchant AM, Tye BK. Cell cycle regulated nuclear localization of MCM2 and MCM3, which are required for the initiation of DNA synthesis at chromosomal replication origins in yeast. Genes Dev. 1993; 7: 2149-2160.
- Yeh S, Chang C. Cloning and characterization of a specific coactivator, ARA70, for the androgen receptor in human prostate cells. Proc Natl Acad Sci USA 1996; 93: 5517-5521.
- Zhu Z, Gandhi M, Nikiforova MN, Fisher AH, Nikiforov YE. Molecular profile and clinical-pathologic features of the follicular variant of papillary thyroid carcinoma. An unusually high prevalence prevalence of ras mutations. Am J Clin Pathol. 2003 Jul;120(1):71-7.
- Zou L, Elledge SJ. Sensing DNA damage through ATRIP recognition of RPA-ssDNA complexes. Science. 2003 Jun 6;300(5625):1542-8.

Attached manuscript #II

Bellelli R, Castellone MD, Ugolini C, Nappi TC, Salerno P, Cantisani MC, Basolo F, Garcia-Rostan G, Salvatore G, Santoro M.

FOXM1 is a molecular determinant of the mitogenic and invasive phenotype of anaplastic thyroid carcinoma

<u>Manuscript in preparation</u>

FOXM1 is a molecular determinant of the mitogenic and invasive phenotype of anaplastic thyroid carcinoma

Roberto Bellelli, Maria Domenica Castellone, Clara Ugolini, Tito Claudio Nappi, Paolo Salerno, Maria Carmela Cantisani, Fulvio Basolo, Ginesa Garcia-Rostan, Giuliana Salvatore, Massimo Santoro.

Dipartimento di Biologia e Patologia Cellulare e Molecolare, "L. Califano", Universita' Federico II c/o Istituto di Endocrinologia ed Oncologia Sperimentale "G. Salvatore", C.N.R. Napoli, Italy (RB, MDC, TCN, PS, MS); Department of Surgery, University of Pisa, Pisa-Italy (CU, FB); Institute of Biology and Molecular Genetics ,Valladolid University, Valladolid, Spain (GG-R); Dipartimento di Studi delle Istituzioni e dei Sistemi Territoriali, Università Parthenope, Napoli, Italy (GS).

To whom correspondence should be addressed:

Massimo Santoro, Dipartimento di Biologia e Patologia Cellulare e Molecolare

University of Naples "Federico II", Via Pansini, 5, 80131- Naples, Italy

Telephone: (+39) 081-7463056; Fax: (+39) 081-7463037

Email: masantor@unina.it

Abstract

Anaplastic thyroid carcinoma (ATC) is a very aggressive thyroid cancer. We previously identified an ATC gene expression signature, featuring the overexpression of a set of genes involved in cell cycle progression and mitotic spindle checkpoints. Upregulation of Forkhead box protein M1 (FOXM1) was part of this signature. FOXM1 is a member of the forkhead box family of transcription factors involved in control of cell proliferation, chromosomal stability, angiogenesis and invasion. Here, we show that FOXM1 is overexpressed in ATC compared to normal thyroid, well-differentiated papillary and poorly-differentiated thyroid carcinoma. The FOXM1 isoform predominantly expressed in ATC and ATC-derived cell lines was the FOXM1c splicing variant. Up-regulated FOXM1 expression in human ATC cells was mechanistically linked to loss-of-function of p53 and of FOXO3a, due to the iperactivation of the PI3K-AKT pathway. Knock-down of FOXM1 in ATC cells inibited cell proliferation, arrested cells in G2/M, and reduced invasion through matrigel and cell motility in a wound healing assay. This phenotype was associated to reduced expression of FOXM1 target genes, like cyclin B1, Plk1, Aurora B, Skp2 and uPA. All together these findings suggest that FOXM1 represents an important player in the establishment of the anaplastic phenotype and a potential therapeutic target for this cancer.

Introduction

Anaplastic thyroid carcinoma (ATC) is a rare tumor that accounts for 2% to 5% of all thyroid cancers. ATC ranks among the most lethal solid tumors with a mean survival rate of 4 to 12 months after diagnosis and, though rare, it represents the first cause of death for endocrine neoplasia. ATC usually presents between the 6th and the 7th decade of life as a rapidly enlarging neck mass that extends locally and tends to disseminate to regional nodes and distant sites. Multimodal therapy, including surgery, chemotherapy and radiotherapy does not significally change the natural course of the disease (Kondo et al. 2006; Smallridge et al. 2009).

ATC shares genetic alterations with well-differentiated papillary (PTC) or follicular (FTC) thyroid carcinoma, namely point mutation in RAS and BRAF (Nikiforova et al. 2003; Garcia Rostan et al. 2003). On the other hand, point mutation or gene amplification of PI3K3CA or AKT and loss of PTEN are more frequently found in ATC than well-differentiated carcinomas (Frisk et al. 2002; Garcia-Rostan et al. 2005; Wu et al. 2005; Santarpia et al. 2007; Ricarte-Filho et al. 2009; Saji & Ringel 2010). Accordingly, intercross of transgenic mice expressing oncogenic RAS with PTEN null mice gave rise to highly aggressive ATC (Miller et al. 2009). Moreover, while well differentiated thyroid carcinomas are rarely associated with p53 mutation (less then 10%), the great majority of ATC features p53 mutations (67% to 88%) or disfunction induced by mechanisms such as upregulation of negative p53 regulators like HMGA1, ΔNp73 or HDM2 (Kondo et al. 2006; Pierantoni et al. 2007; Malaguarnera et al. 2007; Smallridge et al. 2009; Nikiforov et al. 2011). Therefore, deregulation of PI3K3CA/AKT and p53 pathways may foster ATC development.

At a variance from well-differentiated thyroid tumors, ATC has a high proliferation rate and a marked aneuploidy (Wreesmann et al. 2002). Recently, we identified a gene expression signature associated with the ATC phenotype, featuring the upregulation of a panel

of genes involved in the G2 and M phases of the cell cycle (Salvatore et al. 2007). This signature overlapped with "proliferation" and “chromosomal instability” signatures which were correlated with mitogenic and aneuploid phenotype of aggressive human cancer types from various tissues (Cartel et al. 2006).

Forkhead box protein M1 (FOXM1) is a member of the forkhead box family of transcription factors (Korver et al. 1997). It promotes cell cycle progression by affecting both the G1/S and the G2/M transitions and it is an important regulator of chromosomal stability (Laoukili et al. 2005). Accordingly, FOXM1 regulates the expression of a large number of G2/M specific genes, such as Cyclin B, Plk1, Nek2 and CENP-F. Interestingly, most of these genes were part of the ATC signature (Salvatore et al. 2007) and one of them, Plk1, was shown to be promising therapeutic target for ATC (Nappi et al. 2009). FOXM1 deletion was associated with mitotic spindle defects and cell death through mitotic catastrophe (Wonsey & Follettie 2005) and compounds targeting FOXM1 transcriptional activity induced apoptosis in cancer cell lines, thereby suggesting it may represent a potential therapeutic cancer target for several cancers (Hegde et al. 2011). FOXM1 has been also shown to regulate the transcription of genes involved in angiogenesis and invasion, thus acting as a master regulator of metastasization (Raychaudhuri & Park 2011). Accordingly, FOXM1 downregulation reduced invasion and migration of pancreatic and breast cancer-derived cell lines (Wang et al. 2007; Ahmad et al. 2010). FOXM1 overexpression has been observed in several human cancers, including basal cell carcinoma (Teh et al. 2002), glioblastoma (Liu et al. 2006) and hepatocellular (Kalinichenko et al. 2004), breast (Wonsey and Follettie 2005), prostate (Kalin et al. 2006) and gastric cancer (Li et al. 2009) and it is often correlated to high proliferative and invasive phenotype and a dismal prognosis.

Recently, Ahmed and co-workers reported that FOXM1 was up-regulated in a fraction (28.4%) of PTC and that chemical or genetic FOXM1 block reduced PTC cell invasiveness

and survival parallel to decreased metalloproteinases (MMP-2 and MMP-9) expression (Ahmed et al. 2011). We reasoned that FOXM1 over-expression could be an important event in fostering the anaplastic phenotype, leading to increased cell proliferation and invasiveness of ATC. Here we show that FOXM1 is upregulated in ATC compared to well-differentiated thyroid tumours and mediates the mitogenic program of ATC cells. We also show that FOXM1 expression in ATC cells is sustained by the PI3K/AKT pathway as well as by the loss-of-function of the p53-p21(CIP1/WAF1)-pRb axis. Finally, FOXM1 knock-down in ATC cells reduced proliferation, survival and invasion of ATC cells. These results suggest that ATC cells remain addicted to FOXM1 and that FOXM1 targeting may represent a strategy for the treatment of ATC.

Materials and methods

Tissue samples and immunohistochemistry. Tumors and normal thyroid tissue samples for immunohistochemical analysis were retrieved from the files of the Pathology Department of the Hospital Central de Asturias (Oviedo University, Asturias, Spain) and of the Hospital Clinico Universitario de Santiago de Compostela (Santiago de Compostela University, Galicia, Spain). Tumors and normal thyroid tissue samples (n.45) for RNA extraction and RT-PCR were retrieved from the files of the Department of Surgery, University of Pisa (Italy). Case selection was based on the histological findings and on the availability of adequate material for RNA extraction. All histological diagnoses were reviewed by two blinded pathologists (G. G-R and C. U) according to the latest recommendations about diagnostic features of PTC, PDC and ATC (Hedinger et al. 1989; DeLellis et al. 2004; Volante et al. 2007). PDC (poorly differentiated carcinomas) were defined as malignant tumors of follicular cells displaying predominant solid/trabecular/insular growth patterns, high grade features such

as mitoses (>3-5 mitoses x 10 HPF) and/or necrosis and convoluted nuclei, with or without concurrent differentiated components of the follicular or papillary type. ATC (anaplastic thyroid carcinomas) were defined as tumors displaying admixtures of spindle, pleomorphic giant, and epithelioid cells, high mitotic activity, extensive coagulative necrosis with irregular borders, and infiltration of vascular walls often accompanied by obliteration of the vascular lumina. Processing of samples and of patient information proceeded in agreement with review board approved protocols. Formalin-fixed and paraffin-embedded 3–5-μm thick tumor sections were deparaffinized, placed in a solution of absolute methanol and 0.3% hydrogen peroxide for 30 min, and treated with blocking serum for 20 min. The slides were incubated with rabbit polyclonal anti-FOXM1 antibody (H-300, Santa Cruz Biotechnology, USA) and processed according to standard procedures. Negative controls by omitting the primary antibody were included. Cases were scored as positive when unequivocal brown staining was observed in the nuclei of tumor cells. Immunoreactivity was expressed as the percentage of positively stained target cells in four intensity categories [-, no staining; +, low/weak; ++ moderate/distinct; +++, high/ intense]. Score values were independently assigned by two blinded investigators (FB and CU) and a consensus was reached on all scores used for computation.

RNA extraction and reverse transcription-PCR. Total RNA was isolated with the RNeasy Kit (Qiagen, Crawley, West Sussex, UK). The quality of the RNAs was verified by the 2100 Bioanalyzer (Agilent Technologies, Waldbronn, Germany); only samples with RNA integrity number (RIN) value > 7 were used for further analysis. One µg of RNA from each sample was reverse-transcribed with the QuantiTect® Reverse Transcription (Qiagen). For quantitative RT-PCR, primers pairs and PCR conditions are available upon request. PCR reactions were done in triplicate and fold changes were calculated with the formula: $2^{-(\text{sample } 1}$

$^{\Delta Ct - sample\ 2\ \Delta Ct)}$, where ΔCt is the difference between the amplification fluorescent threshold of the mRNA of interest and the mRNA of the β-actin used as an internal reference. Semiquantitative RT-PCR was performed to detect the specific FOXM1 splicing isoforms. The following primers were used:

Fox-F2 (5'-GCGACTCTCGAGCATGGAGAATTGTCACCTG-3') and Fox-R2, (5'-GCGCTACTCGAGTTCGGTTTTGATGGT-3'), encompassing A1 exon;

Fox-F3 (5'-GGGCGCACGGCGGAAGATGAA-3') and Fox-R3 (5'-CCACTCTTCCAAGGAGGGCTC-3'), encompassing A2 exon.

Semiquantitative RT-PCR was applied to study FOXM1 target genes, as follows:

Plk1-F: 5'-ATCACCTGCCTGACCATTCCACCAAGG-3';

Plk1-R: 5'-AATTGCGGAAATATTTAAGGAGGGTGATCT-3' (annealing temperature: 60°C);

cyclin B1-F: 5'-AAGGCGAAGATCAACATGGC-3';

cyclin B1-R: 5'-AGTCACCAATTTCTGGAGGG-3' (annealing temperature: 56°C);

aurora B-F: 5'-CCTATCGCCGCATCGTCAAG-3' ;

aurora B-R: 5'-GCAGCACCCTCCGAGAGTTG-3' (annealing temperature: 60°C);

Skp2-F: 5'-AGAGGTGGTATCGCCTAGCGTCT-3';

Skp2-R: 5'-AGGGTACCATCTGGCACGATTCCA-3' (annealing temperature: 56°C);

uPA-F: 5'-AGCGACTCCAAAGGCAGCAATGA-3';

uPA-R: 5'-AGGGTCGCCTCCGGTTGTCT-3' (annealing temperature: 56°C)

Cell cultures. P5 3N cells were provided by F. Curcio (Università di Udine, Udine, Italia) in 2003. 8505C and CAL62 cells were purchased from DSMZ (Deutsche Sammlung von Mikroorganismen und Zellkulturen GmbH, Braunschweig, Germany) in 2006. SW1736 and HTH74 cells were obtained from N.E. Heldin (University Hospital, Uppsala, Sweden) in

2005. OCUT-1, TTA1 and ACT-1 cells were provided by N. Onoda (Osaka University of Medicine, Osaka, Japan) in 2005. All the cells were DNA profiled by short tandem repeat analysis and shown to be unique and identical to those reported in Schweppe *et al*., 2008 (Schweppe et al. 2008). P5 3N were grown as previously described (Curcio et al. 1994). The thyroid cancer cell lines were grown in Dulbecco's modified Eagle's medium (DMEM) (Invitrogen, Groningen, The Netherlands) containing 10% fetal bovine serum. LY294002 was from Calbiochem (Merck Chemicals Ltd. Nottingham UK) and used at 10 μM final concentration. MEK inhibitor PD98059 was from Cell Signaling and used at 50 μM final concentration.

Protein studies. Protein extraction and immunoblotting was carried out according to standard procedures. Anti-FOXM1 antibody (H-300) was from Santa Cruz Biotechnology; monoclonal anti alfa-tubulin was form Sigma-Aldrich (St Louis, MO). Secondary anti-mouse and anti-rabbit antibodies coupled to horseradish peroxidase were from Santa Cruz Biotechnology.

Plasmids, siRNA and transfection. FOXM1 siRNA smart pool was purchased from Dharmacon (Lafayette, CO, USA). The siCONTROL Non-targeting Pool (#D-001206-13-05) was used as a negative control. Cells were transfected with 100 nM siRNA using Dharmafect 3 siRNA reagent following manufacturer's instructions. The HA-FOXM1b plasmid was purchased from Origene Technologies (Rockville, MD); HA-FOXM1c was a kind gift of Dr. KM Yao (University of Hong Kong).

Invasion Assay. *In vitro* invasiveness through Matrigel was assayed using transwell cell culture chambers. Briefly, 8505c confluent cell monolayers were harvested with trypsin/EDTA and centrifuged at 800X*g* for 10 min. The cell suspension ($1X10^5$ cells/well)

was added to the upper chamber of transwells on pre-hydrated polycarbonate membrane filter of 8 μM pore size (Costar, Cambridge, MA, USA) coated with 35μg Matrigel (BD Biosciences). The lower chamber was filled with complete medium. Cell dishes were incubated at 37 °C in 5% CO_2 and 95% air for 24 h. Non-migrating cells on the upper side of the filter were wiped off and migrating cells on the reverse side of the filter were stained with 0.1% crystal violet in 20% methanol for 15 min, counted and photographed. Each experiment was repeated three times.

Wound healing assay. For wound healing assays, 8505c cells were grown up to 80% confluency; a wound of approximately 300 μm width was inflicted to the cell monolayer with a sterile pipette tip. The culture medium was changed to remove nonadherent cells. The progress of wound closure (healing) was monitored with microphotographs of ×10 magnification taken with the Leica DM IL light microscope (Leica Microsystems, Wetzlar, Germany) immediately and 24 hours after the wound. The experiment was repeated three times.

Luciferase assays. Cells were transfected with 500 ng of the reporter plasmid DNA (6XCDX2), together with (when required) p53 wild type, p21 (CIP1/WAF1), E2F4 (kindly donated by M. Crescenzi, Istituto Superiore di Sanità, Rome), AKT-K178M and FOXO-3a by using LipofectAMINE reagent (Invitrogen, Groningen, The Netherlands) according to manufacturer's instructions. A plasmid expressing the enzyme Renilla luciferase (pRL-null) was used as internal control. In all cases, the total amount of transfected plasmid DNA was normalized by adding empty vector DNA. Forty-eight hours after transfection, Firefly and renilla luciferase activity were assayed using the Dual-Luciferase Reporter System (Promega

Corporation), and the Lumat LB9507 luminometer (EG Berthold). Each experiment was done in triplicate.

Statistical analysis. The two-tailed unpaired Student's t test was used for statistical analysis. All P values were two sided and differences were significant when P was less then 0.05. All statistical analysis were carried out using the GraphPad Instat software program (version 3.06.3).

Results

Increased FOXM1 expression in ATC and ATC-derived cell lines. We studied the expression of FOXM1 in normal thyroids and thyroid carcinomas by immunostaining a set of 35 normal thyroids, 51 PTC, 246 PDC and 113 ATC samples. Nuclear positivity was classified as low (+), medium (++) and high (+++), based on the percentages of nuclear positive cells. Results are reported in Table 1 and representative pictures are shown in Fig. 1. FOXM1 was not detectable in normal thyroid cells; consistent with a previous report (Ahmed et al. 2011) 25.4% of PTC and 30.8% PDC show weak/moderate stain. Noteworthy, FOXM1 nuclear expression was strongly increased in ATC (compared to both PTC and PDC: $p < 0.001$), with 42.2% of the samples scoring weak/moderate and 22% showing an intense stain (Table 1).

We performed qRT-PCR analysis on RNA extracted from normal thyroids, PTC and ATC samples (15 each) to verify whether FOXM1 up-regulation was at the RNA level. FOXM1 mRNA expression was significantly higher in ATC samples compared to normal thyroid ($p < 0.001$) and PTCs ($p < 0.001$) (Fig. 2A).

FOXM1 gene is located on chromosome 12p13.3 and it consists of nine exons, two of which (A1 and A2) are alternatively spliced giving rise to three differentially espressed isoforms: FOXM1a (containing both A1 and A2 exons), FOXM1c (containing only A1) and FOXM1b (lacking both A1 and A2) (Fig. 2B). Only FOXM1b and FOXM1c are active as transcription factors, because of the lack of the inhibitory sequence encoded by exon A2 which renders FOXM1a variant transcriptionally inactive and endowed with dominant negative effects (Ye et al. 1997). We applied RT-PCR and primers designed to amplify the regions containing A1 and A2 exons, generating large or small PCR fragments depending on the presence or not of the targeted exon, to address the relative expression of the three isoforms in normal and tumour thyroid tissues (9 samples for each category). FOXM1b and

FOXM1c plasmids were used to generate PCR products as molecular weight controls. ATC samples predominantly expressed FOXM1c (Fig. 2C). Noteworthy, FOXM1c was reported to be the FOXM1 variant that more strongly triggers proliferation and invasion of cancer cells (Kim et al. 2006).

Deregulation of the p53/p21/E2F and PI3K/AKT/FOXO axis promote FOXM1 overexpression in ATC cells. We investigated the mRNA and the protein levels of FOXM1 in a panel of ATC cell lines. A primary culture of normal thyrocytes, P5-4N, was used as control. ATC cell lines expressed high levels of FOXM1 mRNA (Fig. 3A) and protein (Fig. 3B) as compared to normal cells. As for tissue samples, ATC cell lines expressed FOXM1c isoform (Fig. 3A).

Then, we asked which ATC-associated molecular pathways may trigger FOXM1 up-regulation. FOXM1 has been recently identified as a target of p53-mediated repression, secondary to p21CIP1/WAF1-mediated pRb de-phosphorylation and E2F transcription factor down-regulation (Barsotti & Prives 2009; Pandit et al. 2009). This event is critical for the maintenance of a stable G2 arrest in response to DNA damage. To address whether in ATC cells FOXM1 overexpression depend on p53 loss-of-function, we transfected two ATC-derived cell lines, 8505C and HTH74, with plasmids coding for p53 wildtype, p21(CIP1/WAF1) and E2F4 (a negative regulator of the E2F family) together with a firefly luciferase reporter to monitor FOXM1 transcriptional acivity (6XCDX2) (Kim et al. 2006). As shown in Fig. 4A, adoptive overexpression of p53 wt, p21(CIP1/WAF1) and E2F4 decreased FOXM1 activity, compared to cells transfected with the empty vector ($p<0.001$). Consistently, FOXM1 mRNA levels as measured by qRT-PCR were reduced in p53 wt-, p21(CIP1/WAF1)- and E2F4-transfected cells (Fig. 4B). These findings suggest that p53 loss is a molecular event driving the high FOXM1 transcription levels in ATC, this eventually

unleashing cell cycle progression (see below) from the cell cycle checkpoints and thus facilitating chromosomal instability, a common feature of ATC.

The phosphatidylinositol-3-kinase (PI3K)/AKT pathway is a key regulator of proliferation, apoptosis and motility and is hyperactivated in several cancer types. Thyroid cancer features constitutive activation of the PI3K/AKT pathway due to PI3K3CA amplification or mutation, AKT mutation or PTEN downregulation (Saji & Ringel 2010). These genetic lesions are more prevalent in ATC than in well-differentiated thyroid lesions suggesting a role for PI3K/AKT pathway in the progression of thyroid malignancies (Saji & Ringel 2010). FOXO3a transcription factor is negatively controlled by AKT and, in turn, FOXM1 expression has been reported to be negatively regulated by FOXO3a in breast cancer (McGovern et al. 2009). Thus, we hypothesized that the PI3K/AKT/FOXO3a pathway may influence FOXM1 expression in ATC. To address this possibility, we transfected ATC cells with plasmids coding for dominant negative AKT mutant (K178M) or FOXO3a together with the FOXM1 activity reporter. AKT(K178M) and FOXO3a transfection strongly reduced FOXM1 activity in ATC cells (Fig. 4A). Same results were obtained by treatment with the chemical PI3K inhibitor, LY294002. LY294002 also reduced FOXM1 expression levels (Fig. 4B). Importantly, chemical blockade of the MAPK pathway by the MEK inhibitor PD98059 did not recapitulate this event, suggesting that FOXM1 up-regulation is specifically sustained by the activation of the PI3K/AKT pathway in ATC (Fig. 4).

Down-regulation of FOXM1 expression by siRNA inhibited ATC cell growth and in vitro invasion. We knocked down FOXM1 expression by siRNA in 8505C and HTH74 and monitored cell counts in triplicate at 48 hours. FOXM1 siRNA but not scrambled control caused growth inhibition in both the cell lines tested ($P<0.001$) (Fig. 5A), parallel to FOXM1 mRNA knock-down (see below Fig. 5D).

ATC features a higly invasive and metastatic phenotype. FOXM1 promotes the transcription of genes involved in extracellular matrix degradation and motility, thereby acting as a master regulator of metastasization (Raychaudhuri & Park 2011). Thus, we monitored cell motility (wound closure assay) and invasion (transwell chamber assay) upon FOXM1 knock-down. FOXM1 depletion significantly impaired the capability of ATC cells to close the wound ($p < 0.001$) (Fig. 5B) and to invade through Matrigel ($p < 0.001$) (Fig. 5C) when compared to the scrambled control.

Finally, we tested whether pro-mitogenic and –invasive effects of FOXM1 were mediated by the transcriptional program induced by FOXM1. Indeed, transcriptional effects of FOXM1 includes up-regulation of genes involved in cell proliferation and invasion (Laoukili et al. 2005). As shown in Fig 5D, FOXM1 downregulation in ATC cells blunted the expression of mRNAs related to cell-cycle (Skp2, cyclin B1, aurora B, and Plk1) as well as invasion (UPA). Noteworthy, some of these FOXM1 targets have been previously reported to be up-regulated in ATC (Ito et al. 2002; Chiappetta et al. 2007; Sorrentino et al. 2005; Wiseman et al. 2007; Nappi et al. 2009).

Discussion

At a variance from well differentiated thyroid carcinoma that is treatable with surgery and radioactive iodine ablation, ATC is one of the most aggressive human malignancies and it represents the first cause of death for thyroid cancer. Our understanding of the molecular mechanisms leading to the highly aggressive mitogenic and invasive ATC phenotype is still very limited (Smallridge et al. 2009). FOXM1 oncogenic factor is a master regulator of a transcriptional program including genes mediating cell proliferation, motility, invasion and metastasization and it was indeed included in the set of genes upregulated in ATC identified through our previous gene expression profile screening (Salvatore et al. 2007). This prompted us to explore FOXM1 function in ATC.

In this study, we show that FOXM1 expression is strongly upregulated in ATC. FOXM1 overexpression in ATC tissue samples and cell lines was detected at the protein as well as at the mRNA levels suggesting increased transcription as the main mechanism responsible for its overexpresssion. Recently, FOXM1 expression has been reported to be negatively controlled by p53 and FOXO3a anti-oncogenic transcriptional factors (Barsotti & Prives 2009; Pandit et al. 2009; McGovern et al. 2009). In turn, impaired activity of both these tumor-suppressors is part of the molecular features of ATC, that indeed include p53 loss-of-function, in turn releasing E2F factors from the negative control exerted by the p21(CIP1/WAF1)/pRb axis, as well as PI3K3CA/AKT gain-of-function mutations, in turn mediating a phosphorylation-dependent FOXO3a block (Smallridge 2009; Saji & Ringel 2010). Accordingly, here we show that release from these negative constraints contributes to FOXM1 up-regulation in ATC cells (Fig. 6). Importantly, we show that this pathway is amenable of therapeutic targeting by PI3K chemical inhibitors, drugs that have been recently

proposed as potential therapeutic tools in preclinical models of thyroid cancer (Liu et al. 2011a; Liu et al. 2011b; Xing et al. 2010; Jin et al. 2011; Jin et al. 2009).

We found that FOXM1c was the main splicing variant strongly upregulated in ATC and FOXM1c has been reported to be the isoform endowed with more potent mitogenic and pro-invasive effects (Kim et al. 2006). Finally, by applying RNAi, we show that ATC cells depend on FOXM1 expression for both proliferation and *in vitro* motility and invasion. Mechanistically, FOXM1 ablation downregulated the expression of a set of genes that in turn are candidate mediators of these functions. These findings support a model whereby FOXM1 up-regulation may contribute to the locally invasive, metastatic and mitogenic phenotype of ATC; in turn, release of ATC cells from the normal cell cycle checkpoints may also contribute to the chromosomal instability that characterizes this cancer (Fig. 6).

Our data represent an extension of the findings recently reported by Ahmed and colleagues (2011), who, studying differentiated thyroid carcinomas, demonstrated that FOXM1 was upregulated in a fraction (28.4%) of PTC and correlated with aggressive PTC variants (tall-cell) and expression of molecular markers of invasiveness, such as different metalloproteases. Overall it is feasible that FOXM1 is a mediator of thyroid cancer aggressiveness and therefore involved in most ATC as well as in that fraction of differentiated carcinomas featuring an aggressive behaviour. More importantly, Ahmed and collegues proved that a natural compound, thiostrepton, that reduces FOXM1 transcriptional activity and protein level (Radhakrishnan et al 2006; Kwok et al 2008) impair thyroid cancer cell growth and invasion. All together, these findings suggest that FOXM1 is a molecular determinant of thyroid cancer malignant phenotype and may be exploited as a molecular marker of aggressiveness as well as a molecular target in approaches aimed at inhibiting directly its transcriptional activity or indirectly the pathways sustaining its expression (Fig. 6).

Acknowledgements

We thank F. Curcio for the P5 cells, K.M. Yao for the FOXM1c-HA plasmid, M. Crescenzi for E2F4, and R.H. Costa for the 6XCDX2 reporter plasmid. We thank N.E. Heldin and N. Onoda for providing ATC cells and J. Cameselle-Teijeiro, A. Herrero and M. Fresno – Forcelledo for providing human ATC samples. This study was supported by the Associazione Italiana per la Ricerca sul Cancro (AIRC), the Ministero dell'Università e della Ricerca (MIUR), and by the grant MERIT of MIUR.

References

- Ahmad A, Wang Z, Kong D, Ali S, Li Y, Banerjee S, Ali R, Sarkar FH. FoxM1 down-regulation leads to inhibition of proliferation, migration and invasion of breast cancer cells through modulation of extra-cellular matrix degrading factors. Breast cancer Res Treat. 2010 Jul;122(2):337-46.
- Ahmed M, Uddin S, Hussain AR, Alyan A, Jehan Z, Al-Dayel F, Al-Nuaim A, Al-Sobhi S, Amin T, Bavi P, Al-Kuraya KS. FoxM1 and Its Association with Matrix Metalloproteinases (MMP) Signaling Pathway in Papillary Thyroid Carcinoma. J Clin Endocrinol Metab. 2011 Nov 2.
- Barsotti AM, Prives C. Pro-proliferative FoxM1 is a target of p53-mediated repression. Oncogene. 2009 Dec 3;28(48):4295-305.
- Brunet A, Bonni A, Zigmond MJ, Lin MZ, Juo P, Hu LS, Anderson MJ, Arden KC, Blenis J, Greenberg ME. Akt promotes cell survival by phosphorylating and inhibiting a Forkhead transcription factor. Cell. 1999;96:857-868.
- Cartel SL, Eklund AC, Kohane IS, Harris LN, Szallasi Z. A signature of chromosomal instability inferred from gene expression profiles predicts clinical outcome in multiple human cancers. Nat Genet. 2006 Seo;38(9):1043-8.
- Chiappetta G, De Marco C, Quintiero A, Califano D, Gherardi S, Malanga D, Scrima M, Montero-Conde C, Cito L, Monaco M, Motti ML, Pasquinelli R, Agosti V, Robledo M, Fusco A, Viglietto G. Overexpression of the S-phase kinase-associated protein 2 in thyroid cancer. Endocr Relat Cancer. 2007 Jun;14(2):405-20.
- Curcio F, Ambesi-Impiombato FS, Perrella G, Coon HG. Long-term culture and functional characterization of follicular cells form adult normal human thyroids. Proc Natl Acad sci USA. 1994 Sep 13;91(19):9004-8.

- Frisk T, Foukakis T, Dwight T, Lundberg J, Höög A, Wallin G, Eng C, Zedenius J, Larsson C. Silencing of the PTEN tumor-suppressor gene in anaplastic thyroid cancer. Genes Chromosomes Cancer. 2002 Sep;35(1):74-80
- Garcia-Rostan G, Costa AM, Pereira-Castro I, Salvatore G, Hernandez R, Hermsem MJ, Herrero A, Fusco A, Cameselle-Teijeiro J, Santoro M. Mutation of the PI3K3CA gene in anaplastic thyroid carcinoma. Cancer Res. 2005;15:10199-207.
- Garcia-Rostan G, Zhao H, Camp RL, Pollan M, Herrero A, Pardo J, Wu R, Carcangiu ML, Costa J, Tallini G. ras mutations are associated with aggressive tumor phenotypes and poor prognosis in thyroid cancer. J Clin Oncol. 2003 Sep 1;21(17):3226-35.
- Hedinger C, Williams ED, Sobin LH. The WHO histological classification of thyroid tumors: a commentary on the second edition. Cancer 1989;63:908-11.
- Hegde NS, Sanders DA, Rodrigez R, Balasubramanian S. The transcription factor FOXM1 is a cellular target of the natural product thiostrepton. Nat Chem. 2011 Aug 2;3(9): 725-31.
- Ito Y, Yoshida H, Nakano K, Takamura Y, Kobayashi K, Yokozawa T, Matsuzuka F, Matsuura N, Kuma K, Miyauchi A. Expression of G2-M modulators in thyroid neoplasms: correlation of cyclin A, B1 and cdc2 with differentiation. Pathol Res Pract. 2002;198(6):397-402.
- Jin N, Jiang T, Rosen DM, Nelkin BD, Ball DW. Dual inhibition of mitogen-activated protein kinase kinase and mammalian target of rapamycin in differentiated and anaplastic thyroid cancer. J Clin Endocrinol Metab. 2009 Oct;94(10):4107-12.
- Jin N, Jiang T, Rosen DM, Nelkin BD, Ball DW. Synergistic action of a RAF inhibitor and a dual PI3K/mTOR inhibitor in thyroid cancer. Clin Cancer Res. 2011 Oct 15;17(20):6482-9.

- Kalin TV, Wang IC, Ackerson TJ, Major ML, Detrisac CJ, Kalinichenko VV, Lyubimov A, Costa RH. Increased levels of the FoxM1 transcription factor accelerate development and progression of prostate carcinomas in both TRAMP and LADY transgenic mice. Cancer Res. 2006 Feb 1;66(3):1712-20.
- Kalinichenko VV, Major ML, Wang X, Petrovic V, Kuechle J, Yoder HM, Dennewitz MB, Shin B, Datta A, Raychaudhuri P, Costa RH. Foxm1b transcription factor is essential for development of hepatocellular carcinomas and is negatively regulated by the p19ARF tumor suppressor. Genes Dev. 2004 Apr 1;18(7):830-50.
- Kim IM, Ackerson T, Ramakrishna S, Tretiakova M, Wang IC, Kalin TV, Major ML, Gusarova GA, Yoder HM, Costa RH, Kalinichenko VV. The Forkhead Box m1 transcription factor stimulates the proliferation of tumor cells during development of lung cancer. Cancer Res. 2006 Feb 15;66(4):2153-61.
- Kondo T, Ezzat S, Asa SL. Pathogenetic mechanisms in thyroid follicular-cell neoplasia. Nat Review Cancer. 2006;6:292-306.
- Korver W, Roose J, Clevers H. The winged-helix transcription factor Trident is expressed in cycling cells. Nucleic Acid Research. 1997;25:1715-9.
- Kwok JM, Myatt SS, Marson CM, Coombes RC, Constantinidou D, Lam EW. Thiostrepton selectively targets breast cancer cells through inhibition of FOXM1 expression. Mol Cancer Ther. 2008;7:2022-32.
- Laoukili J, Kooistra MR, Bràs A, Kauw J, Kerkhoven RM, Morrison A, Clevers H, Medema RH. FoxM1 is required for execution of the mitotic programme and chromosomal stability. Nat Cell Biol. 2005 Feb;7(2) :126-36.
- Li Q, Zhang N, Jia Z, Le X, Dai B, Wei D, Huang S, Tan D, Xie K. Critical role and regulation of transcription factor FoxM1 in human gastric cancer angiogenesis and progression. Cancer Res. 2009 Apr 15;69(8):3501-9.

- Liu M, Dai B, Kang SH, Ban K, Huang FJ, Lang FF, Aldape KD, Xie TX, Pelloski CE, Xie K, Sawaya R, Huang S. FoxM1B is overexpressed in human glioblastomas and critically regulates the tumorigenicity of glioma cells. Cancer Res. 2006 Apr 1;66(7):3593-602.
- Liu R, Liu D, Trink E, Bojdani E, Ning G, Xing M. The Akt-specific inhibitor MK2206 selectively inhibits thyroid cancer cells harboring mutations that can activate the PI3K/Akt pathway. J Clin Endocrinol Metab. 2011 Apr;96(4):E577-85.
- Liu R, Liu D, Xing M. The Akt Inhibitor MK2206 Synergizes, but Perifosine Antagonizes, the BRAFV600E Inhibitor PLX4032 and the MEK1/2 Inhibitor AZD6244 in the Inhibition of Thyroid Cancer Cells. J Clin Endocrinol Metab. 2011 Nov 16
- Malaguarnera R, Vella V, Vigneri R, Frasca F. p53 family proteins in thyroid cancer. Endocr Relat Cancer. 2007 Mar;14(1):43-60.
- McGovern UB, Francis RE, Peck B, Guest SK, Wang J, Myatt SS, Krol J, Kwok JM, Polychronis A, Coombes RC, Lam EW. Gefitinib (Iressa) represses FOXM1 expression via FOXO3a in breast cancer. Mol Cancer Ther. 2009 Mar;8(3):582-91.
- Miller KA, Yeager N, Baker K, Liao XH, Refetoff S, Di Cristofano A. Oncogenic Kras requires simultaneous PI3K signaling to induce ERK activation and transform thyroid epithelial cells in vivo. Cancer Res. 2009 Apr 15;69(8):3689-94.
- Myatt SS, Lam EW. The emerging roles of forkhead box (Fox) proteins in cancer. Nat Rev Cancer. 2007 Nov;7(11):847-59.
- Nappi TC, Salerno P, Zitzelsberger H, Carlomagno F, Salvatore G, Santoro M. Identification of Polo-like kinase 1 as a potential therapeutic target in anaplastic thyroid carcinoma. Cancer Res. 2009 Mar 1;69 (5): 1916-223.
- Nikiforov YE, Nikiforova MN. Molecular genetics and diagnosis of thyroid cancer. Nat Rev Endocrinol. 2011 Aug 30;7(10):569-80.

- Nikiforov YE. Genetic alterations involved in the transition from well-differentiated to poorly differentiated and anaplastic thyroid carcinomas. Endocr Pathol. 2004 Winter;15(4):319-27.
- Nikiforova MN, Kimura ET, Gandhi M, Biddinger PW, Knauf JA, Basolo F, Zhu Z, Giannini R, Salvatore G, Fusco A, Santoro M, Fagin JA, Nikiforov YE. BRAF mutations in thyroid tumors are restricted to papillary carcinomas and anaplastic or poorly differentiated carcinomas arising from papillary carcinomas. J Clin Endocrinol Metab. 2003 Nov;88(11):5399-404.
- Pandit B, Halasi M, Gartel AL. p53 negatively regulates expression of FOXM1. Cell Cycle. 2009;8:34257.
- Pierantoni GM, Rinaldo C, Mottolese M, Di Benedetto A, Esposito F, Soddu S, Fusco A. High-mobility group A1 inhibits p53 by cytoplasmic relocalization of its proapoptotic activator HIPK2. J Clin Invest. 2007 Mar;117(3):693-702.
- Radhakrishnan SK, Bhat UG, Hughes DE, Wang IC, Costa RH, Gartel AL. Identification of a chemical inhibitor of the oncogenic transcription factor forkhead box M1. Cancer Res. 2006;66:9731-5.
- Raychaudhuri P, Park HJ. FoxM1: a master regulator of tumor metastasis. Cancer Res. 2011 Jul 1;71(13):4329-33.
- Ricarte-Filho JC, Ryder M, Chitale DA, Rivera M, Heguy A, Ladanyi M, Janakiraman M, Solit D, Knauf JA, Tuttle RM, Ghossein RA, Fagin JA. Mutational profile of advanced primary and metastatic radioactive iodine-refractory thyroid cancers reveals distinct pathogenetic roles for BRAF, PIK3CA, and AKT1. Cancer Res. 2009 Jun 1;69(11):4885-93.
- Saji M, Ringel MD. The PI3K-Akt-mTOR pathway in initiation and progression of thyroid tumors. Mol Cell Endocrinol. 2010; 321:20-28.

- Salvatore G, Nappi TC, Salerno P, Jiang Y, Garbi C, Ugolini C, Miccoli P, Basolo F, Castellone MD, Cirafici AM, Melillo RM, Fusco A, Bittner ML, Santoro M. A cell proliferation and chromosomal instbility signature in anaplastic thyroid carcinoma. Cancer Res. 2007 Nov 1; 67(21): 10148-58.
- Santarpia L, El-Naggar AK, Cote GJ, Myers JN, Sherman SI. Phosphatidylinositol 3-kinase/akt and ras/raf-mitogen-activated protein kinase pathway mutations in anaplastic thyroid cancer. J Clin Endocrinol Metab. 2008 Jan;93(1):278-84.
- Schweppe RE, Klopper JP, Korch C, Pugazhenthi U, Benezra M, Knauf JA, Fagin JA, Marlow LA, Copland JA, Smallridge RC, Haugen BR 2008 Deoxyribonucleic acid profiling analysis of 40 human thyroid cancer cell lines reveals cross-contamination resulting in cell line redundancy and misidentification. J Clin Endocrinol Metab. 2008 Nov; 93(11):4331-41
- Smallridge RC, Marlow LA, Copland JA. Anaplastic thyroid cancer: molecular pathogenesis and emerging therapies. Endocr Relat Cancer. 2009 Mar;16(1):17-44.
- Sorrentino R, Libertini S, Pallante PL, Troncone G, Palombini L, Bavetsias V, Spalletti-Cernia D, Laccetti P, Linardopoulos S, Chieffi P, Fusco A, Portella G. Aurora B overexpression associates with the thyroid carcinoma undifferentiated phenotype and is required for thyroid carcinoma cell proliferation. J Clin Endocrinol Metab. 2005 Feb;90(2):928-35.
- Teh MT, Wong ST, Neill GW, Ghali LR, Philpott MP, Quinn AG. FOXM1 is a downstream target of Gli1 in basal cell carcinomas. Cancer Res. 2002 Aug 15;62(16):4773-80.
- Vivanco I, Sawyers CL. The phosphatidylinositol 3-Kinase AKT pathway in human cancer. Nat Rev Cancer. 2002; 2:489-501.
- Vousden KH, Prives C. Blinded by the light: The growing complexity of p53. Cell. 2009;

137:413-31.

- Wang Z, Banerjee S, Kong D, Li Y, Sarkar FH. Downregulation of Forkhead Box M1 transcription factor leads to the inhibition of invasion and angiogenesis of pancreatic cancer cells. Cancer Res. 2007 Sept 1;67(17):8293-300.
- Wiseman SM, Masoudi H, Niblock P, Turbin D, Rajput A, Hay J, Bugis S, Filipenko D, Huntsman D, Gilks B. Anaplastic thyroid carcinoma: expression profile of targets for therapy offers new insights for disease treatment. Ann Surg Oncol. 2007 Feb;14(2):719-29.
- Wonsey DR & Follettie MT. Loss of the forkhead transcription factor FoxM1 causes centrosome amplification and mitotic catastrophe. Cancer Res. 2005 Jun 15; 65(12) :5181-9.
- Wreesmann VB, Chossein RA, PAtel SG, et al Genome-wide appraisal of thyroid cancer progression Am J Pathol. 2002;161:1549-56.
- Wu G, Mambo E, Guo Z, Hu S, Huang X, Gollin SM, Trink B, Ladenson PW, Sidransky D, Xing M. Uncommon mutation, but common amplifications, of the PIK3CA gene in thyroid tumors. J Clin Endocrinol Metab. 2005 Aug;90(8): 4688-93.
- Xing M. Genetic alterations in the phosphatidylinositol-3 kinase/Akt pathway in thyroid cancer. Thyroid. 2010 Jul;20(7):697-706.
- Ye H, Kelly TF, Samadani U, Lim L, Rubio S, Overdier DG, Roebuck KA, Costa RH. Hepatocyte nuclear factor 3/fork head homolog 11 is expressed in proliferating epithelial and mesenchimal cells of embryonic and adult tissues. Mol Cell Biol. 1997 Mar;17(3):1626-41.

Figure legends

Figure 1. Immunohistochemical analysis of FOXM1 expression in human thyroid tissue samples — Representative captions of a normal thyroid (negative), PTC and PDC (weakly positive: +) and ATC (strongly positive: +++) samples. Original magnification: left (x4), right (x40)

Figure 2. FOXM1 is overexpressed at the mRNA level in human anaplastic thyroid carcinoma samples — A) Quantitative RT-PCR showing increased FOXM1 expression in ATC samples compared to normal thyroids as well as to PTC samples (15 samples for each category). Values are expressed as fold changes of tumor samples with respect to the average expression in normal samples measured with ΔCt method after normalization for actin mRNA levels (***, $p < 0.001$). **B)** Schematic representation of the 3 altervatively spliced FOXM1 variants and the PCR primers used to detect the presence of spliced exons A1 and A2. **C)** RT-PCR to show relative expression of levels the three FOXM1 isoforms in normal thyroids, PTC and ATC (9 samples for each category). Plasmids encoding FOXM1b and FOXM1c were used as PCR templates to generate molecular weight controls for the presence or the absence of exon A1 (primers F2/R2) or A2 (primers F3/A3). Arrows indicate expected migration for RT-PCR products containing (variants FOXM1a and FOXM1c) or lacking exon A1 (FOXM1b) or for RT-PCR products containing (FOXM1a) or lacking exon A2 (FOXM1b and FOXM1c).

Figure 3. FOXM1 is overexpressed at the mRNA and protein level in ATC cells — A) Semiquantitative RT-PCR showing increased levels of FOXM1c in ATC cells compared to normal thyrocytes (P5) (see legend to Figure 2). Levels of 18S rRNA were measured for

normalization. **B)** Western Blot analysis showing increased protein expression of FOXM1 in ATC cells compared to P5 control. Tubulin was used for normalization. These results are representative of at least three independent experiments.

Figure 4. FOXM1 in ATC cells is controlled by the p53/p21/pRb/E2F and PI3K/Akt/FOXO3a pathways — A) The indicated ATC cells were co-transfected with the indicated expression vectors (or the empty vector as control) together with 6XCDX2 containing 6 copies of the FOXM1 binding site fused to firefly luciferase. Alternatively, as indicated cells were treated for 48 h with the PI3K inhibitor LY294002 or the MEK inhibitor PD98059. Cells were co-transfected with renilla luciferase for normalization. Normalized luciferase levels are reported as average results of three independent experiments are reported with 95% confidence intervals. Reporter activity in empty vector-transfected cells was arbitrary set at 10; (***, $p < 0.001$). **B)** FOXM1 mRNA expression levels were measured in the indicated ATC cells 72 h after transfection with the indicated plasmids or treatment with LY294002. The average results of three independent experiments are reported together with 95% confidence interval. FOXM1 expression in mock-transfected cells was arbitrary set at 1.0; (***, $p < 0.001$).

Figure 5. Effect of FOXM1 silencing on ATC cell growth, migration and invasion — A) ATC cells were transfected with either FOXM1-siRNA or the scrambled control or left un-transfected. Cells were harvested at 48 hours and counted. Values represent the average of triplicate experiments with bars indicating 95% confidence intervals; (***, $p < 0.001$). B) 8505C cells, transfected with either FOXM1-siRNA or the scrambled control, were plated at confluence and scratch wounds were inflicted. After 24h, cell plates were photographed and cells closing the wound were counted. The avearage results of three experiments are reported

with bars representing 95% confidence intervals; (***, $p < 0.001$). C) 8505C cells, transfected with either FOXM1-siRNA or the scrambled control, were plated in transwells coated with Matrigel and their migration through Matrigel was measured by staining migrated cells with Giemsa. The avearage results of three experiments are reported with bars representing 95% confidence intervals; (***, $p < 0.001$). D) RNA was extracted from 8505C cells, transfected with either FOXM1-siRNA or the scrambled control or left untransfected and semiquantitative RT-PCR assays were performed to detect expression levels of the indicated mRNAs.

Figure 6. A model for FOXM1 role in thyroid cancer. Schematic representation of the molecular pathways linked to FOXM1 up-regulation in ATC (+ and – refer to activating or inhibitory signal, respectively) and gene targets whose expression is stimulated by FOXM1. This pathway can be therapeutically targeted at multiple levels; as show here and in the Ahmed (2011) study, these levels include FOXM1 itself and PI3K.

Fig 1

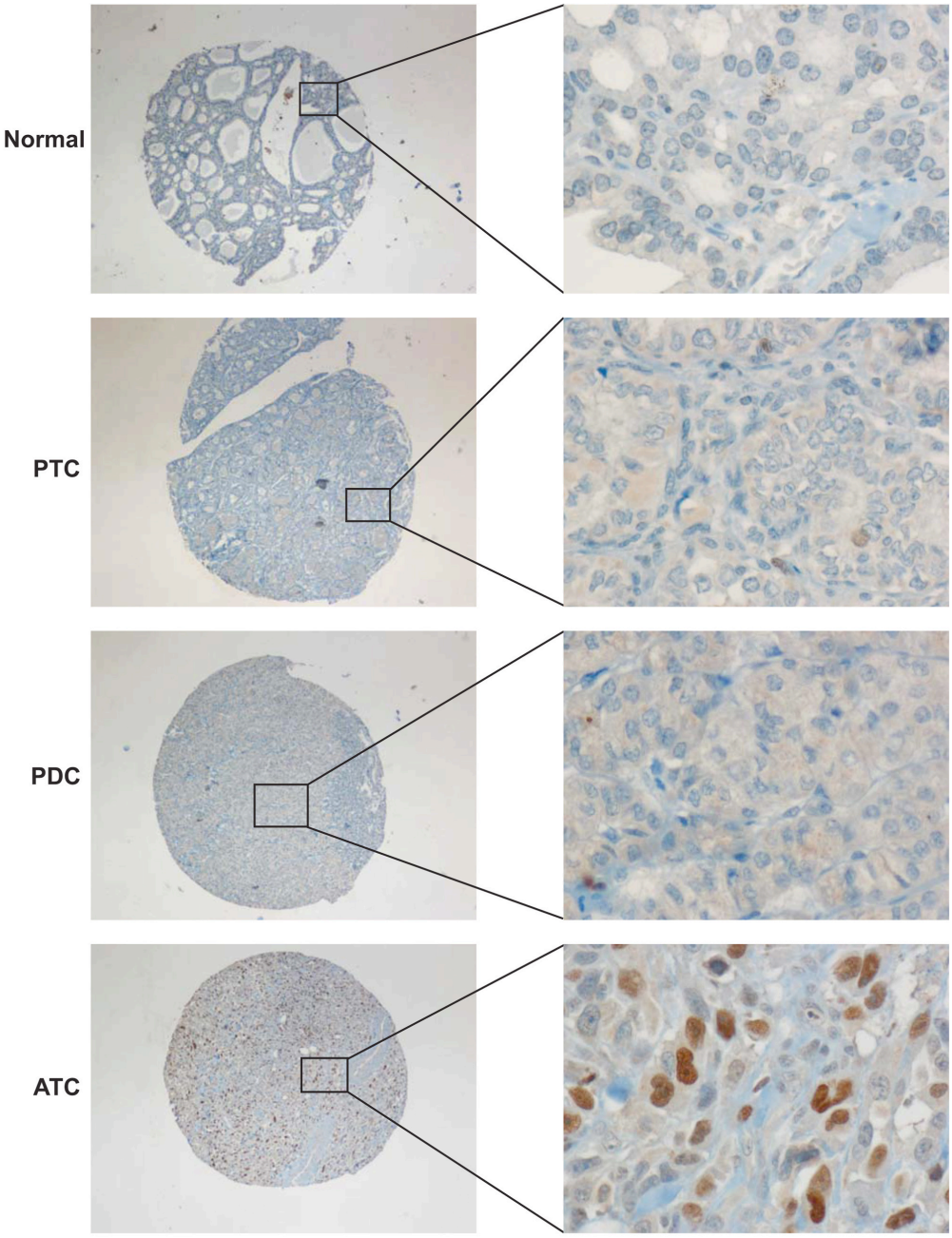

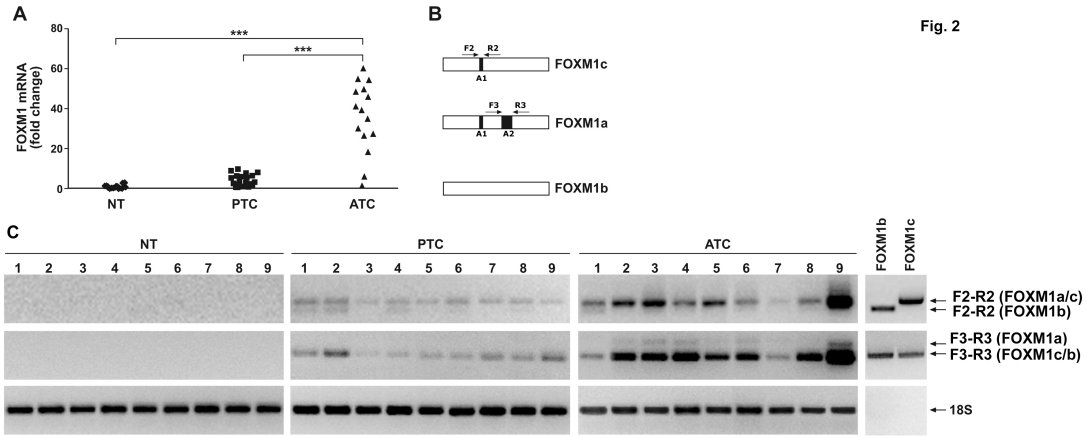
A
FOXM1 mRNA (fold change)
80
60
40
20
0
***
***
NT
PTC
ATC
B
F2
R2
A1
FOXM1c
F3
R3
A1
A2
FOXM1a
FOXM1b
C
NT
PTC
ATC
1 2 3 4 5 6 7 8 9
FOXM1b
FOXM1c
F2-R2 (FOXM1a/c)
F2-R2 (FOXM1b)
F3-R3 (FOXM1a)
F3-R3 (FOXM1c/b)
18S

Fig. 2

Fig. 3

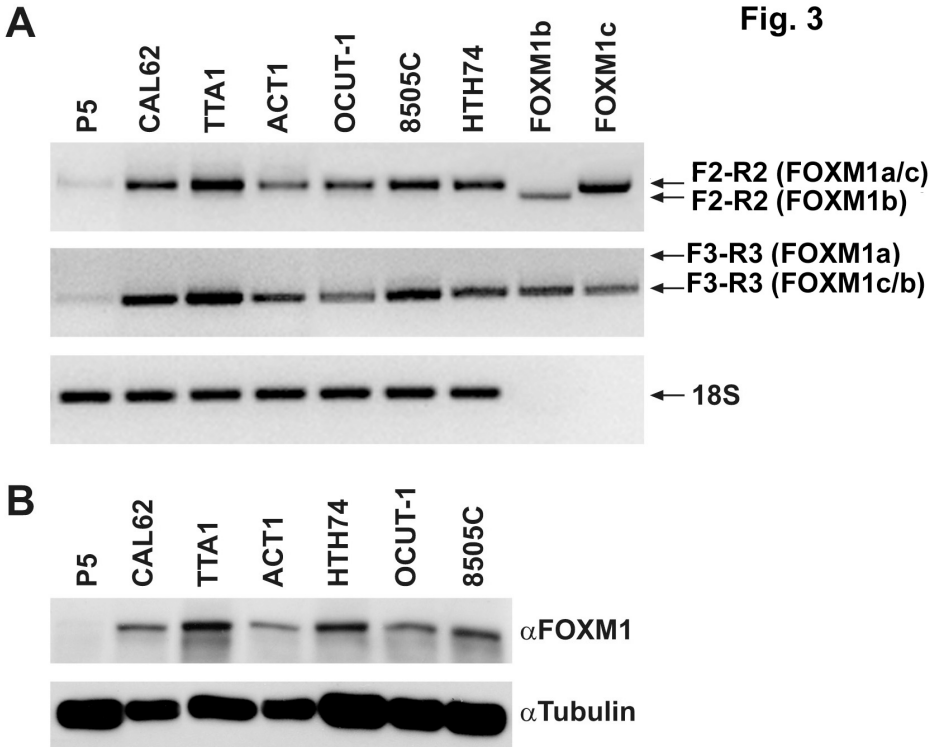
A
P5
CAL62
TTA1
ACT1
OCUT-1
8505C
HTH74
FOXM1b
FOXM1c
F2-R2 (FOXM1a/c)
F2-R2 (FOXM1b)
F3-R3 (FOXM1a)
F3-R3 (FOXM1c/b)
18S
B
P5
CAL62
TTA1
ACT1
HTH74
OCUT-1
8505C
αFOXM1
αTubulin

Fig. 4

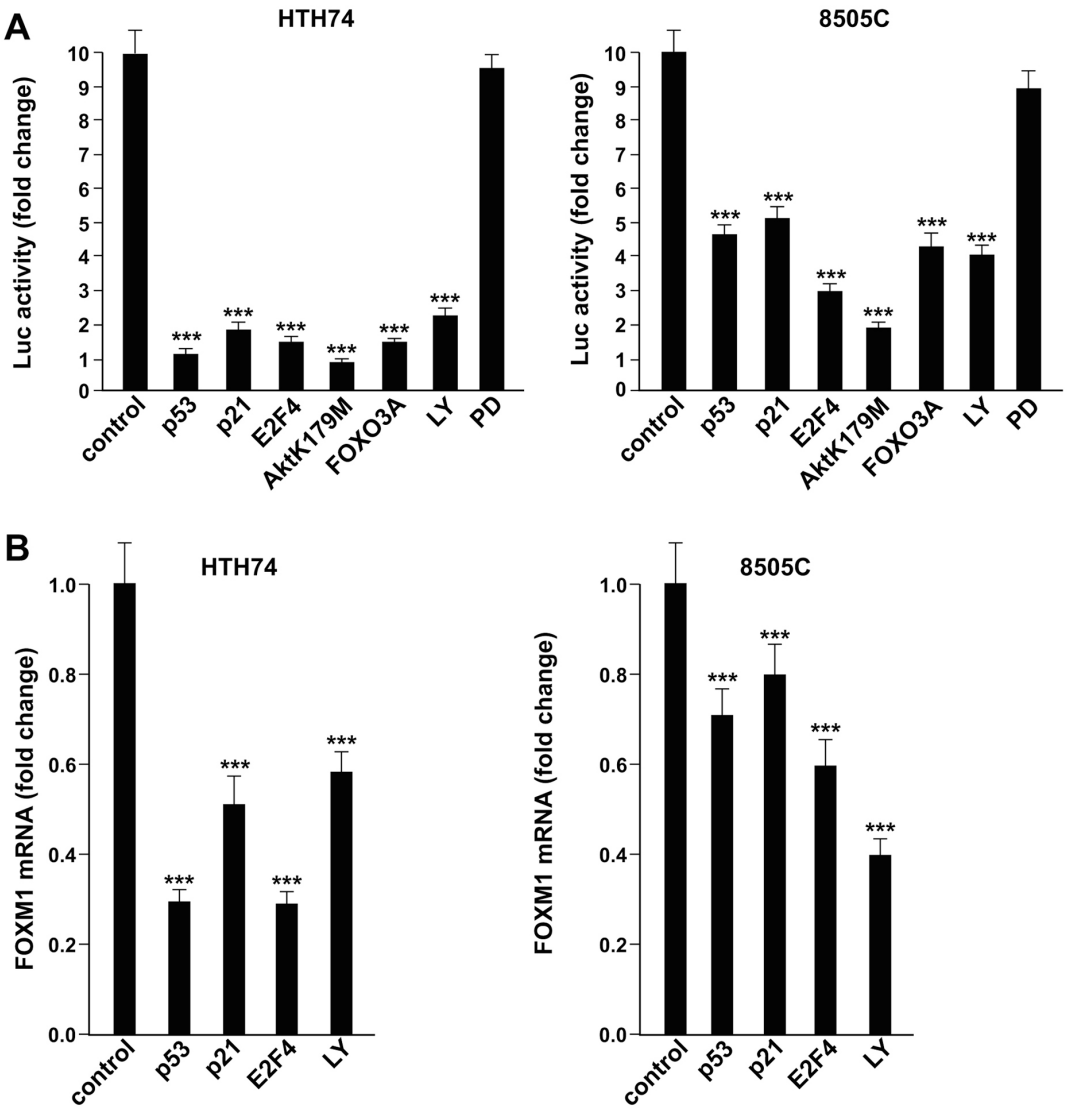
A
HTH74
8505C
Luc activity (fold change)
control
p53
p21
E2F4
AktK179M
FOXO3A
LY
PD
B
HTH74
8505C
FOXM1 mRNA (fold change)
***

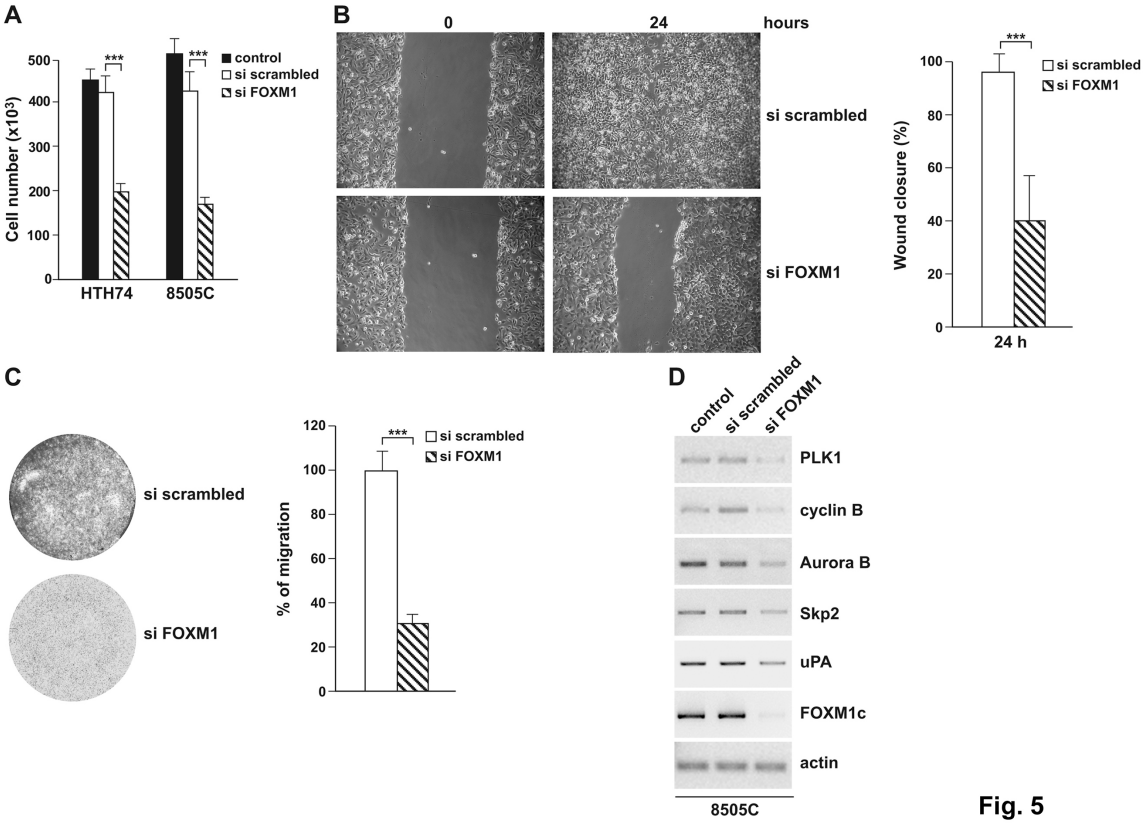
A
Cell number (x10³)
500
400
300
200
100
0
***
***
control
si scrambled
si FOXM1
HTH74
8505C
B
0
24
hours
si scrambled
si FOXM1
***
si scrambled
si FOXM1
Wound closure (%)
100
80
60
40
20
0
24 h
C
si scrambled
si FOXM1
***
si scrambled
si FOXM1
% of migration
120
100
80
60
40
20
0
D
control
si scrambled
si FOXM1
PLK1
cyclin B
Aurora B
Skp2
uPA
FOXM1c
actin
8505C

Fig. 5

Fig. 6

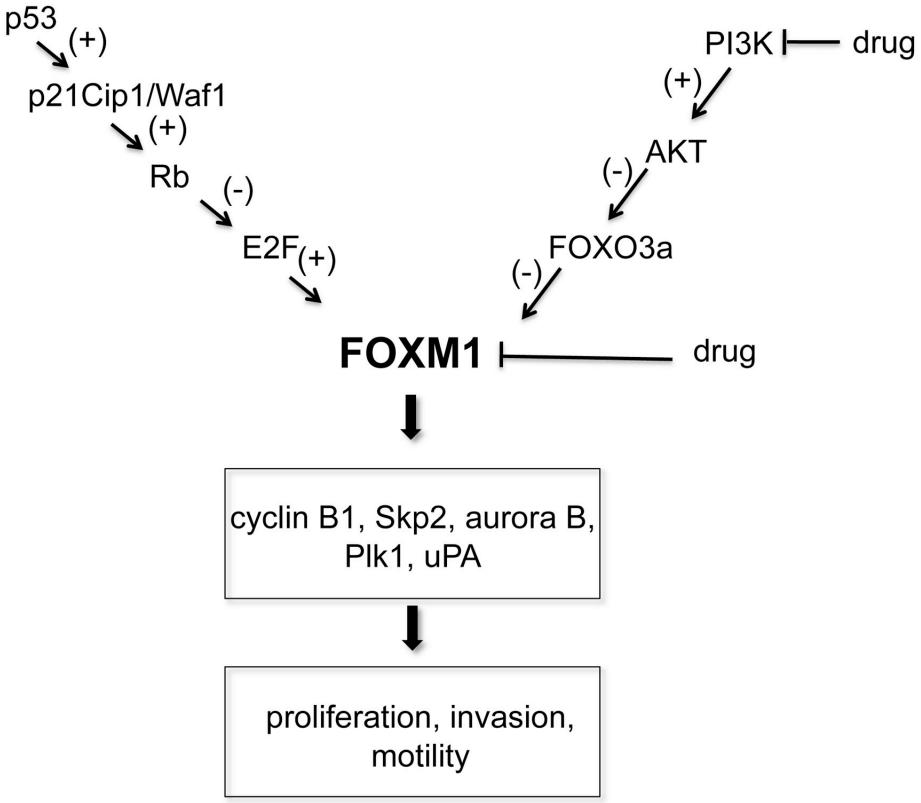
p53
(+)
p21Cip1/Waf1
(+)
Rb
(-)
E2F
(+)
PI3K
drug
(+)
AKT
(-)
FOXO3a
(-)
FOXM1
drug
cyclin B1, Skp2, aurora B, Plk1, uPA
proliferation, invasion, motility

Table 1. FOXM1 expression by immunohistochemistry in human thyroid samples.

Sample	Staining intensity*			
	(-)	(+)	(++)	(+++)
Normal thyroid	100% (35/35)	0% (0/35)	0% (0/35)	0% (0/35)
PTC	74.5% (38/51)	19.6% (10/51)	5.8% (3/51)	0% (0/51)
PDC	67% (165/246)	24.3% (60/246)	6.5% (16/246)	2% (5/246)
ATC	25.6% (29/113)	23% (26/113)	29.2%(33/113)	22.1% (25/135)

*(-) < 5% of cells positive for nuclear FOXM1 expression;
(+) 5-10% of positive cells;
(++) 20-40% of positive cells;
(+++) >50% of positive cells.

Attached Manuscript #III

Castellone MD, Cantisani MC, Perala M, Vidal F, Sadelberg N, **Bellelli R**, Laukkanen MO, Kallioniemi OP, Santoro M.

Identification of EPHRs as new mediators of thyroid carcinogenesis through an RNA interference screening.

Manuscript in preparation

Identification of EPHRs as new mediators of thyroid carcinogenesis through an RNA interference screening.

Maria D. Castellone[1,2], Maria C. Cantisani[1,2], Merja Perala[3], Fey Vidal[3], Niko Sadelberg[3], Roberto Bellelli[1], Mikko O. Laukkanen[4], Olli P. Kallioniemi[3] & Massimo Santoro[1†]

[1]Istituto di Endocrinologia ed Oncologia Sperimentale "G. Salvatore" (IEOS), C.N.R. c/o Dipartimento di Biologia e Patologia Cellulare e Molecolare, "L. Califano", Universita' Federico II, Napoli, Italy; [3]Medical Biotechnology, VTT Technical Research Centre of Finland, Institute for Molecular Medicine Finland and University of Turku, Turku, Finland; [4] Fondazione IRCCS SDN, Naples, Italy.

[2]These authors contributed equally to the work

[†]To whom correspondence should be addressed:
Massimo Santoro, Dipartimento di Biologia e Patologia Cellulare e Molecolare
University of Naples "Federico II", Via Pansini, 5, 80131- Naples, Italy
Telephone: (+39) 081-7463056; Fax: (+39) 081-7463037
Email: masantor@unina.it

ABSTRACT

Background. Thyroid cancer is the most frequently occurring malignancy of the endocrine system, whose incidence is increasing worldwide. Even though recent years have been characterized by significant advances in understanding the molecular basis of thyroid carcinogenesis, leading to the identification of RET and BRAF kinases as major molecular targets in these tumors, still further studies are needed to characterize tumor-initiating genetic events and to identify additional mediators of tumorigenesis and of resistance to conventional therapies. *Methods.* We performed an high-throughput screening of the entire human kinome by transfecting a library of synthetic small interfering RNA (siRNA) in the TPC1 thyroid cancer cell lines, harboring rearrangement of RET-PTC1, in order to identify novel protein kinases required to sustain viability of thyroid carcinoma cells. *Results.* Our data show that knock-down of 21 kinases reduced significantly the viability and the proliferation of thyroid cancer cell lines. Among them, we identified several members of the Ephrine Receptor family (EPHA2, EPHA4 and EPHB2) as regulators of different biological features of thyroid cancer cells such as invasion and migration. *Conclusions.* The identification of EPHs as mediators of thyroid carcinogenesis sheds new light on the molecular mechanisms regulating thyroid transformation and offers novel therapeutic approaches against this malignancy.

INTRODUCTION

The past two decades have witnessed significant progress in understanding molecular mechanisms regulating cancer pathogenesis. Thus, actual efforts are focusing on development of anti-cancer drugs that target proteins involved in carcinogenesis and kill tumor cells while sparing normal cells. Among these drugs, small molecules targeting kinases are proving effective against well-characterized cancers, as many tumors are associated with increase in activity of specific kinases caused by mutational activation, or changes in expression due to gene amplification or translocation (Futreal et al., 2004; Venter et al., 2001; Manning et al., 2002). In a recent study, 23% (120/518) of kinase genes were estimated to function as cancer genes (Greenman et al., 2007), as they mediate most of the signal transduction events in cells by phosphorylation of specific substrates, modifying their activity, cellular location, and/or association with other proteins.

Thyroid cancer is one of the best examples of characterization of the genetic lesions involved in tumor development and progression and of successful therapeutic approaches with specific molecular inhibitors targeting activated proteins. Rearrangements involving RET together with point mutations in the BRAF kinase cover about 70% of Papillary Thyroid Carcinoma (PTC) cases (Santoro *et al*., 1992; García-Rostán *et al*., 2003; Kimura *et al*., 2003; Soares *et al*., 2003; Nikiforova *et al*., 2003a; Nikiforova *et al*., 2003b; Frattini *et al*., 2004; Elisei *et al*., 2008a).

Several compounds able to target the RET and the BRAF kinases are under investigation and some of them have already reached the clinical approval (Santoro and Carlomagno 2006; Schlumberger *et al*., 2009; Sherman, 2009) such as Vandetanib (Zactima, ZD6474) (Astra Zeneca, Wilmington, DE) that has been recently approved (April 2011) from the U.S. Food and Drug Administration (FDA) to treat adult patients with late-stage (metastatic) medullary thyroid cancer (MTC) who are ineligible for surgery and who have

disease that is growing or causing symptoms.

Although most of the genetic lesions involved in thyroid cancer are known, still there is a certain number of PTC (about 30% of cases) where no mutations have been identified yet. In addition, many PTC tumors undergo development of resistance against small molecular inhibitors, due to mutation in the kinase target of the drug or due to the activation of compensatory kinases, that rescue cancer cell proliferation; therefore combination therapies targeting multiple signaling pathways may offer more effective therapeutic strategies.

siRNA screening of the kinome in cancer cells can be exploited to identify molecular mediators of tumorigenesis and to highlight compensating kinases, leading to development of multi target inhibitors able to overtake the mechanism of resistance to drug treatment (Berns et al., 2007; Westbrook et al., 2005; MacKeigan et al., 2005). We have used a high-throughput siRNA screening to characterize functional differences in kinase requirements in human thyroid cells and to find kinases whose roles in proliferation and survival differ in tumor cells as compared to normal cells. Through this screening, we identified 21 "down hits", e.g. kinases whose knock-down reduced by 30% or more TPC1 cell viability. Most of these kinases were essential not only for the viability of TPC1 but also other thyroid cancer cell lines with different genetic backgrounds (RAS or BRAF mutations) but not for normal thyroid cells. Our down-hits include components of multiple signaling pathways. In particular, we identified several members of the EPH (ephrin receptors) family, namely EPHA2, EPHA4 and EPHB2, as over-expressed and functionally active in various thyroid cancer cell lines. The identified EPHs were also up-regulated in human thyroid tumor specimens and their specific knock-down impaired the ability of cancer cells to invade the matrigel and close the wound.

METHODS

Cell Lines, Cell Culture and Tissue Samples

TPC-1 and BCPAP are cell lines derived from papillary thyroid carcinomas and express the RET-PTC1 and BRAF-V600E oncogenes respectively; CAL62, 8505C and SW1736 are derived from undifferentiated- anaplastic carcinomas expressing K-RAS or BRAF-V600E oncogenes as described in supplemental table 1 (Table S1). All thyroid cancer cell lines were grown in Dulbecco's modified Eagle's medium supplemented with 10% FBS (Invitrogen, Carlsbad, CA, USA), L-glutamine and penicillin/streptomycin (Sigma Aldrich, St Louis, MO, USA) (Cerutti *et al*., 1996; Ohta *et al*., 2001; Basolo *et al*., 2002). Nthy-ori 3-1 (ECACC, Wiltshire, UK) represents a normal human thyroid follicular epithelial cell line that has been immortalized by transfection with a plasmid encoding for the SV40 large T gene, grown in RPMI-1640 medium supplemented with 10% FBS. Human primary cultures of normal thyroid cells (P5) were obtained from F. Curcio and cultured as previously described (Curcio *et al*., 1994). All cells were expanded briefly in culture and cryopreserved in multiple replicate vials. This cell bank was tested by ELISA assay (Mycoplasma detection Kit, Cat # 11296744001, Roche, Indianapolis, IN, USA) and found to be free of mycoplasma. To authenticate the cell lines, short tandem repeat genotyping was performed. All cells were maintained in a humidified incubator at 37 C and 5% CO2. A thyroid tumor tissue bank containing a large number of samples (about 300, equally divided among the different subtypes) snap-frozen in liquid nitrogen and maintained at -80°C has been made available through the group of F. Basolo (University of Pisa, Italy). For all of them, formalin-fixed paraffin-embedded material is available. For all cases, clinico-pathological parameters such as age, gender, size, extrathyroidal extension, lymphonode and distant metastases were recorded. The use of these archival tissues in this study was approved by the Ethics Committee of the University of Pisa.

High-Throughput siRNA screening

For primary high-throughput screening, the TPC1 cells were seeded into black, transparent bottom, 384/well plates (BD Biosciences, Heidelberg, Germany) using an automatic MultiDrop dispenser (Thermo Labsystems, Philadelphia, PA, USA). All wells were filled with 1,000 cells/well in a volume of 100 µl of DMEM supplemented with 2.5% FBS without antibiotics. The cells were then transfected with the human kinome siRNA set v 2.0 (Qiagen, Germantown, MD, USA). Each well contained a specific siRNA targeting one of 646 distinct genes. Two siRNAs for each target were used, as well as positive controls (e.g. MAPK-siRNA, PLK1-siRNA), negative controls (scrambled, GFP, buffer) and untransfected cells. 5 µl of 2 micromolar siRNA (10 pmol) was transferred from the stock plate using the robotic liquid handler and mixed to transfection solution, prepared with 0.2 µl of HyPerfect cell culture reagent (Qiagen) diluted in 10 µl of Optimem medium (Invitrogen). Following 10 minutes incubation, the transfection mix was delivered to each well and incubated at room temperature for 1 hour. 72 hours after transfection, 10 µl of Cell Titer Blue reagent (CellTiter Blue Assay, Promega, Madison, WI, USA) diluted 1:1 in cell culture medium were added to each well, to measure the amount of metabolite which is generated by dye reduction in viable cells. Plates were incubated at 37 °C for 6 hours with 5% CO_2 and then transfered to room temperature for overnight incubation, at dark. Cell viability was measured with an EnVision Multilabel plate reader at an excitation wavelength of 530 nm and emission wavelength of 590 nm (Perkin Elmer, Waltham, MA, USA). For each well data were calculated as a ratio on an average of control wells present in each plate, to minimize the effects due to transfection toxicity. The results were expressed as log2 and siRNA effective in reducing cell vitality by at least 30% (loess log ≤-0.67) were considered as negative hits. The primary screening was repeated in duplicate and the results are attached as supplemental informations (Table S2).

Secondary siRNA screen

To confirm the primary screening results, we obtained an independent set of 2 siRNAs for each of the 49 identified hits (with exception of two pseudo-genes: LOC392265 and MGC4796) (Table S3). The catalogue number list of siRNA used is attached as Supplemental table 4. From this analysis 80.8% (38) of the 47 tested genes were significantly reducing cell viability with the new siRNAs, although only those hits (26) that were reducing cell viability by at least 30%, compared to the control, and with at least 3 (out of 4) different siRNAs, passed our confirmation screening. Among these genes, after a preliminary test in normal cells, we identified some hits that were significantly ($p \leq 0.05$) affecting viability also of normal cells (8 genes out of 26). Because our aim was to find kinases that could be important for cancer cells, as mediators of tumorigenesis and as potential therapeutical targets, we excluded from further studies those hits that were affecting also normal cells, limiting our analysis to 18 hits. Moreover, because the Ephrine Receptor Family (EPH) was the best represented group in our list, we reduced the cut off to fish for more member of this protein group and we identified two proteins (EPHA4, EPHB2), located just below the chosen cut off (EPHA4 loess log = -0.3; EPHB2 loess log= -0.4), that we included in our further studies. Our final list contained therefore 20 down hits, that we targeted with siRNA in a broader panel of thyroid cells (BCPAP, 8505C, SW1736, Nthy-ori and P5), as a validation screening. For each of the used cell line, siRNA transfection conditions had been previously set up by using the KDalert GAPDH kit (Ambion, Applied Biosystem, Carlsbad, CA, USA) that measures the efficiency of GAPDH silencing with specific siRNA. The secondary and the validation screenings were repeated three independent times.

Quantitative RT-PCR

The goal of the validation screen was to prioritize the identified hits for further studies. In order to verify the specificity of the siRNAs used in our study, we performed a Quantitative RT-PCR analysis in cancer (TPC1) and normal (Nthy-ori) cells, confirming that the used duplex were knocking down their specific target genes. Moreover we tested the relative expression for every identified gene in a broader panel of thyroid cancer cells, compared to normal cells. For evaluation of mRNA expression, each cell line was grown to 70% confluency, total RNA was extracted with RNeasy mini kit (Qiagen) and subjected to on-column DNase digestion with the RNase-free DNase set (Qiagen) according to the manufacturer's instructions. RNA (1μg) was reverse transcribed using a high-capacity reverse transcriptase kit (Quantitect Reverse® Transcription Kit, Qiagen). Reaction occurred at 42°C for 15 minutes, 99°C for 5 minutes, and subsequent cooling at 5°C for 5 minutes. cDNA amplification was performed using the GeneAmp RNA PCR Core Kit system starting from 2.5 μl of RT product in a reaction volume of 25 μl according to the manufacturer's instructions. Primers were designed by using a software available at http://www-genome.wi.mit.edu/cgi-bin/primer/primer3_www.cgi and synthesized by the Ceinge (Naples, Italy). Quantitative (real-time) reverse transcription polymerase chain reactions (qRT-PCR) were performed by using the SYBR Green PCR Master mix (Applied Biosystems) in the iCycler apparatus (Bio-Rad Laboratories, Berkeley, CA, USA). Fluorescent threshold values were measured in triplicate and fold changes were calculated by the formula: $2^{-(\text{sample 1 } \Delta Ct - \text{sample 2 } \Delta Ct)}$, where ΔCt is the difference between the amplification fluorescent threshold (Ct) of the mRNA of interest and the Ct of the *β* actin mRNA used as housekeeping gene. The list of primers used is attached as Supplemental Table 5 (Table S5). Each result derives from three independent experiments.

Protein Extraction and Immunoblot.

Protein extraction and immunoblotting experiments were performed according to standard procedures. Briefly, cells were harvested in lysis buffer (50 mM HEPES, pH 7.5, 150 mM NaCl, 10% glycerol, 1% Triton X-100, 1 mM EGTA, 1.5 mM MgCl2, 10 mM NaF, 10 mM sodium pyrophosphate, 1 mM Na3VO4, 10 μg aprotinin/ml, 10 μg leupeptin/ml) and clarified by centrifugation at 10,000 g at 4°C. Protein concentration was estimated with a modified Bradford assay (Bio-Rad). Lysates of equal protein concentration (30 μg for total cell lysates and 1 mg for immunoprecipitation) were separated with sodium dodecyl sulfate-polyacrylamide gel electrophoresis (SDS-PAGE) and transferred to Hybond C Extra nitrocellulose membranes (GE Healthcare, Munich, Germany). Membranes were incubated in blocking solution containing 5% nonfat dry milk for 1 hour at room temperature. Incubation with primary antibodies was performed overnight at 4°C, followed by incubation for 1 hour at room temperature with HRP-conjugated anti-mouse or anti-rabbit secondary antibodies (dilution 1:3000) from Amersham Biosciences (Piscataway, NJ, USA). Immunocomplexes were detected with the enhanced chemiluminescence kit (ECL; Amersham Biosciences). Anti-EphA2 antibody (dilution 1:1000 for WB and 1:100 for IP) and anti-phospho-tyrosine (dilution 1:1000) antibodies were from Millipore (Schwalbach, Germany) (05-480 and 05-321, respectively); anti-EphA4 antibody (dilution 1:500 for WB and 1:50 for IP) was from Invitrogen (371600); anti-EphB2 antibody (dilution 1:1000 for WB and 1:100 for IP) was from R&D Systems (Minneapolis, MN, USA); anti phospho-MAPK (dilution 1:1000) and anti phospho-AKT (dilution 1:1000) were from Cell Signaling Technologies (Danvers, MA, USA) (4370 and 4850 respectively). Monoclonal anti–α-tubulin (dilution 1:10 000) was from Sigma-Aldrich (T-9026). All experiments were performed at least three independent times.

Proliferation and survival assays

To test whether siRNA transfection would affect cell proliferation, S-phase entry was evaluated by BrdU incorporation, Cell Proliferation ELISA BrDu (Roche). Briefly, cells were cultured in 96-multiwell plate black, flat bottom (BD Biosciences) in a volume of 100 µl/well. After 72 hours cells were labeled with 10 µM of BrDu labeling solution and incubated at 37°C for additional 2 hours. Cells were then fixed for 30 minutes at room temperature with 200 µl/well of FixDenat buffer, and incubated with 100 µl/well of anti-BrDu-POD (peroxidase) for 90 minutes at room temperature. After three washes, substrate solution was added, plates were kept on a shaker for 3 minutes at room temperature and light emission was read using a microplate luminometer with photomultiplier technology, DL Ready BERTHOLD Technologies Centro (Beckman, Brea, CA, USA). To measure apoptotic cell rate, the Apo-ONE® Homogeneous Caspase-3/7 Assay (Promega) was performed after siRNA transfection as previously described. Blank, e.g. untransfected cells, and negative control, e.g. medium without cells, were performed as well. 100 µl of Apo-ONE® Homogeneous Caspase-3/7 Reagent were added to each well. The fluorescence values were proportional to the amount of caspase-3/7 cleavage activity present in each sample and they were measured with an EnVision Multilabel plate reader (Perkin Elmer). All the experiments were performed in triplicates.

Wound healing assay

For wound healing assays, TPC1 cells transfected with siRNA targeting EPHs and scrambled control were grown to form cell monolayers of 80% confluency in which a wound of approximately 300µm width was inflicted with a sterile pipette tip. The culture medium was exchanged to remove non-adherent cells. The progress of wound closure (healing) was monitored with microphotographs of X10 magnification taken with the Leica DM IL light

microscope (Leica Microsystems, Wetzlar, Germany) immediately and 12 hours after the wound. The experiments were repeated three independent times.

Invasion Assay

In vitro invasiveness through Matrigel was assayed using transwell cell culture chambers according to described procedures. Briefly, TPC1 confluent cell monolayers were harvested with trypsin/EDTA and centrifuged at 800X*g* for 10 min. The cell suspension ($1X10^5$ cells/well) was added to the upper chamber of transwells on pre-hydrated polycarbonate membrane filter of 8 μM pore size (Costar, Cambridge, MA, USA) coated with 35μg Matrigel (BD Biosciences). The lower chamber was filled with complete medium. Cell dishes were incubated at 37 °C in 5% CO_2 and 95% air for 24 h. Non-migrating cells on the upper side of the filter were wiped off and migrating cells on the reverse side of the filter were stained with 0.1% crystal violet in 20% methanol for 15 min, counted and photographed. Each experiment was repeated three times.

Statistical analysis

Experimental data are summarized as the mean values with 95% confidence intervals (CIs). All statistical analyses were performed using a two-tailed Student's t test (GraphPad Prism 3.0, GraphPad Software, San Diego, CA, USA), and differences were considered to be statistically significant at a value of P less than .05.

Cell viability values were log-transformed and then subtracted by the median value of the experimental and negative control wells. These values were then divided by the standard deviation of the plate well values. The raw data were quantile-normalized and analyzed with the R/Bioconductor software (Gentleman RC, Carey VJ, Bates DM, Bolstad B, Dettling M, Dudoit S, Ellis B, Gautier L, Ge Y, Gentry J, Hornik K, Hothorn T, et al. Bio- conductor:

open software development for computational biology and bioinformatics. Genome Biol 2004;5:R80.).

RESULTS

High-throughput screening of human kinases involved in TPC1 cells viability.

To establish the role of all known protein kinases in thyroid carcinogenesis we designed a functional assay using the human papillary thyroid carcinoma cell line TPC1 harboring rearrangement of RET-PTC1 oncogene. Cells were silenced with a library containing 646 synthetic siRNAs targeting all human protein kinases as well as a number of kinase-related and associated proteins. To reduce the off-target effect of siRNAs, the library has been designed to contain two independent duplex targeting the same transcript. The transfection was done by using 10 pmol of siRNA (see methods for details). To monitor transfection efficiency, each plate contained cytotoxic siRNAs targeting genes that are positive regulators of proliferation in all cells (e.g. polo like kinase 1-PLK1 and mytogen activated protein kinase 1-MAPK1), and negative control siRNAs targeting green fluorescente proteine (GFP) or scrambled sequences as well as buffer and un-transfected cells.

Identification of primary hits.

72 hours after transfection of siRNAs we performed a cell titer blue assay to identify genes whose knock-down would affect TPC1 cells viability. Primary hits were defined as genes that, when silenced, reduced viability (normalized on negative control) by at least 30% (loess log $\leq$ -0.67). According to our data, siRNA-targeted downregulation of 7.5% (49 candidates out of 646 tested) of the kinome library resulted in significant reduced cell viability of TPC1 cells (Figure S1, Table S2 and Table S3). Samples that did not reproduce in at least two biological replicates, or those of dubious spots, were excluded from further analysis. To validate the screening results we conducted a secondary confirmation test with an independent set of 2 siRNAs targeting a distinct mRNA region of the 49 identified kinases. From this list we excluded two pseudo-genes (MGC4796 and LOC392265) and we added two other genes

(EPHA4 and EPHB2), belonging to the most represented family in our list, the Ephrin Receptor Family (EPHs), located just below our chosen cut off (EPHA4 loess log = -0.3; EPHB2 loess log= -0.4). With these new siRNAs targeting our 49 down hits, we performed the confirmation screening in TPC1 cells, by using the same conditions as for the primary screen. Confirmed down hits were those genes whose knock-down (mean of different siRNAs) would significantly ($p \leq 0.05$) affect cell viability by at least 25% as compared to the control (loess log $\leq$-0.5). This analysis led to the identification of 28 hits (Table S3). Because our study was aimed to discover new mediators of tumorigenesis and novel potential therapeutic targets in thyroid cancer, we performed a preliminary test in normal thyroid cells and we excluded those kinases (8 out of 28) that were affecting viability of normal and cancer cells indistinctly (CIB3, IHPK3, ITPKA, MAPK7, MARCKS, PAK2, STK33, TESK1). Our final list contain therefore 20 kinases (Table S3). They include logical candidates, like signaling kinases (FYN and AKT2), together with some novel kinases that have not previously been described to play a role in thyroid carcinogenesis. Among them the EPHR family is the best represented, with 6 different members in our list. Although we could exclude off target effects of duplex because we had confirmed our results by using different siRNAs for each gene, still we wanted to verify whether the oligos we used were specifically down-regulating their target transcripts. To this aim, we performed a quantitative RT-PCR in papillary thyroid cancer (TPC1) and normal thyroid cell lines (Nthy-ori 3-1), upon silencing of each of the identified kinase. Our data showed that all targets were significantly depleted by their specific siRNAs in both tested cell lines (Figure S2, S3), suggesting that the observed effects were due to specific gene silencing.

Validation screen.

To test the effect of our identified kinases in other thyroid cancer cell lines, we extended the analysis to a panel of genetically different cell lines of papillary (BCPAP), anaplastic (8505C, Cal62) and normal phenotype (Nthy-ory 3-1 and P5) (Table S1). The optimal transfection conditions for each cell line (number of cells, amount of siRNA and amount of transfection reagent) were previously defined by using the GAPDH Alert kit (Ambion), monitoring efficiency of GAPDH knock-down by specific siRNA. As shown in figure 2, most of the tested gene silencing significantly reduced the viability of all thyroid cancer cell lines while sparing normal cells. Few exceptions were represented by two genes that were affecting TPC1 cells exclusively (LIMK1 and MAP3K6), suggesting their possible connection to the presence of the RET-PTC1 rearrangement, and by other genes such as EPHA5, HCK, MAP3K7IP1, PKN1 and PRKD2 that were required for the viability only of PTC cells (TPC1 and BCPAP), but not of ATC cells (8505C and CAL62), suggesting their link to more differentiated (papillary) cancer histotype.

Characterization of the biological effects of kinase knock-down in thyroid cells.

To further characterize the reduced cell viability caused by the knock-down of our negative hits in thyroid cells, we performed growth curve analysis, BrdU incorporation as well as cleaved caspase-3 measurement assay upon siRNA transfection in TPC1 as well as Nthy-ori 3-1 normal cells. Our data show that in TPC1 cells all siRNAs had a significant ($p \leq 0.05$) cytostatic effect, evaluated as diminished percentage of BrdU incorporation (Figure 3 upper panel), while proliferation of normal Nthy-ory cells was not affected by gene knock-down (Figure 3 lower panel). The reduced BrdU incorporation was paralleled by a decreased number of cancer cells when performing growth curve experiments (Figure S4, S5). On the

other hand, no significant cytotoxic effect was observed in cancer or normal cells when measuring caspase 3 cleavage (Figure S6 or data not shown).

Identification of Ephrin receptors and their ligands in thyroid cancer cells and human samples.

Among the identified genes affecting thyroid cancer cell growth, we focused our attention on the Ephrin Receptors (EPHR), as six different members of this family were among the most prominent down hits in our primary screening (EPHA2, A4, A5, A7, B2 and B6) (Figure 1, Table S2, Table S3). To investigate the role of EPHR in thyroid cancer cells and to better understand the mechanisms of the reduced cell proliferation observed with EPHR siRNAs in TPC1 cells, we first tested whether the EPHR identified among our down hits would be differently expressed in cancer cells with respect to normal cells. By using several thyroid cell lines of different histotype and genotype we performed a quantitative RT-PCR (Q-RT-PCR) and demonstrated that all the 6 EPHRs present among our negative hits were expressed in thyroid cell lines. Moreover, when comparing the relative expression in cancer as compared to normal (Nthy-ori) cells, we found that some of them (EPHA2, EPHA4 and EPHB2) were significantly ($p<0.05$) over-expressed in transformed cells as compared to the normal control cell line (Figure 4A, left panels). To verify whether EPHs could also be present in human tumors, we tested the expression of EPHA2, EPHA4 and EPHB2 in papillary thyroid samples (PTC) and normal thyroids (NT). Our results, shown in figure 4A, right panels, demonstrate that also thyroid tumor samples have significant ($p \leq 0.01$) up-regulation of EPHA2, EPHA4 and EPHB2. These data support recent evidences suggesting strong involvement of EPHR/ephrins in tumorigenesis and correlating their expression levels to invasiveness, metastatization and reduced patient survival rates (Pasquale, 2005).

EPHRs are promiscuous tyrosine kinase receptors, able to bind to transmembrane (ephrins B) or GPI-soluble (ephrins A) ligands. They also mediate the signal transduction either in a paracrine way between two juxtaposed interacting cells, or in an autocrine manner in between the same cells (Pasquale 2005). We therefore screened our panel of thyroid cell lines for the expression of all the known ephrin ligands (EFNs). Our analysis revealed that among all the ligands, only a few (EFNA1, EFNA4, EFNB2) showed significantly ($p< 0.01$) higher expression in cancer as compared to normal cells (Figure 4B, left panels). Interestingly, these ligands can bind to the same EPHs identified from our screening (EPHA2, EPHA4, EPHB2). As for the receptors, also the three ligands were up-regulated in PTC tumor samples as compared to normal thyroid (Figure 4B, right panels).

Because EPHs are tyrosine kinase receptors, they undergo phosphorylation upon activatin. To evaluate the activation of these proteins in thyroid cancer, we studied the EPHA2, EPHA4 and EPHB2 protein expression and phosphorylation status by immunoprecipitation and Western blot analysis. Our data, shown in figure 5A, demonstrate overall increased total amount of EPHs in TPC1, BCPAP, SW1736 and 8505C cancer cells compared to normal Nthy-ory cells. Moreover, our screening cell line, TPC1, express high levels of tyrosine phosphorylated proteins, however when looking at the phosphorylation status in other cell lines, we observed differences among the cells; for instance, BCPAP cells seem to activate mainly EPHA2, while SW1736 cells express high levels of phosphorylated EPHB2 (Figure 5A). According to the EFN expression level results, the differences in activation could be due to the aboundance of specific ligands (EFNA1 for BCPAP and EFNB2 for SW1736), but more detailed studies are needed in order to understand the dynamic of EPHs-EFNs interaction in thyroid cancer cells.

Silencing of EPHRs affects migration and invasiveness of thyroid cancer cells.

To finally study whether the knock-down of the EPHs would affect any of the known pathway controlling thyroid cancer cell growing and metastasizing properties, we performed EPHR siRNA transfection in TPC1, BCPAP and NTHY cells and determined the impact on mitogenic and invasive properties. By performing Western blotting experiments, we observed that in the interfered cells the activation of the most prominent oncogenic pathways (such as MAPK and AKT) was impaired (Figure 5B lower panels). To further characterize the efficiency of protein silencing we tested the same lysates for EPHRs expression, finding that the receptors were significantly reduced in the presence of their specific siRNA (Figure 5B upper panels). To then move to study the biological properties of the interfered cells, we verified whether knock-down of EPHRs would be able to impair cell migration into a "wound" that is created in a cell monolayer and to affect cell invasion of matrigel. Figure 5C shows how in TPC1 cells interfered with siRNAs targeting EPHA2, EPHA4 and EPHB2, there is a reduced ability to close the wound at 12 hours. Figure 5D shows instead how the same siRNA have also ability to impair matrigel invasion of TPC1 cells, supporting the hypothesis that EPHR may have a role in promoting not only mitogenesis but also gain of invasive and angiogenic properties in thyroid cancer cells.

DISCUSSION

Elucidation of the complex signaling pathways governing cancer cell growth and survival has allowed the rational design of targeted inhibitors. Still, a major challenge is that of determining which target to inhibit in each cancer type. The dependence of cancer cells on specific genetic lesions ("oncogene addiction") is under deep investigation, as these lesions are susceptible of pharmacological intervention (Luo *et al*., 2009). However, cancer cells can also be addicted to proteins that, though non mutated *per se*, still are crucial for cancer (but not for normal) cell viability. This phenomenon has been called "non-oncogene addiction" (Luo *et al*., 2009). Thus, as an example, RAS mutated cancer cells can in principle be eradicated by identifying proteins (other than RAS) to which they are addicted to. The identification of such Achilles' heels remains a formidable challenge. Moreover, also in those cases in which cancer-causing oncoprotein can be effectively targeted (for example BCR-ABL in CML), resistance may develop. In some cases, the resistance is mediated by secondary mutations in the oncoprotein that impairs drug binding; in other cases, resistance is caused by the activation of alternative pathways with which cancer cells escape the treatment (Gramza *et al*., 2009; Milojkovic *et al*., 2009).

RNAi technology has provided a powerful approach to tackle these tasks, because it allows searching for proteins to which cancer cells are addicted to or that mediate cancer cell resistance (Luo *et al*., 2009). We applied an RNAi-based screen to identify protein kinases to which thyroid cancer cells may are addicted to. We focused our attention on protein kinases (and associated proteins) because of their frequent involvement in human cancer (in thyroid cancer in particular) and because of their "druggability". Initially, we conducted the screening in the TPC1 cell line, expressing the RET/PTC1 rearrangement. Then, we extended the study to other thyroid cancer cell lines bearing BRAF or RAS oncogenes. At the end, we have identified a set of 20 genes that, when silenced, impaired the viability of the various thyroid

cancer cells. Importantly, sensitivity to knock-down of these genes was not cell line-specific and, therefore, not oncogene-specific (RET/PTC, BRAF, RAS). Indeed, on average, all the 4 cancer cell lines were equally susceptible to their blockade.

These findings anticipate that BRAF mutant thyroid cancers may be susceptible to the inhibition of most of our down hits, an important concept because BRAF mutations are recognized as risk factors for thyroid cancer to progress to radioiodine refractory disease (Xing, 2007). Inhibition of most of our 20 genes may exert efficacy also in RAS mutant thyroid cancers; this is also important because, as mentioned above, RAS oncoproteins have been difficult to be targeted directly. Moreover, several of the used cancer cell lines bear p53 mutations. Therefore, efficacy of our siRNAs was not negatively affected by p53 mutations; this is another important point given the role that p53 mutation exerts on cancer cell resistance to pharmacological therapy (Wiman, 2010). Finally, the two non tumorigenic thyroid cell types were in general refractory to the effects of the identified siRNAs, a fact that warrants a good therapeutic window for approaches aimed at inhibiting them in thyroid cancer.

None of our identified hits has been previously directly involved in thyroid cancer; exceptions were AKAP9 that was found rearranged with BRAF in radiation-associated PTC (Ciampi et al., 2005) and GRK4 that was found overexpressed in thyroid nodules (Voigt et al., 2004). Although our hits are involved in several pathways and cellular functions, the list was enriched for: i) EPHR; ii) SRC family kinases (FYN, HCK); iii) proteins involved in the p38 MAPK pathway (MAP3K6, MAP3K7IP1, MAPKAPK2) or other MAPK cascades (RPS6KA6 in the ERK; MAP3K6 in the JNK); iv) proteins involved in the PI3K/mTOR signaling (AKT2). Involvement of these cascades in thyroid cancer is well established. Moreover, both PI3K and ERK are key effectors of RET-derived oncogenes (Melillo *et al*., 2005; Lodyga *et al*., 2009). Also SRC family kinases were previously involved in RET/PTC signal transduction (Melillo *et al*., 1999) and as targets for kinase inhibitors in thyroid cancer

(Schweppe *et al*., 2009). Finally, JNK and p38MAPK were activated by RET/PTC (Chiariello *et al*., 1998) and p38 targeting was effective in reducing proliferation of TPC1 cells (Mariggiò *et al*., 2007). Blockage of the 20 hits quite homogenously affected cell proliferation but not cell survival. This suggests that they are primarily involved in sustaining proliferation. However, this does not exclude that specific hits may also exert additional functions. In fact, EPH receptors, for instance, were important also for cancer cell migration and invasion. RTK receptors of the EPH family were the largest group (8/21, 40%) among the hits identified. Indeed, four members of the A family (EPHA2, EPHA4, EPHA5, EPHA7) and two of the B family (EPHB2 and EPHB6), were included among them. All of them (with the exception of EPHA5, that was required for TPC1 and BCPAP only) were required for the viability of all thyroid cancer cells. Three of them (EPHA2, EPHA4 and EPHB2) were over-expressed in most of the neoplastic cell lines as compared to normal thyroid cells and were constitutively phosphorylated in different cancer cell lines but not in NTHY cells. Knock-down of EPHA2, EPHA4 and EPHB2 not only reduced proliferation and affected MAPK and AKT activation, but also impaired cell motility and invasiveness of TPC1 cells. Finally, EPHA2, and to a lower extent EPHA4 and EPHB2, were over-expressed in PTC and ATC comparing to normal thyroid specimens. Mechanism of overexpression and activation of EPH in thyroid cancer cells remain to be addressed. Intriguingly, EPH expression is stimulated by the RAS-RAF-ERK axis (Macrae *et al*., 2005); being virtually always activated in thyroid cancer (through RET, RAS or BRAF), this pathway may explain EPH overexpression in thyroid cancer cells. EPHB receptors bind promiscuously to the 3 transmembrane ephrins B (EFN-B), while EPHA receptors bind promiscuously to the 5 GPI-linked ephrins A (EFN-A). Interestingly, EFNA1, major ligand for EPHA2, EFNA4, ligand for EPHA4 and EFNB2, ligand for EPHB2 were also overexpressed in TPC1 and other thyroid cancer cells. EPH-EFN complexes emanate bidirectional signaling: forward signals that depend on EPH tyrosine-

kinase activity, and reverse signals depending on SRC family kinases associated to the cytosolic side of EFN (Pasquale, 2010). Forward signaling controls many functions including cell migration, invasion, proliferation ad survival. Among them, perhaps, the most typical EPH-mediated effect is the generation of a "repulsive" inter-cellular force that leads to cell-cell detachment and scattering (Pasquale, 2005). Importantly, such a migration-promoting role was exerted by EPHA2, EPHA4 and EPHB2 in thyroid cancer cells.

Our conclusion from these observations is that in thyroid cancer EPHA2, EPHA4 and EPHB2 are overexpressed and constitutively phosphorylated; moreover, their knock-down impair cell proliferation and inhibits migration and invasiveness. Therefore, these EPHs behave as *bona fide* oncogenes, and their inhibition with small molecule inhibitors has the potential to improve treatment of those cancers that are dependent on these molecules for their growth and invasiveness. However, whether these effects are opposite to those that EPH may mediate in normal thyrocytes and the biochemical mechanism for such a subversion need to be further investigated as well as more studies are required to clarify the EPH-EFN interaction in thyroid tumor as well as in tumor microenviroment (endothelial cells and pericytes) where it has been described to promote angiogenesis (Pasquale, 2010).

REFERENCES

1 Futreal PA, Coin L, Marshall M, Down T, Hubbard T, Wooster R, et al. A census of human cancer genes. *Nat Rev Cancer.* 2004;4(3):177-83.

2 Venter JC, Adams MD, Myers EW, Li PW, Mural RJ, Sutton GG, et al. The sequence of the human genome. *Science.* 2001;291(5507):1304-51.

3 Manning G, Whyte DB, Martinez R, Hunter T, Sudarsanam S. The protein kinase complement of the human genome. *Science.* 2002;298(5600):1912-34.

4 Greenman C, Stephens P, Smith R, Dalgliesh GL, Hunter C, Bignell G, et al. Patterns of somatic mutation in human cancer genomes. *Nature.* 2007;446(7132):153-8.

5 Santoro M, Carlomagno F, Hay ID, Herrmann MA, Grieco M, Melillo R, et al. Ret oncogene activation in human thyroid neoplasms is restricted to the papillary cancer subtype. *J Clin Invest.* 1992;89(5):1517-22.

6 Garcia-Rostan G, Zhao H, Camp RL, Pollan M, Herrero A, Pardo J, et al. ras mutations are associated with aggressive tumor phenotypes and poor prognosis in thyroid cancer. *J Clin Oncol.* 2003;21(17):3226-35.

7 Kimura ET, Nikiforova MN, Zhu Z, Knauf JA, Nikiforov YE, Fagin JA. High prevalence of BRAF mutations in thyroid cancer: genetic evidence for constitutive activation of the RET/PTC-RAS-BRAF signaling pathway in papillary thyroid carcinoma. *Cancer Res.* 2003;63(7):1454-7.

8 Soares P, Trovisco V, Rocha AS, Lima J, Castro P, Preto A, Máximo V, Botelho T, Seruca R, Sobrinho-Simões M. BRAF mutations and RET/PTC rearrangements are alternative events in the etiopathogenesis of PTC. *Oncogene.* 2003;22(29):4578-80.

9 Nikiforova MN, Lynch RA, Biddinger PW, Alexander EK, Dorn GW 2nd, Tallini G, et al. RAS point mutations and PAX8-PPAR gamma rearrangement in thyroid tumors: evidence for distinct molecular pathways in thyroid follicular carcinoma.

10 *J Clin Endocrinol Metab.* 2003;88(5):2318-26.

11 Nikiforova MN, Kimura ET, Gandhi M, Biddinger PW, Knauf JA, Basolo F, et al. BRAF mutations in thyroid tumors are restricted to papillary carcinomas and anaplastic or poorly differentiated carcinomas arising from papillary carcinomas.

12 *J Clin Endocrinol Metab.* 2003;88(11):5399-404.

13 Frattini M, Ferrario C, Bressan P, Balestra D, De Cecco L, Mondellini P, et al. Alternative mutations of BRAF, RET and NTRK1 are associated with similar but distinct gene expression patterns in papillary thyroid cancer. *Oncogene.* 2004;23(44):7436-40.

14 Elisei R, Ugolini C, Viola D, Lupi C, Biagini A, Giannini R, et al. BRAF(V600E) mutation and outcome of patients with papillary thyroid carcinoma: a 15-year median follow-up study. *J Clin Endocrinol Metab.* 2008;93(10):3943-9.

15 Santoro M and Carlomagno F. Drug insight: Small-molecule inhibitors of protein kinases in the treatment of thyroid cancer. *Nat Clin Pract Endocrinol Metab.* 2006;2(1):42-52.

16 Schlumberger M and Sherman SI. Clinical trials for progressive differentiated thyroid cancer: patient selection, study design, and recent advances. *Thyroid.* 2009;19(12):1393-400.

17 Sherman SI. Tyrosine kinase inhibitors and the thyroid. *Best Pract Res Clin Endocrinol Metab.* 2009;23(6):713-22.

18 Berns K, Horlings HM, Hennessy BT, Madiredjo M, Hijmans EM, Beelen K, et al. A functional genetic approach identifies the PI3K pathway as a major determinant of trastuzumab resistance in breast cancer. *Cancer Cell.* 2007;12(4):395-402.

19 Westbrook TF, Stegmeier F, Elledge SJ. Dissecting cancer pathways and vulnerabilities with RNAi. *Cold Spring Harb Symp Quant Biol.* 2005;70:435-44.

20 MacKeigan JP, Murphy LO, Blenis J. Sensitized RNAi screen of human kinases and phosphatases identifies new regulators of apoptosis and chemoresistance. *Nat Cell Biol.* 2005;7(6):591-600.

21 Cerutti J, Trapasso F, Battaglia C, Zhang L, Martelli ML, Visconti R, et al. Block of c-myc expression by antisense oligonucleotides inhibits proliferation of human thyroid carcinoma cell lines. *Clin Cancer Res.* 1996;2(1):119-26.

22 Ohta K, Endo T, Haraguchi K, Hershman JM, Onaya T. Ligands for peroxisome proliferator-activated receptor gamma inhibit growth and induce apoptosis of human papillary thyroid carcinoma cells. *J Clin Endocrinol Metab.* 2001;86(5):2170-7.

23 Basolo F, Giannini R, Toniolo A, Casalone R, Nikiforova M, Pacini F, et al. Establishment of a non-tumorigenic papillary thyroid cell line (FB-2) carrying the RET/PTC1 rearrangement. *Int J Cancer.* 2002;97(5):608-14.

24 Curcio F, Ambesi-Impiombato FS, Perrella G, Coon HG. Long-term culture and functional characterization of follicular cells from adult normal human thyroids. *Proc Natl Acad Sci U S A*. 1994;91(19):9004-8.

25 Pasquale EB. Eph receptor signalling casts a wide net on cell behaviour. *Nat Rev Mol Cell Biol.* 2005;6(6):462-75

26 Luo J, Solimini NL, Elledge SJ. Principles of cancer therapy: oncogene and non-oncogene addiction. *Cell.* 2009;136(5):823-37.

27 Gramza AW, Corless CL, Heinrich MC. Resistance to Tyrosine Kinase Inhibitors in Gastrointestinal Stromal Tumors. *Clin Cancer Res.* 2009;15(24):7510-7518.

28 Milojkovic D and Apperley J. Mechanisms of Resistance to Imatinib and Second-Generation Tyrosine Inhibitors in Chronic Myeloid Leukemia. *Clin Cancer Res* 2009;15(24): 7519-7527.

29 Xing M. BRAF mutation in papillary thyroid cancer: pathogenic role, molecular bases, and clinical implications. *Endocr Rev.* 2007;28(7): 742-62.

30 Wiman KG. Pharmacological reactivation of mutant p53: from protein structure to the cancer patient. *Oncogene.* 2010;29(30): 4245-52.

31 Ciampi R, Knauf JA, Kerler R, Gandhi M, Zhu Z, Nikiforova MN, et al. Oncogenic AKAP9-BRAF fusion is a novel mechanism of MAPK pathway activation in thyroid cancer. *J Clin Invest.* 2005;115(1):94-101.

32 Voigt C, Holzapfel HP, Meyer S, Paschke R. Increased expression of G-protein-coupled receptor kinases 3 and 4 in hyperfunctioning thyroid nodules. *J Endocrinol.* 2004;182(1):173-82.

33 Melillo RM, Castellone MD, Guarino V, De Falco V, Cirafici AM, Salvatore G, et al. The RET/PTC-RAS-BRAF linear signaling cascade mediates the motile and mitogenic phenotype of thyroid cancer cells. *J Clin Invest.* 2005;115(4):1068-81.

34 Lodyga M, De Falco V, Bai XH, Kapus A, Melillo RM, Santoro M et al. XB130, a tissue-specific adaptor protein that couples the RET/PTC oncogenic kinase to PI 3-kinase pathway. *Oncogene.* 2009;19;28(7):937-49.

35 Melillo RM, Barone MV, Lupoli G, Cirafici AM, Carlomagno F, Visconti R, et al. Ret-mediated mitogenesis requires Src kinase activity. *Cancer Res.* 1999;59(5):1120-6.

36 Schweppe RE, Kerege AA, French JD, Sharma V, Grzywa RL, Haugen BR. Inhibition of Src with AZD0530 reveals the Src-Focal Adhesion kinase complex as a novel therapeutic target in papillary and anaplastic thyroid cancer. *J Clin Endocrinol Metab.* 2009;94(6):2199-203.

37 Chiariello M, Visconti R, Carlomagno F, Melillo RM, Bucci C, de Franciscis V,et al. Signalling of the Ret receptor tyrosine kinase through the c-Jun NH2-terminal protein

kinases (JNKS): evidence for a divergence of the ERKs and JNKs pathways induced by Ret. *Oncogene.* 1998;16(19):2435-45.

38 Mariggiò S, Filippi BM, Iurisci C, Dragani LK, De Falco V, Santoro M, et al. Cytosolic phospholipase A2 alpha regulates cell growth in RET/PTC-transformed thyroid cells. *Cancer Res.* 2007;67(24):11769-78.

39 Macrae M, Neve RM, Rodriguez-Viciana P, Haqq C, Yeh J, Chen C, Gray JW, McCormick F. A conditional feedback loop regulates Ras activity through EphA2. *Cancer Cell.* 2005;8(2):111-8.

40 Pasquale EB. Eph receptors and ephrins in cancer: bidirectional signalling and beyond. *Nat Rev Cancer.* 2010;10(3):165-80.

Table 1: List of identified down hits.

Symbol	Gene name	GenbankID
AGC	**protein kinase C family**	
AKT2	v-akt murine thymoma viral oncogene homolog 2	NM_001626
CIT	citron (rho-interacting, ser/thre kinase 21)	NM_007174
PKN1	protein kinase N1	NM_002741
PRKACB	protein kinase cAMP dependent, catalitic, beta	NM_182948
RPS6KA6	ribosomal protein S6 kinase, 90kDa, polypeptide 6	NM_014496
Atypical		
SMG1	PI-3-kinase-related kinase SMG-1	NM_014006
CAMK	**calcium/calmodulin-dependent protein kinases**	
CAMKIINα	calcium/calmodulin-dependent protein kinase	NM_018584
CIB3	calcium and integrin binding family member 3	NM_054113
STK33	serine/threonine kinase 33	NM_030906
CK1		
CSNK1G2	casein kinase 1, gamma 2	NM_001319
CMGC		
CDK4	cyclin-dependent kinase 4	NM_000075
HIPK1	homeodomain interacting protein kinase 1	NM_152696
PLK3	polo-like kinase 3	NM_004073
KAP	**Kinase-associated protein**	
AKAP9	A kinase (PRKA) anchor protein (yotiao) 9	NM_005751
MAP2K1IP1	mitogen-activated protein kinase kinase 1 interacting protein 1	NM_021970
MAP3K7IP1	mitogen-activated protein kinase kinase kinase 7 interacting protein 1	NM_006116
Other		
AAK1	AP2 associated kinase 1	NM_014911
AK3	adenylate kinase 3	NM_013410
CDKN2A	cyclin-dependent kinase inhibitor 2A	NM_000077
DGKB	diacylglycerol kinase, beta 90kDa	NM_004080
GRK4	G protein-coupled receptor kinase 4	NM_182982
IHPK3	inositol hexaphosphate kinase 3	NM_054111
ITPKA	inositol 1,4,5-trisphosphate 3-kinase A	NM_002220
NEK3	NIMA (never in mitosis gene a)-related kinase 3	NM_002498
PIP5K1C	phosphatidylinositol-4-phosphate 5-kinase, type I, γ	NM_012398
SORCS3	sortilin-related VPS10 domain containing receptor 3	NM_014978
TK1	thymidine kinase 1, soluble	NM_003258
UCKL1	uridine-cytidine kinase 1-like 1	NM_017859
ULK4	unc-51-like kinase 4	NM_017886
STE	**MAPK cascade family**	
MAP3K6	mitogen-activated protein kinase kinase kinase 6	NM_004672
MAP4K1	mitogen-activated protein kinase kinase kinase kinase 1	NM_007181
MAPK7	mitogen-activated protein kinase 7	NM_002749
MAPKAPK2	mitogen-activated protein kinase-activated protein kinase 2	NM_004759
MARCKS	myristoylated alanine-rich protein kinase C substrate	NM_002356
PAK2	p21 (CDKN1A)-activated kinase 2	NM_002577
PXK	PX domain containing serine/threonine kinase	NM_017771
STK10	serine/threonine kinase 10	NM_005990
TK	**tyrosine kinases**	
EPHA2	EPH receptor A2	NM_004431
EPHA4	EPH receptor A4	NM_004438
EPHA5	EPH receptor A5	NM_004439
EPHA7	EPH receptor A7	NM_004440
EPHB2	EPH receptor B2	NM_017449
EPHB6	EPH receptor B6	NM_004445
FYN	FYN oncogene	NM_002037
HCK	hemopoietic cell kinase	NM_002110
TKL	**tyrosine kinases like**	

ACVR1B	Ser/ Thr protein kinase receptor R2 precursor	NM_004302
ACVRL1	Ser/ Thr protein kinase receptor R3 precursor,	NM_000020
LIMK1	LIM domain kinase 1	NM_002314
TESK1	testis-specific kinase 1	NM_006285

FIGURE LEGENDS

Figure 1: Confirmation screening in TPC1 cells.

TPC1 cells were transfected with two independent siRNAs, targeting different regions of the 49 identified genes. Results of cell titer blue are shown. Our confirmed hits were those siRNAs that reduced viability of at least 25% (loess log ≤-0.5, shown as dotted line). The values shown are the means of two siRNAs transfections and the bars represent the upper and lower 95% confidence intervals for three independent experiments. ∗*P*= .05.

Figure 2: Validation screening in thyroid cell lines.

Several thyroid normal (Nthy-ori 3-1 and P5) and cancer cell lines (BCPAP, CAL62 and 8505C) were transfected with siRNAs targeting our identified 20 down hits. The values represent cell titer blue incorporation, expressed as Loess Log of cell viability. Values of three independent experiments with upper and lower 95% confidence intervals are shown. ∗*P*= .05.

Figure 3: Effect of siRNAs on cell proliferation.

TPC1 and NTHY were transfected with siRNAs targeting our 20 hits and S-phase entry was monitored by using luminescence. Proliferation obtained from scrambled transfected cells was normalized as 100%, and the values shown are the means and upper 95% confidence intervals for three independent experiments. ∗*P*= .05.

Figure 4: Expression analysis of EPHs in human thyroid cell lines and samples.

EPHA2, EPHA4 and EPHB2 expression level was analyzed in a panel of thyroid cancer cell lines of different genotype and hystotype (see also Table S1). The bar graphs illustrate the ß-actin normalized EPHs (**A**) and ephrines (**B**) mRNA levels in cancer cells relative to those of normal cells and in patient samples relative to those of normal thyroid tissues. Data shown are

the mean values and upper 95% confidence intervals of the intensity levels from three independent PCR amplifications. ∗*P*= .05. ∗∗*P*= .01.

Figure 5, A: EPHs protein and phosphorylation levels. EPHA2, EPHA4 and EPHB2 immunoprecipitation show higher levels in cancer cells compared to normal cells (upper lane); moreover, although with differences among the cell lines, cancer cells express more phosphorylated protein (middle lane). Protein have been normalized on tubulin expression levels (lower lane). **B:** Knock-down of EPHs impairs activation of MAPK and AKT signaling pathways. TPC1 and NTHY have been transfected with siRNA against EPHA2, EPHA4 and EPHB2 receptors. After testing efficiency of silencing with specific EPH antibodies, we probed the same lysates for phosphorylation (activation) of MAPK and AKT. Our data show that all the three EPHs are somehow affecting MAPK and AKT activation , as their silencing impairs the phosphorylation of both pathways. Normalization has been performed using tubulin antibody. **C:** EPHs control migration and invasion of thyroid cancer cells. Wounds of 300 μM width were set in a 80% confluent monolayer of TPC1 scrambled or EPHA2, EPHA4 and EPHB2 interfered. The vertical dotted lines indicate the margins of wound. Representative micrographs are shown. Magnification = ×10. Scale bar = 200 μM. Closure of the wound 12 at hours was measure and scrambled transfection was used as control. The means and 95% confidence intervals (error bars) from three independent experiments are presented. P values were calculated using two-sided Student t test. ∗∗*P*= .01. **D:** Cell migration was analyzed using Boyden chamber assay and expressed as percentage of solvent-treated TPC1 scrambled interfered cells. The means and 95% confidence intervals (error bars) from three independent experiments are presented. P values were calculated using two-sided Student t test. ∗*P*= .05. ∗∗*P*= .01.

FIGURES

Figure 1: Confirmation screening in TPC1 cells.

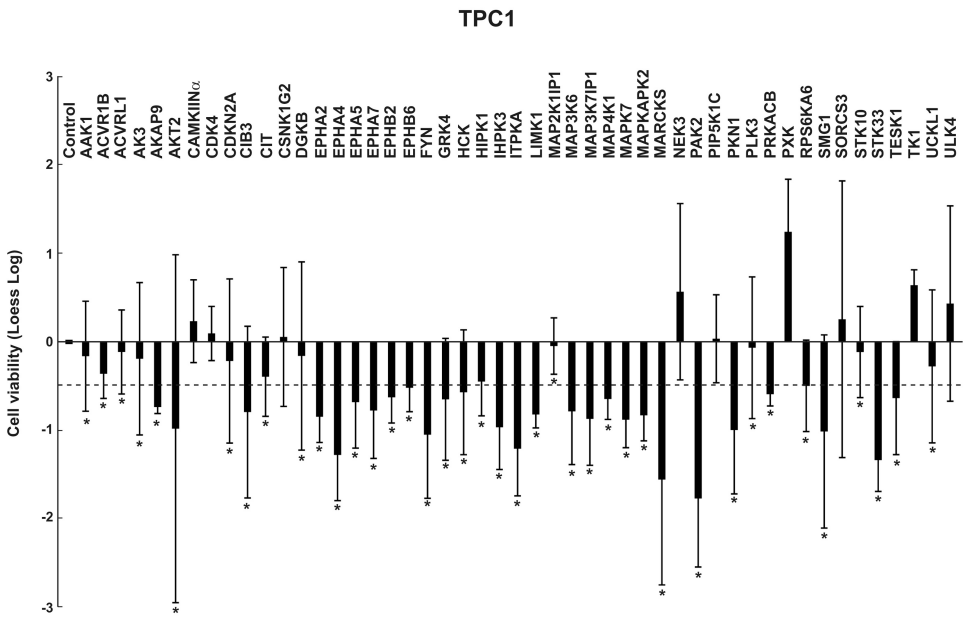

Figure 2: Validation screening in thyroid cell lines.

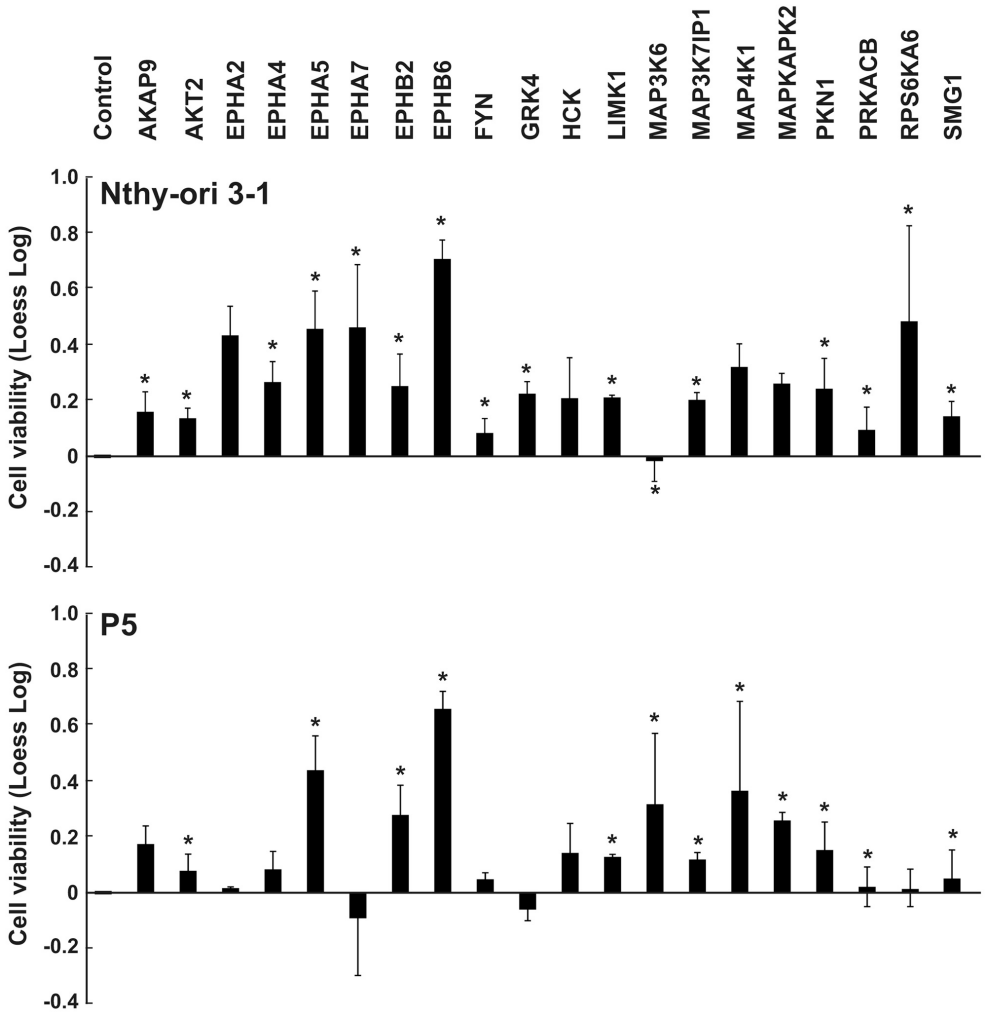

Figure 2: Validation screening in thyroid cell lines (cont'nd).

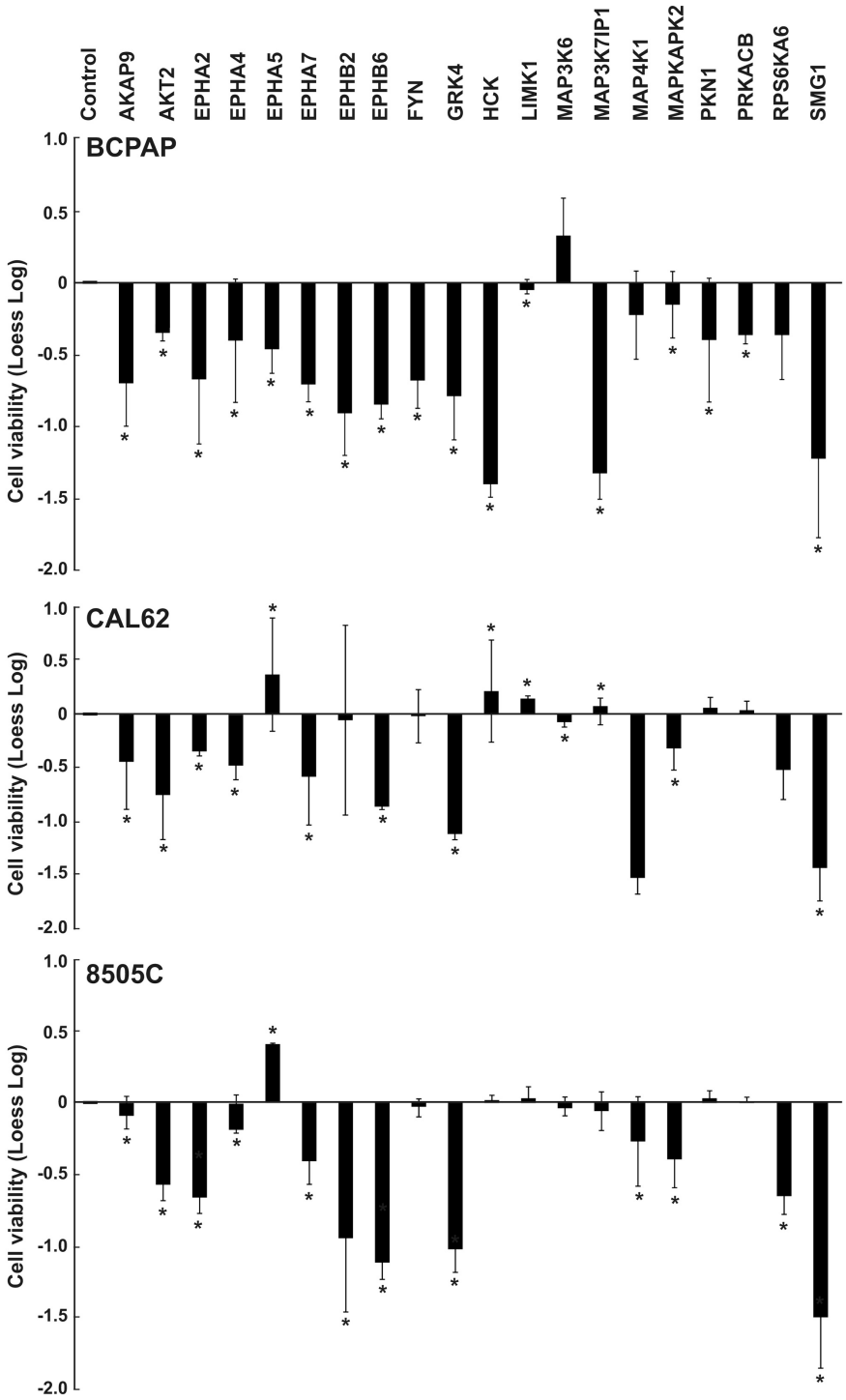

Figure 3: Effect of siRNAs on cell proliferation.

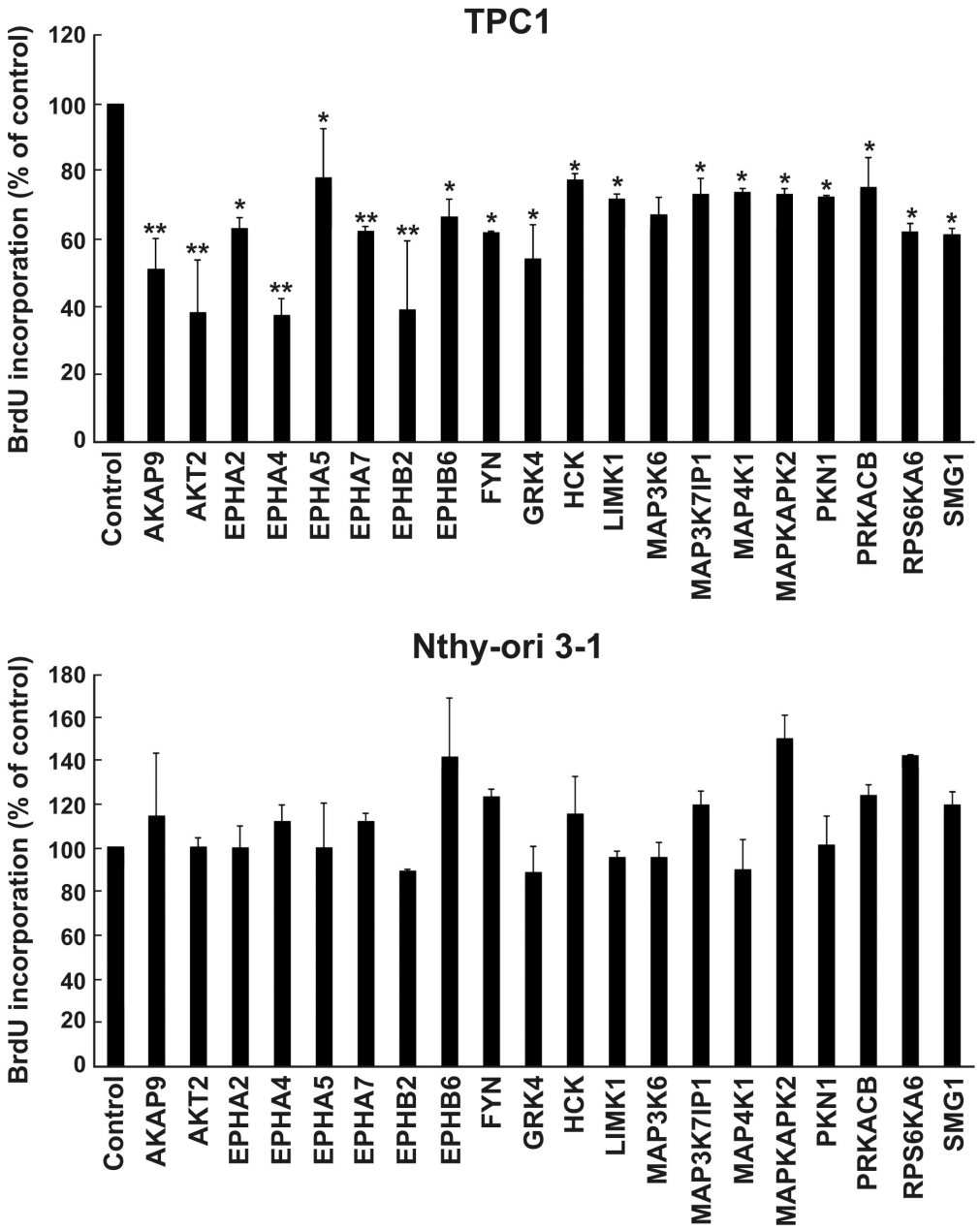

Figure 4: Expression analysis of EPHs in human thyroid cell lines and samples.

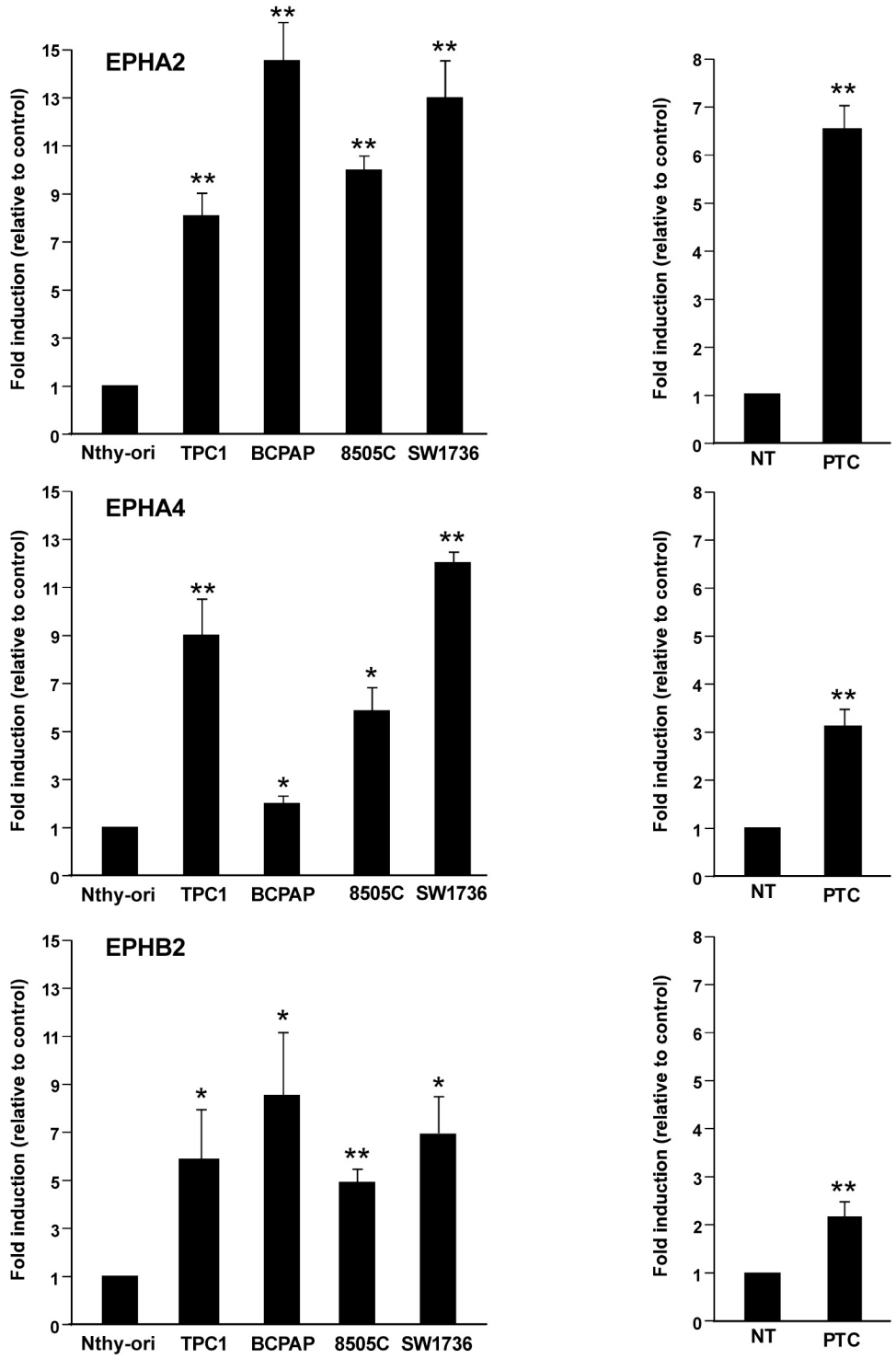

Figure 4: Expression analysis of EPHs in human thyroid cell lines and samples (cont'nd)

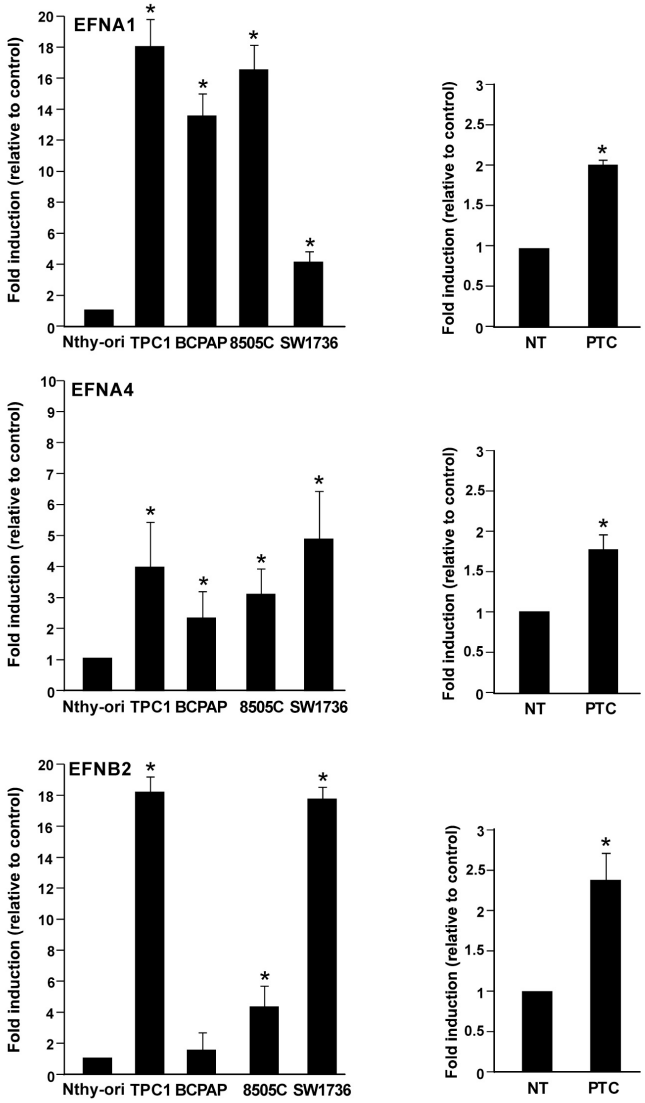

Figure 5: EPHs protein and phosphorylation levels

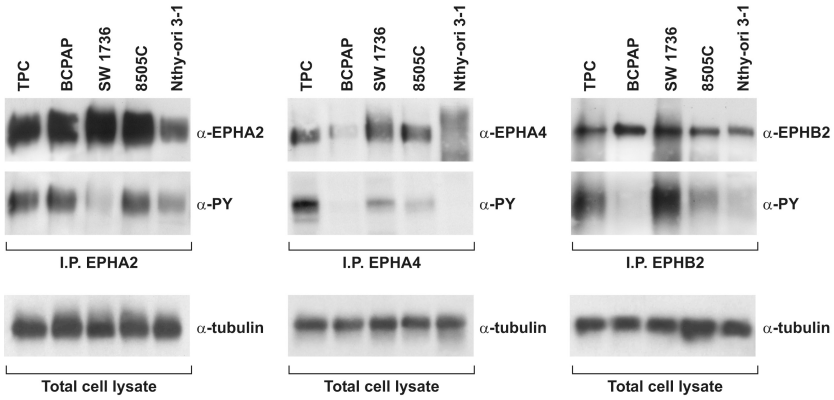

Figure 5: EPHs protein and phosphorylation levels (cont'nd).

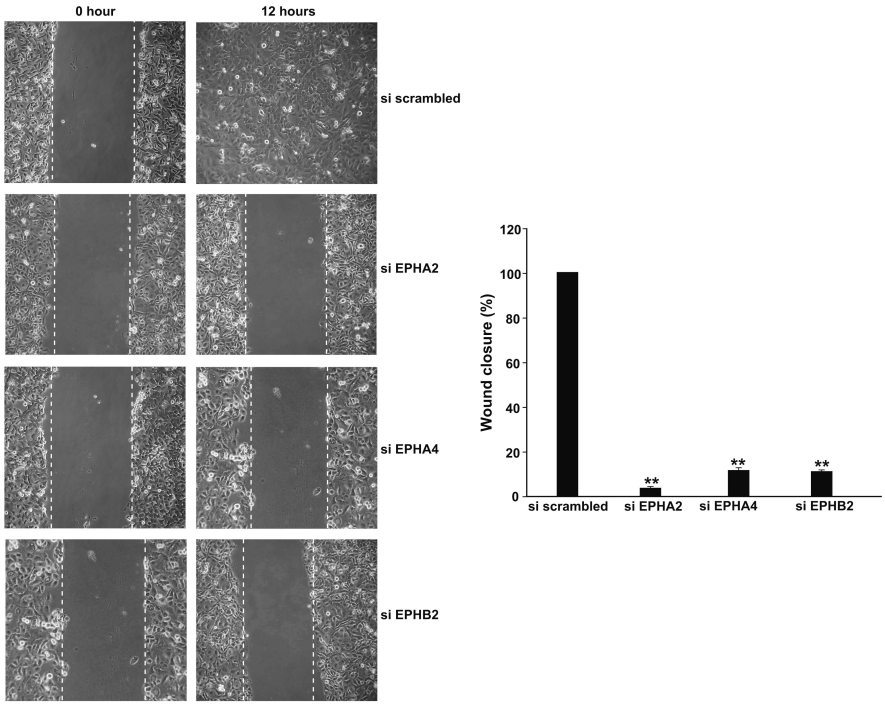

Figure 5: EPHs protein and phosphorylation levels (cont'nd).

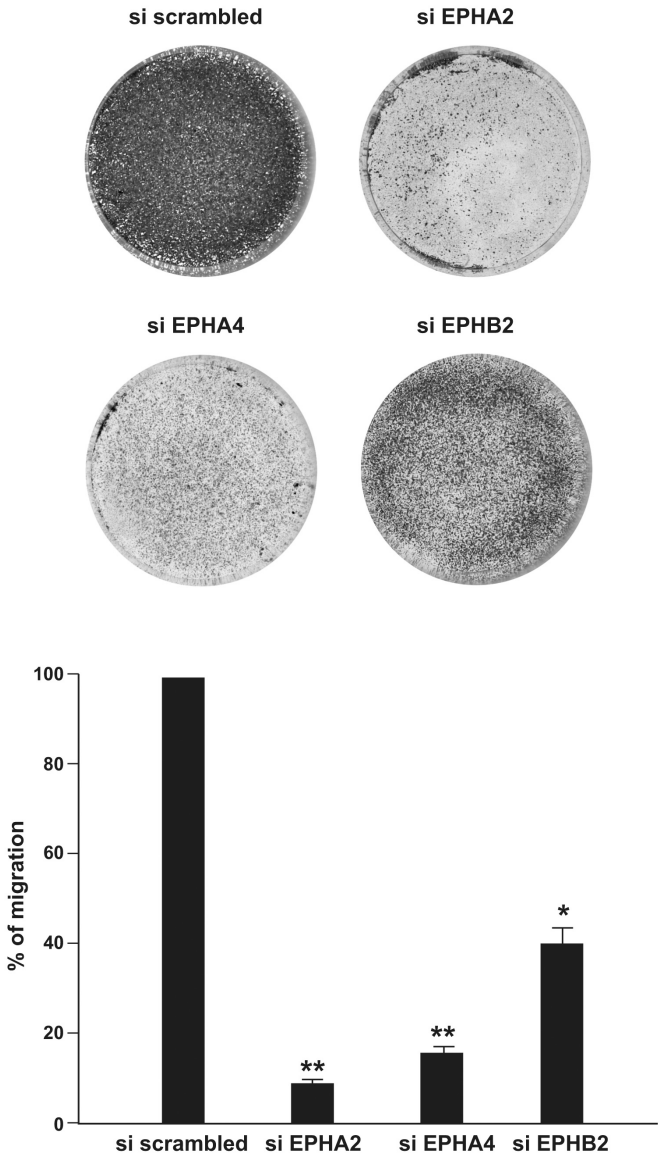

Figure 5: EPHs protein and phosphorylation levels (cont'nd).

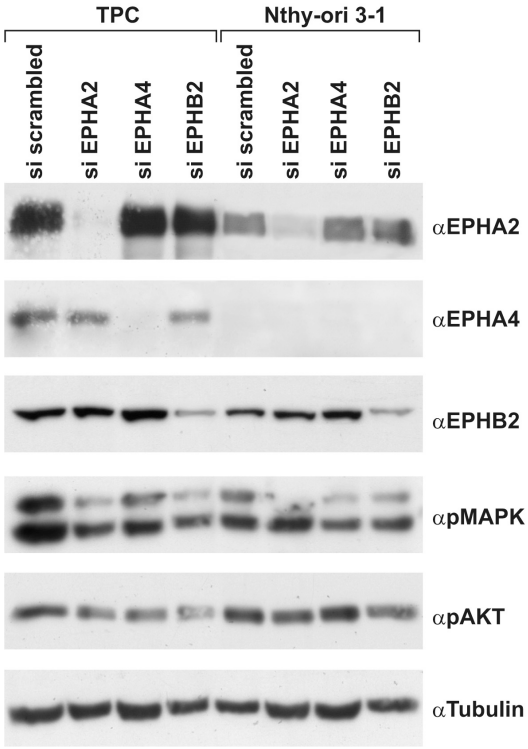

Identification of EPHRs as new mediators of thyroid carcinogenesis through an RNA interference screening.

Maria D. Castellone et al.

Supplementary Informations

Supplementary Tables

Table S2: List of used cells lines

Cell line	Type	Oncogene
BCPAP	PTC	Braf V600E
CAL62	ATC	KRAS
NTH-ory 3-1	NT	-
P5	NT	-
SW1736	ATC	Braf V600E
TPC1	PTC	RET/PTC1
8505C	ATC	Braf V600E

Table S3: List of used siRNA

	siRNA1	siRNA2	siRNA3	siRNA4
AAK1	SI02224579	SI02224586	SI00108717	SI00108724
ACVR1B	SI02622046	SI00288127	SI03070977	SI03117107
ACVRL1	SI02659972	SI00000154	SI02758392	SI04894687
AK3	SI02224453	SI02224460	SI03084305	SI03102253
AKAP9	SI00080948	SI03024854	SI02223963	SI02223970
AKT2	SI00299166	SI00287672	SI00299173	SI00287679
CAMKIINalpha	SI02224873	SI02224880	SI00112882	SI00112889
CDK4	SI00604744	SI00001428	SI00299789	SI00299803
CDKN2A	SI02659503	SI02664396	SI02664403	SI00299817
CIB3	SI02225223	SI02225230	SI02647666	SI02647673
CIT	SI02224243	SI00095088	SI00095074	SI04438840
CSNK1G2	SI00605171	SI00605178	SI03073217	SI03105690
DGKB	SI02225265	SI02225272	SI03043103	SI03050551
EPHA2	SI02223508	SI04434990	SI00300181	SI00300188
EPHA4	SI04435018	SI04435025	SI02223522	SI02223529
EPHA5	SI00063686	SI00063672	SI02223536	SI00287511
EPHA7	SI00063707	SI03091851	SI02223543	SI02223550
EPHB2	SI02642626	SI02224796	SI02224789	SI04026330
EPHB6	SI00063805	SI00063826	SI02665292	SI02758441
FYN	SI02654729	SI02659545	SI00605451	SI03095218
GRK4	SI02649920	SI02622501	SI02622508	SI03032092
HCK	SI02627807	SI02665320	SI02659986	SI02665327
HIPK1	SI00288001	SI00288008	SI03054233	SI04903899
IHPK3	SI02659846	SI02659853	SI04441318	SI00148092
ITPKA	SI00605500	SI00605507	SI00034482	SI00034489
LOC392265	SI00538776			
LIMK1	SI00036057	SI00605542	SI00605549	SI00036064
MAP2K1IP1	SI02225027	SI02225034	SI00131845	SI00131859
MAP3K6	SI00066955	SI04438042	SI00288218	SI00288225
MAP3K7IP1	SI04900049	SI02660329	SI02758903	SI04952311
MAP4K1	SI00095130	SI04438854	SI02224250	SI02224257
MAPK7	SI00606039	SI02629445	SI00606046	SI03024924
MAPKAPK2	SI00068033	SI00068012	SI02223697	SI00288246
MARCKS	SI00605584	SI00605591	SI00036603	SI04897060
MGC4796	SI00287910	SI00287917	SI00141687	SI00141694
NEK3	SI02225293	SI02225300	SI04897193	SI04897193
PAK2	SI00039802	SI00605710	SI00301077	SI00301084
PIP5K1C	SI02224376	SI00099953	SI02758966	SI00099967
PKN1	SI00042350	SI00605962	SI00605955	SI00042357
PLK3	SI02223466	SI00059388	SI02223473	SI00059395
PRKACB	SI03063228	SI03022740	SI02225468	SI02225461
PXK	SI02224817	SI02224824	SI00119609	SI00119616
RPS6KA6	SI00106603	SI04379592	SI00287609	SI02659748
SMG1	SI02640148	SI00102753	SI02622333	SI00102767
SORCS3	SI00108983	SI02641100	SI00108990	SI00108997
STK10	SI02224047	SI02224054	SI04713569	SI04713576
STK33	SI02660210	SI02660203	SI02660217	SI00139741
TESK1	SI02224117	SI02224124	SI04379522	SI00086919
TK1	SI00049931	SI02223193	SI02223200	SI02223200
UCKL1	SI00288484	SI00288491	SI04439939	SI04439939
ULK4	SI04901631	SI04025490	SI02812061	SI02812068

Table S4: List of primers used for QPCR

	REVERSE	FORWARD
AAK1	GGGTTTTGGTTGGGGAAC	AAGAGGGCCACTGTTCAGC
ACVR1B	GGCAGCTGATATTCTTCATGG	ATATTGGGAGATTGCTCGAAGA
ACVRL1	CTGCTCCGAAGGAGGTTG	CCACCTCTGCAACCACAA
AK3	GCTTTCTGGCTTCTTTGTGG	TCTCATTCAGCGTGAGGATG
AKAP9	CTTTGTCGAAACTGGGCAAG	GGAGGACGAGGAGAGACAGA
AKT2	ACACACCCCAGCTGCCCTCA	CGCCAAGCCCAACCACTCTGG
CAMKIINalpha	GAGGCCAGCAACAGATTCTC	GGAGGGACACCACTACCTGA
CDK4	AGGGAGACCCTCACGCCAGC	CTCTGCGTCCAGCTGCTCCG
CDKN2A	AAAACCCTCACTCGCGGCGG	GTGCGTGGGTCCCAGTCTGC
CIB3	TCACGGAAAACATGTCCAAA	CTCGTGCCCCTCGACTATAC
CIT	CAGAAGGAGGTGGAGCTGAA	CTTGCTCCAAACTTCGCTTT
CSNK1G2	AGTTCAACGCCTGGTTTTTG	CTTCGAGAAGCCCGACTATG
DGKB	CTCCTGAAGTGGGCAGAGTC	GGACTGCATTGTGTTTGGTG
EPHA2	CCAGGCAGGCTACGAGAA	GGCTCTCAGATGCCTCAAAC
EPHA4	TCCAAGTTCACAGATGTCTCGTTGAC	TCTATGCCCTGCACCCGTCCA
EPHA5	TCTGGAGGACGTGCCTTCTCCT	TGACAGTGCGTGAATCCAAT
EPHA7	GGTCAGATGGAGCCCTGTAA	AAGCAGGCTACCAGCAAAAA
EPHB2	CCAGCAGAACTTGCATCTTG	TCTTTGGAGGGCCTGGAT
EPHB6	CGGAACTCCTGCTCTATTGC	TGCTGGTGAATAGCCACTTG
FYN	CATCTTTTCGGCCAAGTTTT	CAGCAATTATGTGGCTCCAG
GRK4	CACAATCACTTCGGTCCTCA	GAGGCACATTGAATTCTTGGA
HCK	GCAATCTGGGCTGAGAAGTC	TGGCAGTGAAGACGATGAAG
HIPK1	TTTTGTGAAGCTATTGATATGTGGT	GCAAGCCTTGTGTTTGTGAA
IHPK3	GAGCATACGGTGTGCAAGC	AGAGGTGCACTGTGACGGTA
ITPKA	TACATGTCCTTCCGCAGCTT	GTGTGCTCGACTGCAAAATG
LOC392265		
LIMK1	TGTCCTTGGCAAAGCTCACT	GGGGCATCATCAAGAGCA
MAP2KIP1	TGTCAGATAGAGATGGAGTACCTGTT	AAACCAGGTCGCAAAGCAT
MAP3K6	CGGGGGAGATGTTGGAGT	TCTCCTTGATGGCGATGC
MAP3K7IP1	CTGAGCCAACCCCAGAGA	GGAGCTTGCTGCAGAGTGA
MAP4K1	GCCACCAAGATGCTCAGTC	CCGGGATTCTTCAGTTTGTC
MAPK7	GGTCGCTTTCCATCAGGTC	AAATGGCGGACACAATTCC
MAPKAPK2	TCTCGTACACATCCACGATCC	GAGGACCCAGGAGAAATTCG
MARCKS	TTTACCTTCACGTGGCCATT	ATGGGTGCCCAGTTCTCC
MGC4796	TCCGCTTCATTCTCAGCTCT	AGCATGACCACAGACCCATT
NEK3	TATTAGGGTGTTTCATTTTGGCTA	GCCATGAAAGAAATAAGGCTTC
PAK2	GATAACGGTTTGGCCAGTTTC	AAGGGGTTCAGCCAAAGAAT
PIP5K1C	CTGGGTCGGGGGCTGCATAGA	CACCGACATCTACTTTCCCACCG
PKN1	CTCTTCGATGCGCAGCTC	CACATCCGCATGCAACT
PLK3	GTGGTCCCCGTAGAAGTTCA	CTACATGGAGCAGCACCTCA
PRKACB	CTTTGGCTAGAAACTCTTTCACG	TGACCCCTTCTTGCCATC
PXK	GGGCCAAGGTCAGCCCAGCTTA	GAACCAAAGTGGGAGGTGGTGGA
RPS6KA6	GCAACTCAAACTGTGCAGGA	CGGCGAGGTAAATGGTCTTA
SMG1	GCACTATCAGTTCTGGGTTGCCAGT	TAATGAGCCGCAGAGCCCCGG
SORCS3	TTCCTCTCAGGTCCACATCC	ACGCGTGGGATTTACTTCAC
STK10	CTTCGGCAAGGTTTACAAGG	TCAATCTCCACGATGTAGTCCTC
STK33	TGTAATTGGCATCAGGGACA	CTTCGGTGAGACCAACCAAT
TESK1	GGTGCTGGGTTCCAGGTT	AACTCTGGTGGGGGATGACT
TK1	AATGGCTTCCTCTGGAAGGT	AGACACTCGCTAACAGCAGCA
UCKL1	GGTAAGCTGGTTGTTCTGGA	TTCAGGACTGCGTCGTACAG
ULK4	ACCCCTCACAACTTCTGGTG	GGCAAAAGTGGAAGGTGAAA

Supplementary Figures

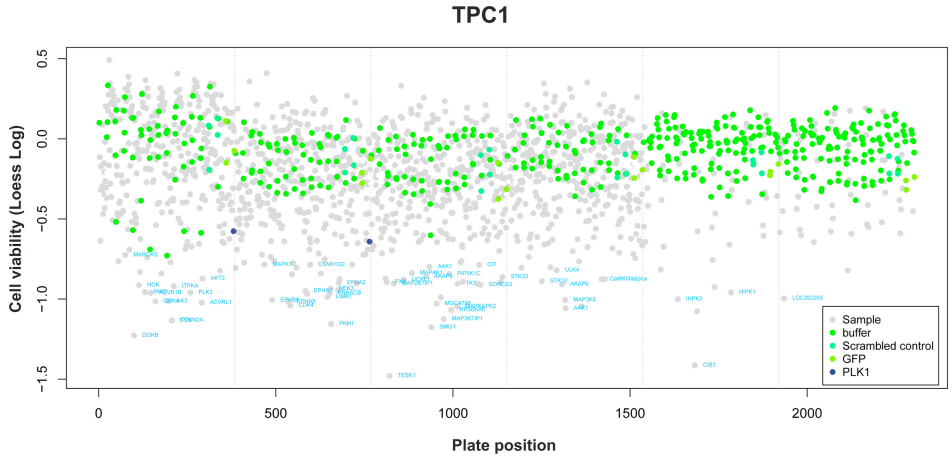

Figure S1: Plot of screening data.

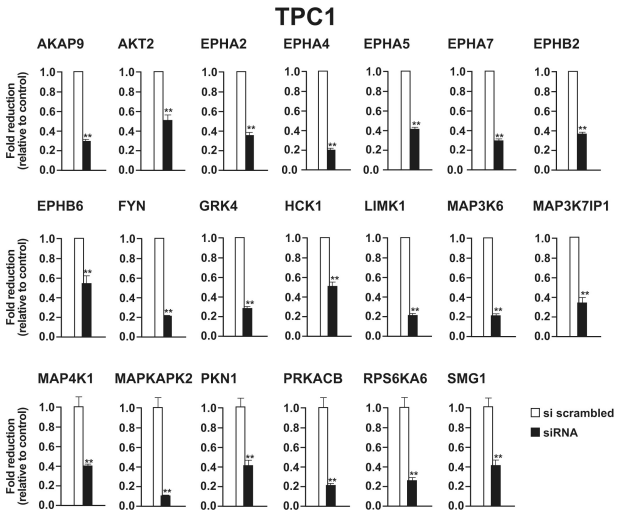

Figure S2, S3: All used siRNAs silence their specific targets. Gene expression of the 20 down hits has been tested in TPC1 (**S2**) and NTHY (**S3**) cells transfected with their siRNAs compared to control, scrambled transfected, cells. Hystograms express fold reduction compared to control. Error bars represent upper 95% confidence intervals from three independent experiments. ∗*P*= .05. ∗∗*P*= .01.

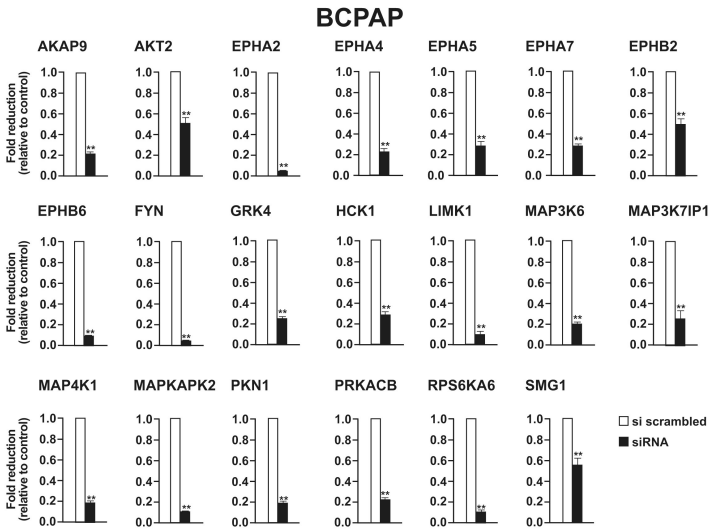

Figure S2, S3: All used siRNAs silence their specific targets. Gene expression of the 20 down hits has been tested in TPC1 (**S2**) and NTHY (**S3**) cells transfected with their siRNAs compared to control, scrambled transfected, cells. Hystograms express fold reduction compared to control. Error bars represent upper 95% confidence intervals from three independent experiments. ∗*P*= .05. ∗∗*P*= .01.

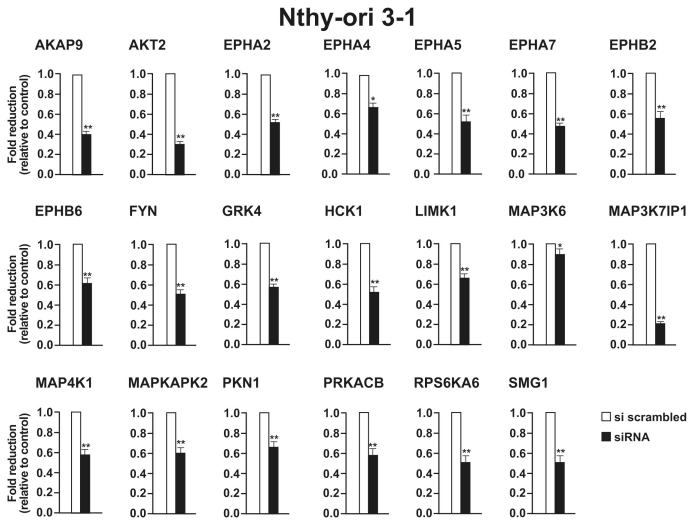

Figure S4, S5: Knock-down of our down hits reduce number of thyroid cancer cells but not of normal cells. Cell count was performed 72 hours after transfection of siRNA in TPC1 (**S4**) and NTHY (**S5**) cells. Error bars represent upper 95% confidence intervals from three independent experiments. ∗*P*= .05. ∗∗*P*= .01.

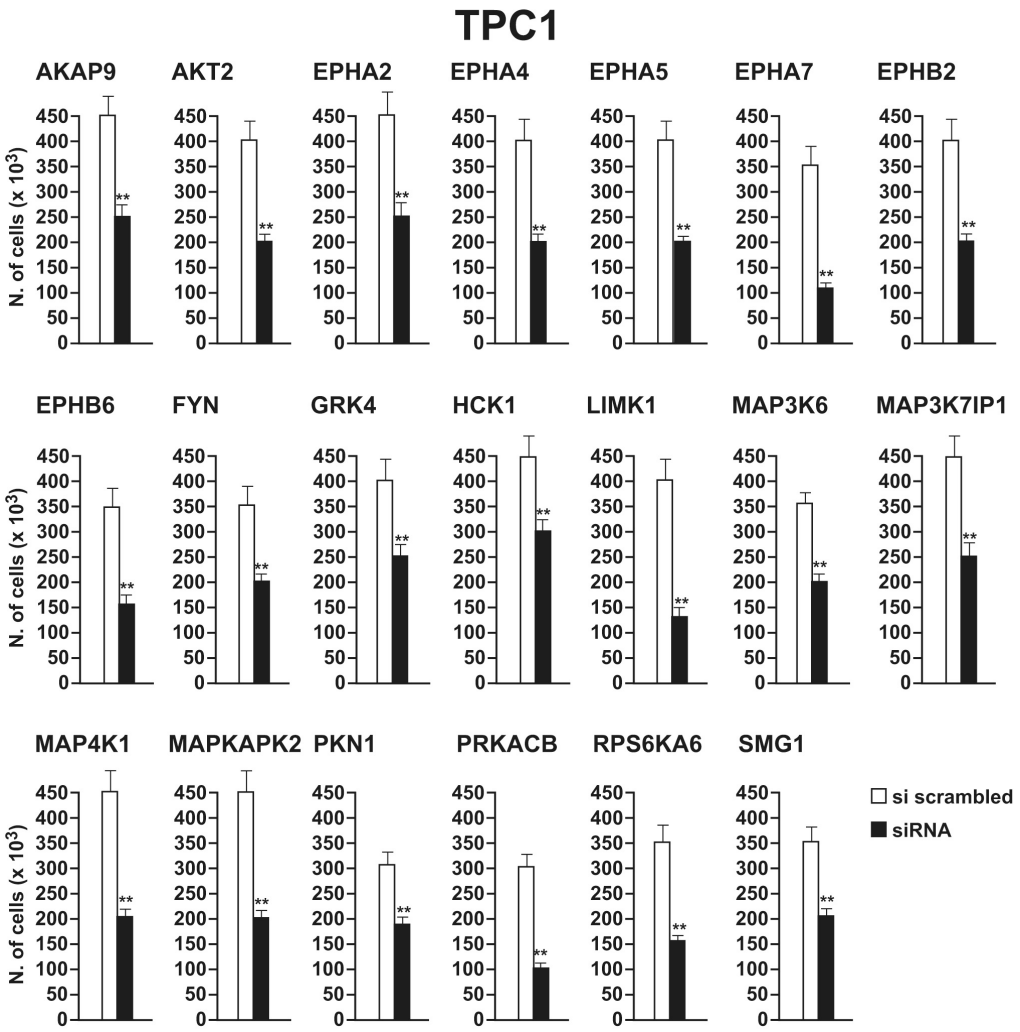

Figure S4, S5: Knock-down of our down hits reduce number of thyroid cancer cells but not of normal cells. Cell count was performed 72 hours after transfection of siRNA in TPC1 (**S4**) and NTHY (**S5**) cells. Error bars represent upper 95% confidence intervals from three independent experiments. ∗*P*= .05. ∗∗*P*= .01.

Attached Manuscript #IV

Castellone MD, De Falco V, Rao DM, **Bellelli R**, Muthu M, Basolo F, Fusco A, Gutkind JS, Santoro M.

The beta-catenin axis integrates multiple signals downstream from RET/papillary thyroid carcinoma leading to cell proliferation. Cancer Res. 2009 Mar 1;69(5):1867-76

The β-Catenin Axis Integrates Multiple Signals Downstream from RET/Papillary Thyroid Carcinoma Leading to Cell Proliferation

Maria Domenica Castellone,[1] Valentina De Falco,[1] Deva Magendra Rao,[1,2] Roberto Bellelli,[1] Magesh Muthu,[1] Fulvio Basolo,[3] Alfredo Fusco,[1] J. Silvio Gutkind,[4] and Massimo Santoro[1]

[1]Istituto di Endocrinologia ed Oncologia Sperimentale "G. Salvatore," Consiglio Nazionale delle Ricerche, c/o Dipartimento di Biologia e Patologia Cellulare e Molecolare "L. Califano," Universita Federico II, Naples, Italy; [2]Department of Genetics, Institute of Basic Molecular Sciences, University of Madras, Madras, India; [3]Division of Pathology, Department of Surgery, University of Pisa, Pisa, Italy; and [4]National Institute of Dental and Craniofacial Research, NIH, Bethesda, Maryland

Abstract

RET/papillary thyroid carcinoma (RET/PTC) oncoproteins result from the in-frame fusion of the RET receptor tyrosine kinase domain with protein dimerization motifs encoded by heterologous genes. Here, we show that RET/PTC stimulates the β-catenin pathway. By stimulating PI3K/AKT and Ras/extracellular signal–regulated kinase (ERK), RET/PTC promotes glycogen synthase kinase 3β (GSK3β) phosphorylation, thereby reducing GSK3β-mediated NH_2-terminal β-catenin (Ser33/Ser37/Thr41) phosphorylation. In addition, RET/PTC physically interacts with β-catenin and increases its phosphotyrosine content. The increased free pool of S/T(nonphospho)/Y(phospho)β-catenin is stabilized as a result of the reduced binding affinity for the Axin/GSK3β complex and activates the transcription factor T-cell factor/lymphoid enhancer factor. Moreover, through the ERK pathway, RET/PTC stimulates cyclic AMP–responsive element binding protein (CREB) phosphorylation and promotes the formation of a β-catenin-CREB-CREB-binding protein/p300 transcriptional complex. Transcriptional complexes containing β-catenin are recruited to the cyclin D1 promoter and a cyclin D1 gene promoter reporter is active in RET/PTC–expressing cells. Silencing of β-catenin by small interfering RNA inhibits proliferation of RET/PTC–transformed PC Cl3 thyrocytes, whereas a constitutively active form of β-catenin stimulates autonomous proliferation of thyroid cells. Thus, multiple signaling events downstream from RET/PTC converge on β-catenin to stimulate cell proliferation. [Cancer Res 2009;69(5):1867–76]

Introduction

Papillary thyroid carcinoma (PTC) features chromosomal aberrations that result in the fusion of the tyrosine kinase domain of the RET receptor with the NH_2 terminus of heterologous proteins, thereby generating the RET/PTC oncoproteins (1). Although there is large variation according to the geographic area and the detection method, the fraction of PTC samples positive for RET/PTC oncogenes is estimated to be 20% to 40%; this fraction increases up to 80% in PTC developed in radiation-exposed individuals (1). RET/PTC1 (H4-RET) and RET/PTC3 (NCOA4-RET) are the most prevalent variants (1). Fusion with protein partners that have protein-protein interaction motifs provides RET/PTC kinases with dimerizing interfaces, thereby resulting in ligand-independent dimerization and constitutive kinase activation. Autophosphorylation of RET Y1062 plays a particularly important role in cell transformation (2). Accordingly, when phosphorylated, Y1062 acts as the binding site for several protein tyrosine binding proteins, namely, Shc, IRS1/2, FRS2, and DOK1/4/5 (2). This mediates recruitment of growth factor receptor binding protein 2/son of sevenless homologue complexes (2–5) and Gab-family adaptors (2, 6–8) leading to Ras/RAF/extracellular signal–regulated kinase (ERK) and PI3K/AKT signaling (9–11). Moreover, RET/PTC depends on the phosphorylation of Y1062 for recruitment at the inner surface of the cell membrane (2–5).

RET/PTC–mediated transformation requires the Ras/RAF/ERK cascade (11–13). In line with this observation, oncogenic conversion of a member of the RAF family, BRAF, is frequently detected in PTC (1, 14). In addition, deregulation of the PI3K signaling, through activation of PI3K and AKT serine/threonine kinase or loss of PTEN phosphatase, is prevalent in thyroid cancer (15, 16). PI3K signaling is mitogenic for thyrocytes (15, 16).

β-Catenin is a multifunctional protein that plays an important role in signal transduction. In normal resting cells, β-catenin is mainly localized to the adherens junctions, whereas free cytosolic β-catenin is recruited to a "destruction" complex that includes the scaffolding protein Axin, the tumor suppressor adenomatous polyposis coli (APC), and glycogen synthase kinase 3β (GSK3β). This complex facilitates the NH_2-terminal serine/threonine phosphorylation of β-catenin by GSK3β, thereby targeting β-catenin for degradation by the ubiquitin-proteasome (17). When the pathway is activated, as it occurs in the presence of Wnt ligands, β-catenin is stabilized. Stabilization of β-catenin results in its nuclear accumulation and interaction with T-cell factor/lymphoid enhancer factor (TCF/LEF) or other transcription factors and in activation of genes required for cell proliferation (e.g., *c-Myc* and *cyclin D1*; ref. 18). PI3K/AKT induces Ser9/21 GSK3β phosphorylation and inhibition of GSK3β-mediated phosphorylation of β-catenin (19). p90RSK, a Ras/ERK downstream kinase, also phosphorylates and inhibits GSK3β thereby leading to β-catenin up-regulation (17, 20, 21). In this pathway, ERK associates with a docking motif, FKFP (residues 291–294), of GSK3β and phosphorylates it at Thr43 to prime it for subsequent phosphorylation at Ser9/21 by p90RSK (22).

Up-regulation of β-catenin occurs in a variety of cancers, namely, colorectal, breast, and ovarian cancers (17, 18). Mutations that activate β-catenin occur late in thyroid tumor progression, being detected in undifferentiated (anaplastic) thyroid carcinomas (23). Increased free β-catenin pools have been observed in thyroid carcinomas secondary to reduced E-cadherin expression (24). It has been recently reported that oncogenic point mutants of RET (2A-RET and 2B-RET), which are associated with medullary thyroid

Requests for reprints: Massimo Santoro, Dipartimento di Biologia e Patologia Cellulare e Molecolare "L. Califano," Università Federico II di Napoli, via S. Pansini 5, 80131 Naples, Italy. Phone: 39-081-7463056; Fax: 39-081-7463037; E-mail: masantor@unina.it.

doi:10.1158/0008-5472.CAN-08-1982

cancer, phosphorylate β-catenin on Y654 thereby promoting β-catenin escape from APC/Axin/GSK3β–mediated destruction (25). This prompted us to investigate the functional connection between RET/PTC and the β-catenin signaling cascades.

Materials and Methods

Cell lines. HEK293T cells were grown in DMEM supplemented with 10% FCS (Invitrogen). The human thyroid cancer cell lines, derived from papillary (TPC-1 and BCPAP) or anaplastic (OCUT-1 and 8505C) thyroid carcinoma, were grown in DMEM containing 10% fetal bovine serum (FBS). 8505C were from DSMZ (Deutsche Sammlung von Mikroorganismen und Zellkulturen GmbH). OCUT-1 were a gift of K. Hirakawa and N. Onoda (Osaka, Japan). TPC-1 harbors a RET/PTC1 rearrangement; BCPAP, OCUT-1, and 8505C harbor a BRAF V600E mutation (26). Normal human thyrocytes were isolated from normal thyroid tissue obtained from a patient who underwent thyroid surgery and cultivated in RPMI supplemented with 20% FBS. PC Cl3 (hereafter called "PC") is a differentiated thyroid follicular cell line derived from 18-mo-old Fischer rats. PC cells were cultured in Coon's modified Ham's F-12 medium supplemented with 5% calf serum and a mixture of six hormones, including thyrotropin (10 milliunits/mL), hydrocortisone (10 nmol/L), insulin (10 μg/mL), apo-transferrin (5 μg/mL), somatostatin (10 ng/mL), and glycyl-histidyl-lysine (10 ng/mL; Sigma). RET/PTC–expressing PC cells have been described previously (11). To obtain PC cells stably expressing the RET/PTC(4F) or RET/PTC(3F) mutants, transfections were done by the calcium phosphate coprecipitation technique as described previously (11) and mass populations of several 10 cell clones were isolated for each transfection by G418 selection. Equal levels of expression of RET/PTC mutants were confirmed by immunoblotting. Transient transfections were carried out with the Lipofectamine reagent according to the manufacturer's instructions (Life Technologies).

Cell growth and staining. For growth curves, 0.5×10^5 cells were seeded in triplicate and counted at the indicated time points. DNA synthesis rate was measured with the 5′-bromo-3′-deoxyuridine (BrdUrd) Labeling and Detection kit from Boehringer Mannheim. Briefly, cells were seeded on glass coverslips, pulsed for 1 h with BrdUrd (final concentration of 10 μmol/L), fixed, and permeabilized. Coverslips were incubated with anti-BrdUrd mouse monoclonal and rhodamine-conjugated secondary antibodies (Jackson ImmunoResearch Laboratories) and mounted in Moviol on glass slides. Cell nuclei were identified by Hoechst 33258 (final concentration, 1 μg/mL; Sigma) staining. The fluorescent signal was visualized with an epifluorescent microscope (Axiovert 2, Zeiss; equipped with a ×100 lens) interfaced with the image analyzer software KS300 (Zeiss). At least 100 cells were counted in five different microscopic fields; results were average fractions of BrdUrd-positive cells ± SD.

Tissue samples. Archival frozen thyroid tissue samples from 12 patients affected by PTC (T1–T12) and 2 normal thyroids (N1–N2) were retrieved from the files of the Pathology Department of the University of Pisa. The study was approved by the Institutional Ethics Committee. Sections (4 μm thick) of paraffin-embedded samples were stained with H&E for histologic examination to ensure that the samples met the diagnostic criteria required for the identification of PTC (enlarged nuclei with fine dusty chromatin, nuclear grooves, single or multiple micro/macro nucleoli, and intranuclear inclusions; ref. 27). According to a previous characterization, three of these PTC samples had a RET/PTC1 rearrangement (T2, T7, and T12) and six had a BRAF V600E mutation (T1, T4, T5, T6, T8, and T10; ref. 11). Snap-frozen tissue samples were kept in liquid nitrogen for storage at −80°C until protein extraction was done.

Plasmids. Unless otherwise specified, RET/PTC3 is the RET/PTC form used in this study. The RET/PTC3 constructs were cloned in pBABE and pCDNA3.1 (Invitrogen). They encode the short (RET-9) RET/PTC3 spliced form and are described elsewhere (11). For simplicity, we numbered the residues of RET/PTC proteins according to the corresponding residues in unrearranged RET. Briefly, RET/PTC(K−) is a kinase-dead mutant carrying the substitution of the catalytic lysine (residue 758 in full-length RET) with a methionine. RET/PTC(4F) is a mutant in which the four autophosphorylation sites (Y826, Y1015, Y1029, and Y1062) of the COOH-terminal tail are mutated to phenylalanines; in RET/PTC(3F), the Y1062 has been added back. Plasmids encoding the dominant-negative Ras(N17), MEK(DN), and AKT(DN); the constitutively active Ras(V12), BRAF(V600), and β-catenin (S374A); and the TCF/LEF reporter system are described elsewhere (28).

Antibodies and compounds. Anti-RET is an affinity-purified polyclonal antibody raised against the tyrosine kinase protein fragment of human RET. Anti–β-catenin (610153) and anti–E-cadherin (610181) were purchased from Becton Dickinson (BD Transduction Laboratories). Anti–phospho-p44/42 mitogen-activated protein kinase [MAPK; recognizing MAPK (ERK1/2) when phosphorylated either individually or dually on Thr202 and Tyr204], anti–p44/42 MAPK, anti–phospho-AKT (specific for AKT phosphorylated at Ser473), anti-AKT, anti–phospho-Ser21/9 GSK, anti-GSK, and anti–phospho-β-catenin (Ser33/37/Thr41) were purchased from Cell Signaling. Anti-tubulin was from Sigma. Monoclonal anti–phospho-β-catenin (Y654) antibody was from Abcam. Anti–cyclic AMP-responsive element binding protein (CREB), anti–phospho-S133 CREB (06-519), and anti-Tcf4 (05-511) were from Upstate Biotechnology, Inc. Anti–CREB-binding protein (CBP), anti-p300, anti-SP1, and anti–c-Myc antibody were from Santa Cruz Biotechnology. Secondary antibodies coupled to horseradish peroxidase were from Amersham Pharmacia Biotech. Cycloheximide was purchased from Sigma and used at 10 μg/mL final concentration. LY294002 was from Calbiochem (Merck Chemicals Ltd.) and used at 10 μmol/L final concentration. MAPK/ERK kinase (MEK)-1/2 inhibitor UO126 was from Cell Signaling and used at 10 μmol/L final concentration.

Protein studies. Immunoblotting experiments were done according to standard procedures. Protein concentration was estimated with a modified Bradford assay (Bio-Rad). Immune complexes were detected with the enhanced chemiluminescence kit (Amersham Pharmacia Biotech). Signal intensity was analyzed with the Phosphorimager (Typhoon 8600, Amersham Pharmacia Biotech) interfaced with the ImageQuant software. For immunoprecipitations, total lysates were incubated with 2 μg antibody for 2 h at 4°C. Antibody-antigen complexes were collected with 30 μL of protein G-Sepharose or protein A-Sepharose beads overnight at 4°C with gentle rotation. The samples were centrifuged, washed, eluted in sample buffer, and run on SDS-polyacrylamide gel. Nuclear extraction was done as described elsewhere (29). Briefly, cells were harvested in lysis buffer [10 mmol/L Tris-HCl (pH 7.9), 10 mmol/L KCl, 1.5 mmol/L $MgCl_2$, 1 mmol/L DTT, 1 mmol/L phenylmethyl-sulfonylfluoride (PMSF), supplemented with 60 mmol/L NaF, 60 mmol/L β-glycerophosphate, and protease inhibitors (aprotinin, leupeptin, and pepstatin; 40 mg/mL)] and lysed by shearing with 15 passages through a 26-gauge needle mounted in a 1-mL syringe. Nuclei were recovered by centrifugation at 3,000 × *g* for 10 min. Nuclear proteins were extracted in 50 mmol/L Tris-HCl (pH 7.5), containing 0.3 mol/L sucrose, 0.42 mol/L KCl, 5 mmol/L $MgCl_2$, 0.1 mmol/L EDTA, 20% glycerol, 2 mmol/L DTT, 0.1 mmol/L PMSF, 60 mmol/L NaF, 60 mmol/L β-glycerophosphate, leupeptin, and aprotinin. Cytosolic fractions were recovered after membrane fraction removal by 100,000 × *g* ultracentrifugation.

Pull-down assay. The GST-RET/PTC3 and GST-RET/TK plasmids were generated by PCR amplification of full-length RET/PTC3 or the isolated RET component of the RET/PTC3 protein (RET residues 718–1072) and fusion to the glutathione *S*-transferase (GST) coding sequence into the pEBG vector (kindly provided by S. Meakin, Laboratory of Neural Signaling, Cell Biology Group, The John P. Robarts Research Institute, London, Ontario, Canada; ref. 30). GST-RET/PTC3 and GST-RET/TK fusion proteins were purified from transiently transfected cell lysates using glutathione-Sepharose according to standard procedures. HEK293T cells were serum starved for 18 h and lysed in an ice-cold buffer. Protein lysates (2 mg) were incubated overnight with 30 μg of GST-RET/PTC3 and GST-RET/TK fusion proteins. Pellet beads were collected by centrifugation (14,000 × *g*) and washed with lysis buffer. The beads were resuspended in 2× Laemmli buffer and subjected to Western blotting.

Reporter assay. To evaluate the TCF/LEF transcriptional activity, we used a pair of luciferase reporter constructs, TOP-FLASH and the negative control FOP-FLASH (Upstate Biotechnology). TOP-FLASH contains three copies of the TCF/LEF binding site (AAGATCAAAGGGGGT) upstream of

the thymidine kinase minimal promoter; FOP-FLASH contains a mutated TCF/LEF binding site (AAGGCCAAAGGGGGT). Cells were transiently transfected by one of these reporters together with pRL-TK (encoding the Renilla luciferase) in triplicate, as instructed by the manufacturer (Promega Corporation). Luciferase activity was measured 48 h after transfection with the Dual-luciferase reporter assay system (Promega). TCF/LEF activity was determined by the TOP-FLASH/FOP-FLASH ratio after normalization for Renilla luciferase activity. Light emission was quantified with a Berthold Technologies luminometer (Centro LB 960). Data were represented as average fold change ± SD with respect to the negative control.

RNA silencing. Predesigned duplex small interfering RNA (siRNA) against rat β-catenin (190086, 190087, and 190088) were provided by Ambion. The scrambled oligonucleotide was synthesized by Proligo, and the sequence was 5′-AGGAUAGCGUGGAUUUCGGUTT-3′. The day before transfection, cells were plated in six-well dishes at 30% to 40% confluency. Transfection was done using 5 μg of duplex RNA and 6 μL of Oligofectamine reagent (Invitrogen). Cells were harvested at 48 h posttransfection or counted at different time points for evaluating cell growth.

Chromatin immunoprecipitation. Chromatin was extracted from RET/PTC– or empty vector–transfected HEK293T cells. Chromatin immunoprecipitation assay was done by using the chromatin immunoprecipitation assay kit (Upstate Biotechnology), following the manufacturer's instructions. Chromatin was fixed by directly adding formaldehyde (1%, v/v) to the cell culture medium. Nuclear extracts were isolated and then

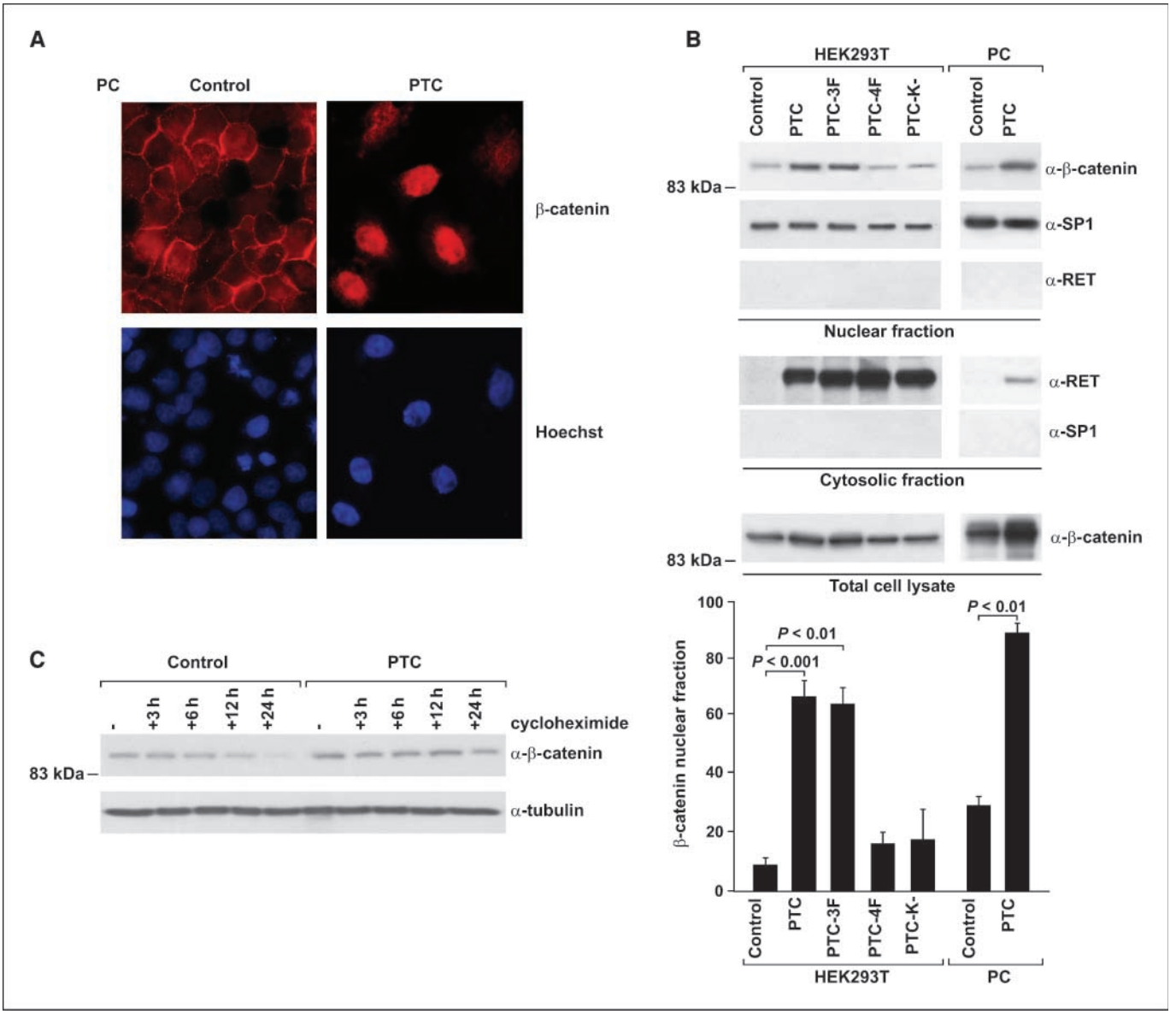

Figure 1. RET/PTC stabilizes β-catenin and promotes its nuclear accumulation. *A,* immunofluorescence for β-catenin in PC cells transiently transfected with RET/PTC. Note the increase of nuclear staining in transfected cells. Hoechst stain was used to visualize cell nuclei; parallel transfection with green fluorescent protein showed that ~20% of the cells expressed exogenous DNA (data not shown). *B,* nuclear translocation of β-catenin on RET/PTC expression. HEK293T cells were transfected with RET/PTC or the indicated mutants [mock transfected (*Control*)]. PC-RET/PTC cells or parental PC were also used. Subcellular fractions were obtained and nuclear extracts (50 μg) probed with anti–β-catenin. The purity of the fractions was assessed by verifying the absence of SP1 in the cytosolic fraction and of RET/PTC in the nuclear fraction. Total β-catenin levels were also measured in unfractionated extracts. *Columns,* mean percentage of nuclear β-catenin with respect to total levels from five independent determinations; *bars,* SD. Reported *P* values were calculated by Student's *t* test. *C,* HEK293T cells transiently expressing RET/PTC or a control vector were treated with cycloheximide for different time points. Lysates (30 μg) were run on SDS-PAGE, and β-catenin levels were determined by immunoblot.

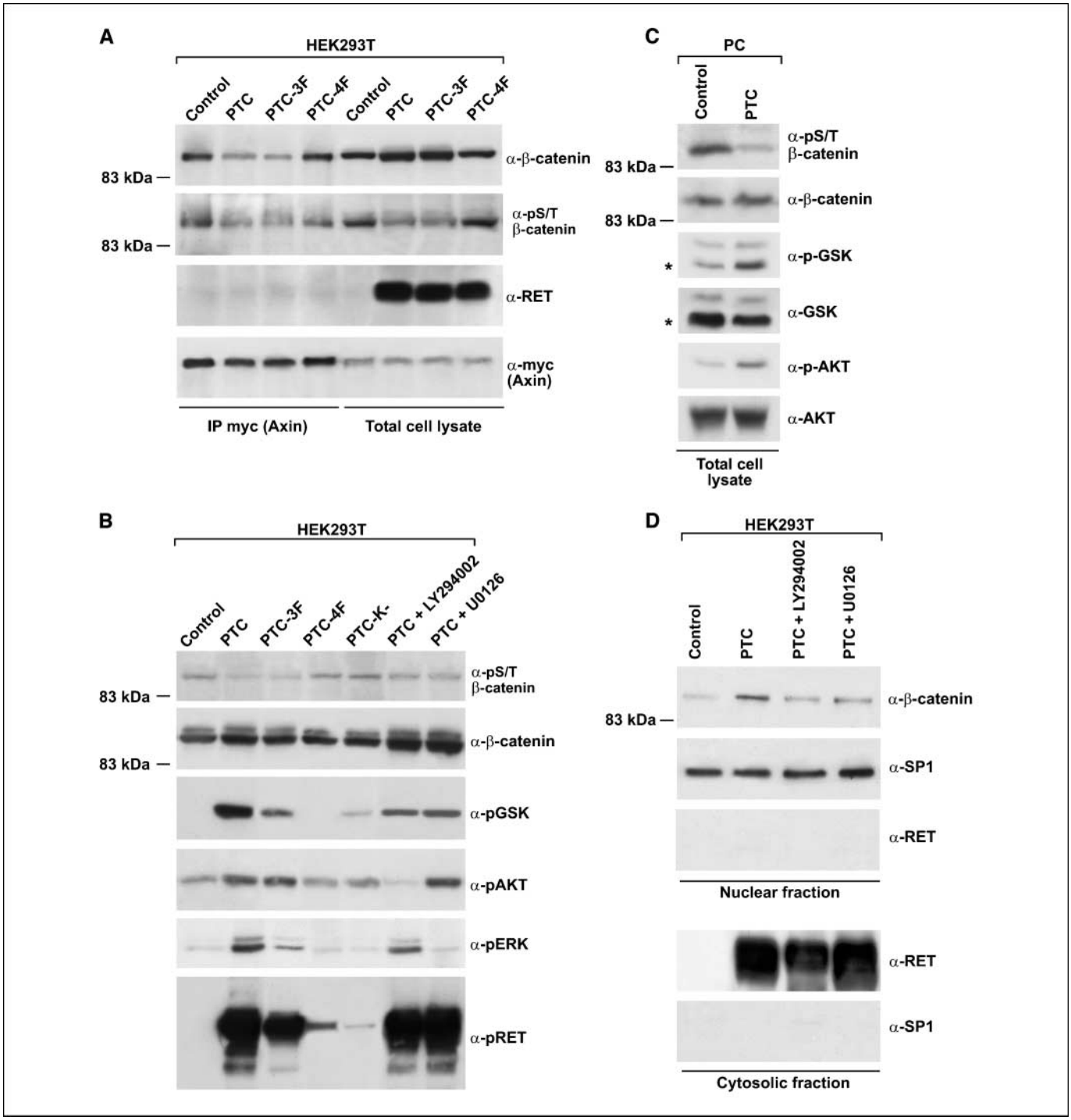

Figure 2. RET/PTC induces the dissociation of the β-catenin degradation complex. *A,* HEK293T cells were transfected with a myc-tagged Axin together with RET/PTC or the indicated mutants. Protein complexes containing Axin were recovered by immunoprecipitation (1 mg) with anti-myc tag and blotted against β-catenin or S/T-phosphorylated β-catenin (phospho-Ser33/37/Thr41). Myc-Axin and RET/PTC protein levels in total cell lysates are shown for normalization. *B* and *C,* phosphorylation levels of GSK3β, β-catenin (phospho-Ser33/37/Thr41), AKT, ERK, and RET (Y905) were measured by immunoblot of total cell lysates (50 μg) harvested from HEK293T (*B*) or PC (*C*) cells expressing the indicated RET/PTC variants or treated with the indicated compounds. GSK3β antibodies may recognize both GSK-3α (51 kDa) and GSK3β (46 kDa) proteins; *, GSK3β migration (*C*). *D,* nuclear accumulation of β-catenin (measured as in Fig. 1*B*) in HEK293T cells transfected with RET/PTC and treated or not with chemical PI3K or MEK inhibitors. Representative data of at least three independent experiments.

fragmented through sonication. Transcription factor–bound chromatin was immunoprecipitated with β-catenin, CREB, or TCF antibodies; cross-linking was reversed; and the isolated genomic DNA amplified by quantitative PCR using primers spanning either the CRE site (Fig. 4*D*) or the TCF/LEF binding site (data not shown) of the human cyclin D1 promoter: CRE-forward, 5′-AACGTCACACGGACTACAGG-3′; CRE-reverse, 5′-TGTTCCATGGCTGGGGCTCTT-3′; TCF-forward, 5′-GAGCGCATGC-TAAGCTGAAA-3′; TCF-reverse, 5′-GGACAGACGGCCAAAGAATC-3′.

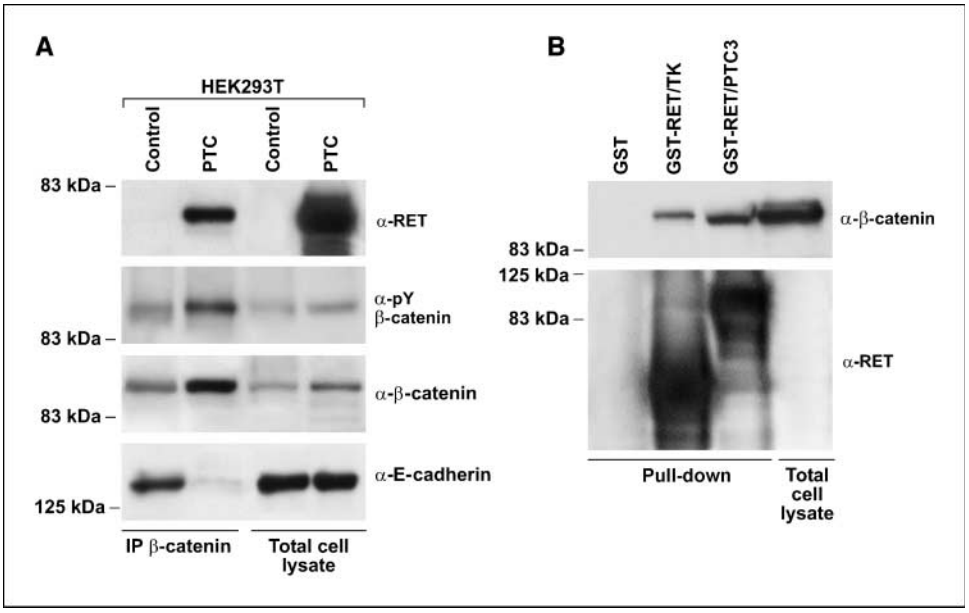

Figure 3. RET/PTC interaction with β-catenin. *A,* protein lysates (2 mg) from mock-transfected or RET/PTC–transfected HEK293T cells were immunoprecipitated with anti–β-catenin and probed with tyrosine-phosphorylated β-catenin (pY654), RET, or E-cadherin antibodies. Expression levels in total cell lysates are shown for normalization. *B,* full-length RET/PTC3 and the isolated RET component of the RET/PTC3 (deprived of the NCOA4 region) protein were produced as GST-fusion proteins and used to pull down β-catenin from HEK293T protein lysates. Immunoblot was stained with anti–β-catenin; recombinant RET proteins input is also reported.

Fluorescent threshold values (C_t) were measured in triplicate for immunoprecipitated samples as well as for an aliquot of the input DNA. Results were calculated by the following formula: $2^{-[\Delta Ct/Ct\ \text{input DNA}]}$, where ΔC_t is the difference between the C_t of the specific antibody-immunoprecipitated DNA and the C_t of mock-immunoprecipitated DNA. Results are average ± SD of triplicate samples.

Statistical analysis. Student's *t* test was used for statistical analysis. All *P* values were two sided and differences were significant when $P < 0.05$.

Results

RET/PTC promotes the nuclear accumulation of β-catenin. Thyroid follicular PC cells transiently transfected with RET/PTC accumulated nuclear β-catenin, a hallmark of β-catenin activation (Fig. 1*A*). By biochemical fractionation, although total β-catenin levels were increased on RET/PTC expression, nuclear β-catenin levels were proportionally increased to a greater extent, thereby accounting for the increase in the nuclear β-catenin fraction in HEK293T or PC cells [7-fold ($P < 0.001$) or 3.6-fold ($P < 0.01$), respectively] on transient or stable RET/PTC expression (Fig. 1*B*). β-Catenin nuclear accumulation depended on RET/PTC kinase activity because it was reduced by a kinase-dead mutant (K−). The residual, albeit not significant, activity of PTC(K−) might depend on RET kinase rescue operated by other tyrosine kinases, such as epidermal growth factor receptor, as recently shown (31). Moreover, β-catenin accumulation depended on RET/PTC autophosphorylation because it was not exerted by a RET/PTC mutant (PTC-4F) whose major autophosphorylation sites (Y826, Y1015, Y1029, and Y1062) were mutated to phenylalanine (Fig. 1*B*). Y1062 was essential because nuclear accumulation of β-catenin was restored when tyrosine Y1062 was added back to the 4F mutant (PTC-3F; $P < 0.01$; Fig. 1*B*). There was no detectable difference in the mRNA levels of β-catenin between RET/PTC–positive and RET/PTC–negative cells, which suggests that the increase in β-catenin occurred at the posttranscriptional level (data not shown). Accordingly, the half-life of β-catenin increased in RET/PTC–expressing cells (>24 hours) versus control HEK293T (~12 hours; Fig. 1*C*).

RET/PTC targets the Axin-GSK3β-β-catenin complex. The pathway leading to β-catenin activation involves a series of events that result in the dissociation of β-catenin from Axin, a scaffold protein that forms a large molecular complex with APC, Dsh, and GSK3β (17, 18). Transient RET/PTC expression in HEK293T cells decreased the amount of β-catenin coprecipitating with myc-tagged Axin; this effect depended on Y1062, as shown when we used the PTC-4F mutant (Fig. 2*A*). Secondary to the assembly of the Axin-GSK3β-β-catenin complex, phosphorylation of β-catenin by GSK3β in NH_2-terminal Ser33, Ser37, and Thr41 promotes its ubiquitin-dependent proteolytic degradation (19–22). RET/PTC expression in HEK293T reduced amounts of S/T-phosphorylated β-catenin coprecipitating with Axin (Fig. 2*A*). Moreover, transient RET/PTC expression in HEK293T (Fig. 2*A* and *B*) and stable expression in PC (Fig. 2*C*) reduced overall S/T β-catenin phosphorylation by immunoblot, an effect that depended on RET/PTC kinase and Y1062 (Fig. 2*B*). β-Catenin phosphorylation is affected by GSK3β. In turn, the activity of GSK3β can be blocked by both AKT- (19) and ERK pathway–mediated phosphorylation at Ser9 (22). RET/PTC stimulates both the PI3K/AKT and the ERK pathways by recruiting several adaptors to phosphorylated Y1062 (2). RET/PTC–triggered phosphorylation of AKT and ERK paralleled the phosphorylation of GSK3β-Ser9 and the consequent reduction of phospho-S/T β-catenin (Fig. 2*B* and *C*). PTC-4F had a significantly reduced activity with respect to wild-type RET/PTC (Fig. 2*B*). In addition, PTC-3F (although expressed at lower levels) had a reduced effect on GSK3β phosphorylation, suggesting that COOH-terminal tyrosines other than Y1062 may participate to this pathway. LY294002, a PI3K inhibitor, partially impaired GSK3β phosphorylation and increased β-catenin S/T phosphorylation; these effects were associated with a reduction in AKT phosphorylation (Fig. 2*B*). In addition, treatment with U0126, a MEK inhibitor, reduced phosphorylation of GSK-3β and partially rescued phospho-S/T β-catenin (Fig. 2*B*). Finally, treatment with LY294002 or U0126 reduced nuclear accumulation of β-catenin (Fig. 2*D*).

RET/PTC increases β-catenin phosphotyrosine content. β-Catenin interacts directly with the oncogenic tyrosine kinases c-src

(32), c-MET (33), RON (34), c-erbB-2 (35), and BCR-ABL (36), thereby resulting in β-catenin phosphorylation on tyrosine residues. More importantly, Gujral and colleagues (25) recently reported that MEN2-associated RET point mutants bind to β-catenin and phosphorylate it on tyrosine 654. We tested whether this mechanism was also used by RET/PTC. In HEK293T cells, RET/PTC coimmunoprecipitated with β-catenin (Fig. 3*A*), and on RET/PTC expression, tyrosine-phosphorylated β-catenin (pY654) increased; overall increased β-catenin levels may partially account for these effects (Fig. 3*A*). The binding of β-catenin to RET/PTC paralleled its dissociation from E-cadherin (Fig. 3*A*). Moreover, recombinant GST-RET/PTC3 and GST-RET/TK proteins were able to pull down β-catenin from HEK293T cell lysates, showing an interaction, either direct or mediated by intermediate protein(s), between the RET component of RET/PTC and β-catenin (Fig. 3*B*).

RET/PTC stimulates TCF/LEF– and CREB-mediated cyclin D1 transcription. Nuclear β-catenin forms complexes with members of the TCF and LEF family of DNA-binding proteins, and this process results in activation of target gene promoters. RET/PTC stimulated the activity of a luciferase TCF/LEF–dependent reporter gene system (TOPflash) in both HEK293T and PC cells ($P < 0.01$; Fig. 4*A*). The mutant TOPflash reporter (FOPflash), bearing a mutated TCF/LEF site, was used to subtract background. This activity depended on the integrity of the RET/PTC kinase and of the Y1062 multidocking site ($P < 0.05$; Fig. 4*A, left*). Again, other tyrosines besides Y1062 likely played a role because the PTC-3F mutant was impaired with respect to wild-type RET/PTC (Fig. 4*A, left*). TOPflash expression was partially reduced by treatment with LY294002 and U0126 and by the coexpression of dominant negative mutants for Ras (N17), MEK (MEKDN), and AKT (AKTDN; $P < 0.05$). Constitutively active BRAF (V600E) and Ras (V12) stimulated the TCF/LEF reporter in HEK293T cells, although to a lesser extent than RET/PTC. A transcriptionally active form of β-catenin (S374A) served as a positive control (Fig. 4*A*).

Besides TCF/LEF, β-catenin recruits the activated form (serine 133 phosphorylated) of CREB, thereby resulting in a transcriptionally active complex, which in turn binds CBP/p300 (37–40). TCF/LEF and CREB collaborate in regulating the transcription of TCRα (41) and WISP-1 (42). Finally, RET signaling through Y1062 and Ras/ERK increases S133 phospho-CREB levels (2). To determine whether RET/PTC affected the binding of CREB to β-catenin, we immunoprecipitated β-catenin from PC cells in the presence or absence of RET/PTC and probed the immunocomplexes with anti-CREB and anti-CBP/p300 antibodies. Expression of RET/PTC significantly increased the amounts of β-catenin bound to CREB and CBP/p300 (Fig. 4*B*). Chemical blockade of MEK by U0126 reduced this association, and this effect was paralleled by a reduction in CREB phosphorylation on Ser133 and ERK phosphorylation (Fig. 4*B*). In a mirror experiment, RET/PTC expression increased not only TCF/LEF-β-catenin (Fig. 4*C, bottom*) but also CREB-β-catenin protein complexes (Fig. 4*C, top*). In HEK293T cells, formation of both complexes was reduced when kinase-dead and 4F mutants were used (Fig. 4*C, right*). Instead, by immunoprecipitating CREB and staining with TCF/LEF, we did not detect TCF/LEF-CREB interaction, suggesting that β-catenin–containing TCF/LEF and CREB complexes are distinct (Fig. 4*C, middle*).

Cyclin D1 promoter contains adjacent TCF/LEF (at −81 bp) and CREB (at −58 bp) binding sites (40). We used chromatin immunoprecipitation to measure β-catenin, TCF/LEF, and CREB binding to the region of the cyclin D1 promoter that contains CREB and TCF/LEF binding sites. For PCR, we used two primer pairs spanning the CRE (Fig. 4*D*) and TCF (data not shown) sites, respectively. With both primer sets, binding of β-catenin, TCF/LEF, and CREB to the cyclin D1 promoter was greatly increased on RET/PTC expression ($P < 0.05$; Fig. 4*D*). Because the binding sites for CREB and TCF/LEF are just a few nucleotides apart on the cyclin D1 promoter, this experiment left open possibilities that the two β-catenin–containing (CREB and TCF/LEF) complexes can be either identical or distinct; however, the lack of coimmunoprecipitation in Fig. 4*C* favors the possibility that the two complexes are distinct.

RET/PTC–mediated mitogenic signaling depends on β-catenin. In PC cells, RET/PTC–mediated increase in β-catenin activity was paralleled by accumulation of the TCF/LEF and CREB target protein cyclin D1 and, more weakly, c-Myc (Fig. 5*A*). We knocked down β-catenin by RNA interference in parental and RET/PTC–expressing PC cells. As shown in Fig. 5*A*, β-catenin–specific siRNA, but not the scrambled control, reduced the expression of β-catenin by >50% in both PC and PC-PTC cells. Moreover, β-catenin siRNA reduced cyclin D1 and, more weakly, c-Myc levels in RET/PTC–expressing cells. β-Catenin RNA interference reduced hormone-independent proliferation of PC-PTC cells (Fig. 5*B, bottom*), whereas a constitutively active form of β-catenin (S374A) stimulated hormone-independent growth of PC cells (Fig. 5*B, top*). We generated mass populations of PTC-4F– and PTC-3F–expressing PC cells. On hormone deprivation, we counted S-phase cells on a 1-hour BrdUrd pulse after transient transfection with scrambled or β-catenin specific siRNA. Similarly to wild-type PTC, PTC-3F–expressing, but not PTC-4F–expressing, cells incorporated BrdUrd in the absence of hormones in a β-catenin–dependent manner ($P < 0.01$). Taken together, these findings show that β-catenin is a mediator of the RET/PTC mitogenic signaling in thyrocytes.

Finally, to study the β-catenin pathway in human PTC samples, we measured levels of GSK3β-Ser9 and S/T β-catenin phosphorylation compared with normal thyroid samples ($n = 2$) in a small set of PTC ($n = 12$) samples (three RET/PTC positive, six BRAF V600E positive, and the remainder RET/PTC and BRAF negative). Reduced levels of β-catenin S/T phosphorylation was visible in virtually all the tumor samples; increased levels of GSK3β-Ser9 phosphorylation and total β-catenin were detectable in ~75% and 50% of them, respectively (Fig. 5*D, left*). Similarly, thyroid carcinoma cell lines positive either for RET/PTC1 (TPC-1) or for BRAF V600E (BCPAP, 8505C, and OCUT-1) showed reduced levels of S/T β-catenin and increased GSK3β-Ser9 phosphorylation when compared with a primary culture of normal thyrocytes (Fig. 5*D, right*).

Discussion

Here we describe the functional interaction between the RET/PTC and the β-catenin signaling pathways. β-Catenin activation by RET/PTC occurred through several coordinated mechanisms (Fig. 6). As previously reported by Gujral and colleagues (25) for point mutant RET, RET/PTC induced the tyrosine phosphorylation of β-catenin, thereby mobilizing the fraction of β-catenin associated to E-cadherin and increasing its free cytosolic pool. RET/PTC-mediated activation of PI3K/AKT and Ras/ERK contributed to promote β-catenin stabilization through inactivation of

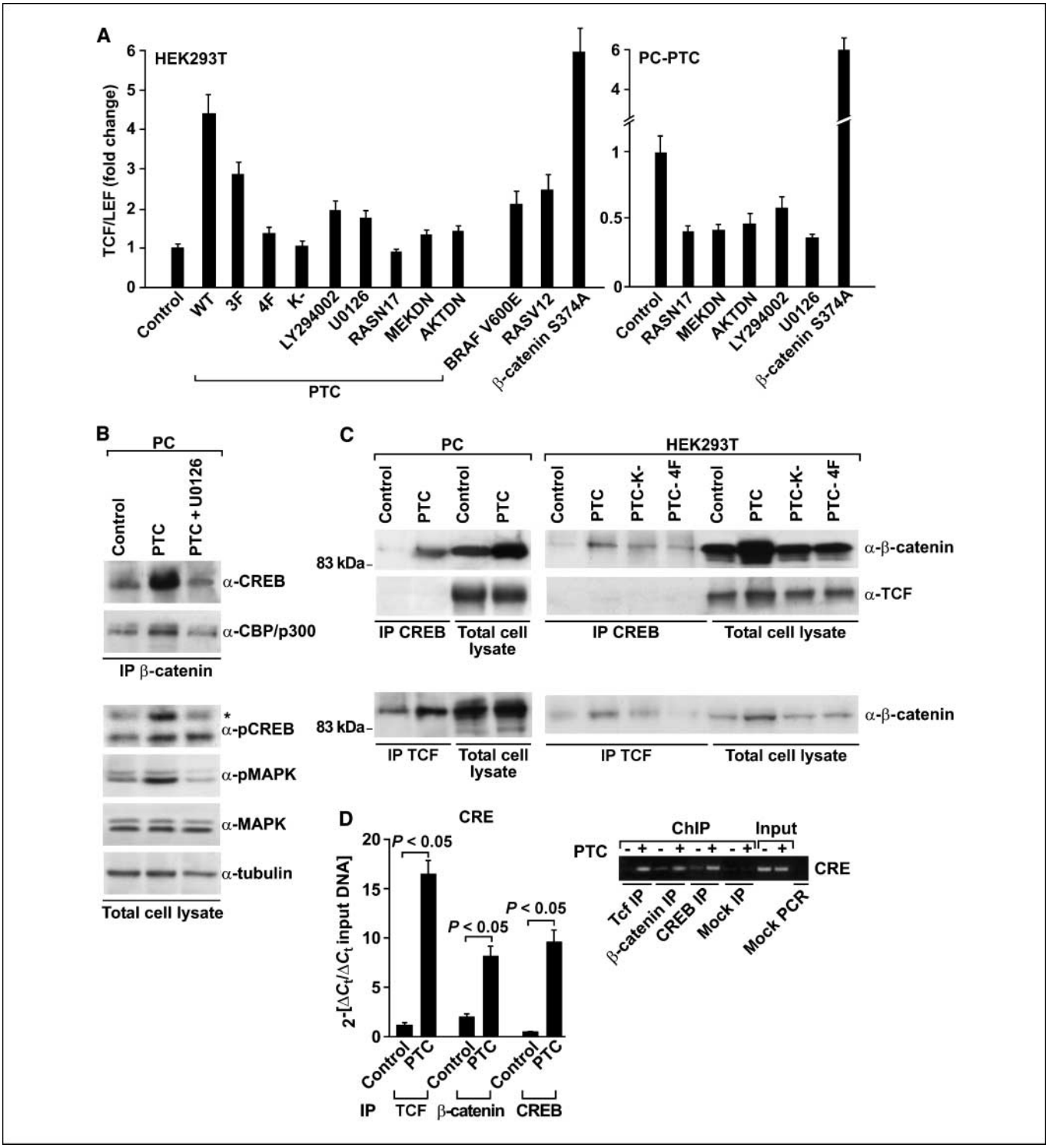

Figure 4. RET/PTC–mediated activation of TCF/LEF and CREB transcription factors. *A,* HEK293T (*left*) and PC-PTC cells (*right*) were transfected with the indicated plasmids together with the TOPflash reporter and, when indicated, treated with the chemical inhibitors. Luciferase activity was expressed as fold increase with respect to mock-transfected cells. *Columns,* average results of three independent assays; *bars,* SD. Reported *P* values were calculated by Student's *t* test. *B,* cellular lysates (1 mg) from PC and PC-PTC cells, treated or not with U0126, were immunoprecipitated with anti–β-catenin and probed with CREB and CBP/p300 antibodies. The CREB antibody may also recognize, besides CREB (43 kDa), CREM (30 kDa) and activating transcription factor-1 (38 kDa); *, CREB migration. Phosphorylation of CREB (S133) and ERK (MAPK) was measured in total cell lysates by immunoblot. Tubulin was used for normalization. *C,* lysates from PC or PC-PTC cells (*left*) and HEK293T cells transiently expressing the indicated RET/PTC constructs (*right*) were immunoprecipitated with CREB and TCF antibodies and probed for β-catenin or TCF antibodies, as reported. *D,* chromatin immunoprecipitation (*ChIP*) was done in HEK293T cells transfected with RET/PTC or the empty vector (*control*). Processed DNA was immunoprecipitated with TCF, β-catenin, or CREB antibodies and subjected to real-time PCR (*bar graphs*) with amplimers spanning the CRE site of the cyclin D1 promoter. *Columns,* mean of triplicate samples; *bars,* SD. Fluorescent threshold values (C_t) were measured for immunoprecipitated samples as well as for an aliquot of the input DNA. Reported *P* values were calculated by Student's *t* test. Semiquantitative PCR (ethidium bromide stain) was also done with the same primers by using 1 μL of the DNA and 25 cycles of amplification. Amplification of the expected fragments in the input samples indicated equal input; mock PCR was done without template.

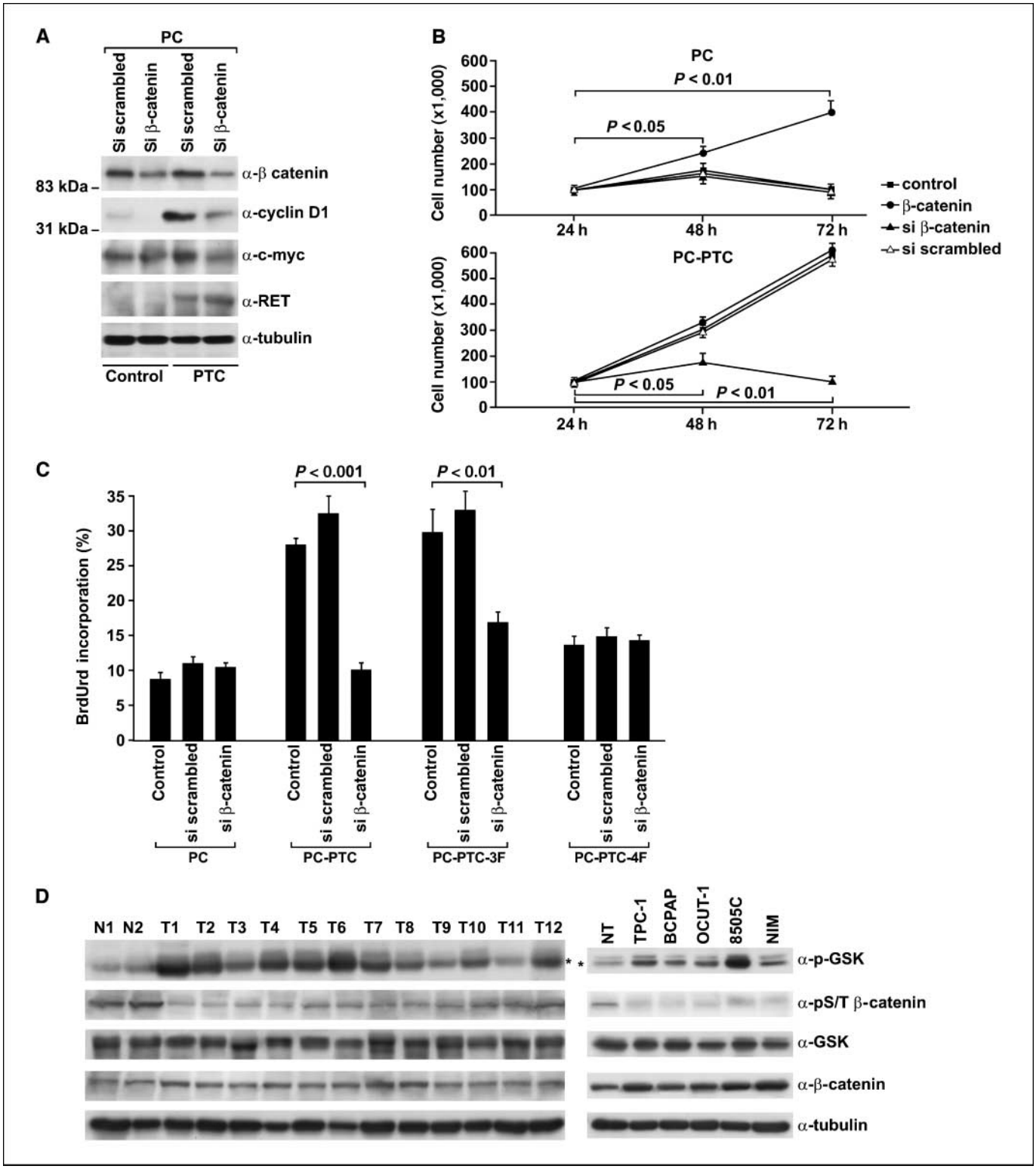

Figure 5. β-Catenin contributes to autonomous growth of RET/PTC–expressing thyroid cells. *A,* β-catenin was knocked down by transient transfection with specific siRNA (*si β-catenin*) in parental or RET/PTC–expressing PC cells. As a control, cells were treated with scrambled siRNA (*si scrambled*). Protein levels were measured by immunoblot with the indicated antibodies. *B,* proliferation in the absence of hormones of parental, constitutively active β-catenin (S374A) or β-catenin siRNA transiently transfected PC or PC-PTC cells was measured by cell counts. *Points,* mean of triplicate samples; *bars,* SD. Reported *P* values were calculated by Student's *t* test. *C,* mass populations of PTC-4F– and PTC-3F–expressing PC cells were generated by stable transfection and marker selection. On hormone deprivation and transfection with scrambled or β-catenin–specific siRNA (as in *A*), cells were pulsed (1 h) with BrdUrd, and BrdUrd-positive cells were analyzed by immunofluorescence. At least 100 cells were counted in five different microscopic fields. *Columns,* mean fractions of BrdUrd-positive cells; *bars,* SD. Reported *P* values were calculated by Student's *t* test. *D,* phosphorylation levels of GSK3β and β-catenin (phospho-Ser33/37/Thr41) were measured by immunoblot of total cell lysates (50 μg) harvested from PTC (*T1–T12*) and normal thyroid (*N1–N2*) tissue samples (*left*) or thyroid carcinoma and normal human primary cells (*NT*; *right*). GSK3β antibodies may recognize both GSK-3α (51 kDa) and GSK3β (46 kDa) proteins; *, GSK3β migration.

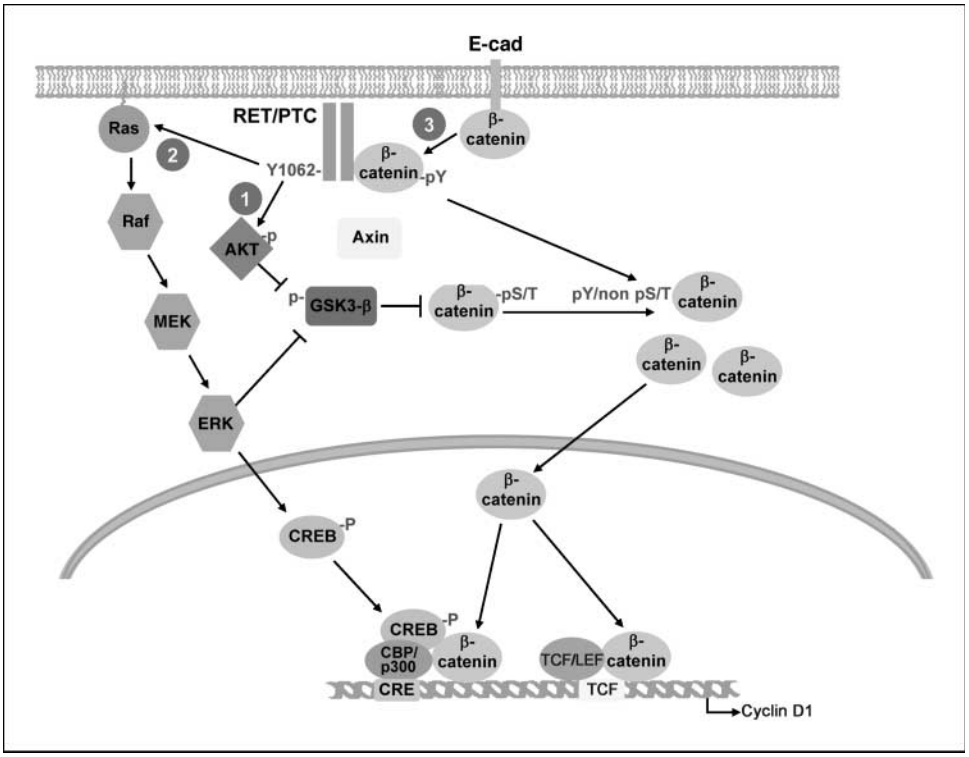

Figure 6. A summary of the pathways leading to β-catenin induction by RET/PTC. *1* and *2,* RET/PTC activates PI3K/AKT and Ras/MEK/ERK. This leads to GSK3β phosphorylation, thereby relieving its negative control on β-catenin, and to an increase of the free β-catenin protein pool. *2,* through ERK activation, RET/PTC induces S133 phosphorylation of CREB, which associates in a complex with β-catenin and CBP/p300 to stimulate transcription of cyclin-D1. *3,* RET/PTC directly binds β-catenin and increases its phosphotyrosine content, thereby decreasing the E-cadherin–bound pool and increasing the free β-catenin pool. Free β-catenin enters the nucleus and participates in at least two different transcription complexes with CREB/p300 and with TCF/LEF, both ultimately involved in the regulation of cyclin D1.

GSK3β. However, neither pathway was probably sufficient because chemical blockade of either one reduced but did not abrogate β-catenin accumulation. Finally, RET/PTC signaling favored the formation of transcriptional complexes containing β-catenin by triggering ERK-mediated CREB phosphorylation. Ser133-phosphorylated CREB formed a protein complex with CBP and β-catenin, which participated in the transcription of cyclin D1. TCF/LEF and CREB binding sites coexist in the promoters of some β-catenin target genes, such as *cyclin D1* (40), *TCRα* (41), and *WISP-1* (42), and collaborate in their firing. Accordingly, our findings suggest that downstream of RET/PTC, β-catenin participates in two distinct transcriptional complexes, one with TCF/LEF and another one with CREB, and that both are recruited to cyclin D1 promoter. The particularly important role played by Y1062 in signaling to β-catenin in the case of RET/PTC with respect to full-length RET mutants (25) may be explained by differential signaling mechanisms between the distinct RET oncogenic forms and the cytosolic localization of RET/PTC that relies on Y1062 to be recruited to the cell membrane (2–4). Finally, β-catenin expression is required for RET/PTC–mediated autonomous proliferation of PC thyrocytes.

It is possible that β-catenin activity cooperates with other signaling cascades activated by RET/PTC to mediate mitogenic activity. Cytosolic β-catenin is recruited to a "destruction" complex that includes APC and GSK3β. Loss of APC tumor suppressor reduces the activity of the β-catenin destruction complex (17, 21). Of direct relevance to thyroid tumorigenesis, patients affected by familial APC [familial adenomatous polyposis (FAP)] and harboring APC mutations are predisposed to thyroid carcinoma (43). Furthermore, the RET/PTC oncogene is activated in some FAP-associated thyroid carcinomas (44). Therefore, our data support a model whereby two different lesions concomitantly present in FAP-associated thyroid carcinoma (i.e., RET/PTC activation and APC loss of function) may converge to enhance the activity of the β-catenin signaling cascade. On the other hand, direct β-catenin mutations are restricted to aggressive and undifferentiated types of thyroid carcinomas (23).

β-Catenin targeting approaches for cancer therapy are currently being explored. For example, a conditionally replicative adenovirus, which kills only cells with a hyperactive β-catenin pathway, significantly inhibited the growth of undifferentiated (anaplastic) thyroid cancers (45). ICG-001, an inhibitor of the β-catenin/CBP transcriptional complex, efficiently induced apoptosis of colon cancer cells (46). Prostaglandin E_2 (PGE_2) also promotes β-catenin signaling (28), and PGE_2 synthesis inhibitors, nonsteroidal anti-inflammatory drugs, in an adjuvant or preventive setting are being tested already in cancer. Our data, together with those reported by Gujral and colleagues (25), suggest that β-catenin targeting approaches could have therapeutic potential in thyroid cancer.

Disclosure of Potential Conflicts of Interest

No potential conflicts of interest were disclosed.

Acknowledgments

Received 5/28/2008; revised 11/20/2008; accepted 12/8/2008; published OnlineFirst 02/17/2009.

Grant support: Associazione Italiana per la Ricerca sul Cancro, Naples OncoGEnomic Center, Istituto Superiore di Oncologia, Ministero dell'Istruzione, Università e Ricerca (MIUR), Ministero della Salute, the project Applicazioni Biotecnologiche dalle molecole all'uomo (MoMa), and European Commission contract no. 03695 (GenRisk-T). M.D. Castellone was recipient of a fellowship from the Accademia Nazionale dei Lincei, Rome, Italy. D.M. Rao and M. Muthu were recipients of fellowships from MIUR in the frame of an India-Italy cooperation program.

The costs of publication of this article were defrayed in part by the payment of page charges. This article must therefore be hereby marked *advertisement* in accordance with 18 U.S.C. Section 1734 solely to indicate this fact.

We thank F. Carlomagno, R.M. Melillo, G. Salvatore, P. Salerno, and G. Vecchio for their support; K. Hirakawa and N. Onoda for OCUT-1 cells; and Jean Ann Gilder for text editing.

References

1. Ciampi R, Nikiforov YE. RET/PTC rearrangements and BRAF mutations in thyroid tumorigenesis. Endocrinology 2007;148:936–41.
2. Hayashi H, Ichihara M, Iwashita T, et al. Characterization of intracellular signals via tyrosine 1062 in RET activated by glial cell line-derived neurotrophic factor. Oncogene 2000;19:4469–75.
3. Asai N, Murakami H, Iwashita T, Takahashi M. A mutation at tyrosine 1062 in MEN2A-Ret and MEN2B-Ret impairs their transforming activity and association with shc adaptor proteins. J Biol Chem 1996;271:17644–9.
4. Alberti L, Borrello MG, Ghizzoni S, Torriti F, Rizzetti MG, Pierotti MA. Grb2 binding to the different isoforms of Ret tyrosine kinase. Oncogene 1998;17:1079–87.
5. Melillo RM, Santoro M, Ong SH, et al. Docking protein FRS2 links the protein tyrosine kinase RET and its oncogenic forms with the mitogen-activated protein kinase signaling cascade. Mol Cell Biol 2001;21:4177–87.
6. Besset V, Scott RP, Ibanez CF. Signaling complexes and protein-protein interactions involved in the activation of the Ras and phosphatidylinositol 3-kinase pathways by the c-Ret receptor tyrosine kinase. J Biol Chem 2000; 275:39159–66.
7. Hadari YR, Gotoh N, Kouhara H, Lax I, Schlessinger J. Critical role for the docking-protein FRS2 α in FGF receptor-mediated signal transduction pathways. Proc Natl Acad Sci U S A 2001;98:8578–83.
8. De Falco V, Guarino V, Malorni L, et al. RAI(ShcC/N-Shc)-dependent recruitment of GAB 1 to RET oncoproteins potentiates PI3-K signalling in thyroid tumors. Oncogene 2005;24:6303–13.
9. Miyagi E, Braga-Basaria M, Hardy E, et al. Chronic expression of RET/PTC 3 enhances basal and insulin-stimulated PI3 kinase/AKT signaling and increases IRS-2 expression in FRTL-5 thyroid cells. Mol Carcinog 2004; 41:98–107.
10. Segouffin-Cariou C, Billaud M. Transforming ability of MEN2A-RET requires activation of the phosphatidylinositol 3-kinase/AKT signaling pathway. J Biol Chem 2000;275:3568–76.
11. Melillo RM, Castellone MD, Guarino V, et al. The RET/PTC-RAS-BRAF linear signaling cascade mediates the motile and mitogenic phenotype of thyroid cancer cells. J Clin Invest 2005;115:1068–81.
12. Knauf JA, Kuroda H, Basu S, Fagin JA. RET/PTC-induced dedifferentiation of thyroid cells is mediated through Y1062 signaling through SHC-RAS-MAP kinase. Oncogene 2003;22:4406–12.
13. Mitsutake N, Miyagishi M, Mitsutake S, et al. BRAF mediates RET/PTC-induced mitogen-activated protein kinase activation in thyroid cells: functional support for requirement of the RET/PTC-RAS-BRAF pathway in papillary thyroid carcinogenesis. Endocrinology 2006; 147:1014–9.
14. Xing M. BRAF mutation in papillary thyroid cancer: pathogenic role, molecular bases, and clinical implications. Endocr Rev 2007;28:742–62.
15. Shinohara M, Chung YJ, Saji M, Ringel MD. AKT in thyroid tumorigenesis and progression. Endocrinology 2007;148:942–7.
16. Coulonval K, Vandeput F, Stein RC, Kozma SC, Lamy F, Dumont JE. Phosphatidylinositol 3-kinase, protein kinase B and ribosomal S6 kinases in the stimulation of thyroid epithelial cell proliferation by cAMP and growth factors in the presence of insulin. Biochem J 2000;348 Pt 2:351–8.
17. Reya T, Clevers H. Wnt signalling in stem cells and cancer. Nature 2005;434:843–50.
18. Peifer M, Polakis P. Wnt signaling in oncogenesis and embryogenesis—a look outside the nucleus. Science 2000;287:1606–9.
19. Rubinfeld B, Albert I, Porfiri E, Fiol C, Munemitsu S, Polakis P. Binding of GSK3β to the APC-β-catenin complex and regulation of complex assembly. Science 1996;272:1023–6.
20. Desbois-Mouthon C, Cadoret A, Blivet-Van Eggelpoel MJ, et al. Insulin and IGF-1 stimulate the β-catenin pathway through two signalling cascades involving GSK-3β inhibition and Ras activation. Oncogene 2001; 20:252–9.
21. Brembeck FH, Rosario M, Birchmeier W. Balancing cell adhesion and Wnt signaling, the key role of β-catenin. Curr Opin Genet Dev 2006;16:51–9.
22. Ding Q, Xia W, Liu JC, et al. Erk associates with and primes GSK-3β for its inactivation resulting in upregulation of β-catenin. Mol Cell 2005;19:159–70.
23. Garcia-Rostan G, Tallini G, Herrero A, D'Aquila TG, Carcangiu ML, Rimm DL. Frequent mutation and nuclear localization of β-catenin in anaplastic thyroid carcinoma. Cancer Res 1999;59:1811–5.
24. Motti ML, Califano D, Baldassarre G, et al. Reduced E-cadherin expression contributes to the loss of p27kip1-mediated mechanism of contact inhibition in thyroid anaplastic carcinomas. Carcinogenesis 2005;26: 1021–34.
25. Gujral TS, van Veelen W, Richardson DS, et al. A novel RET kinase-β-catenin signaling pathway contributes to tumorigenesis in thyroid carcinoma. Cancer Res 2008;68:1338–46.
26. Schweppe RE, Klopper JP, Korch C, et al. DNA profiling analysis of 40 human thyroid cancer cell lines reveals cross-contamination resulting in cell line redundancy and misidentification. J Clin Endocrinol Metab 2008;93:4331–41.
27. Hedinger C, Williams ED, Sobin LH. The WHO histological classification of thyroid tumors: a commentary on the second edition. Cancer 1989;63:908–11.
28. Castellone MD, Teramoto H, Williams BO, Druey KM, Gutkind JS. Prostaglandin E2 promotes colon cancer cell growth through a Gs-axin-β-catenin signaling axis. Science 2005;310:1504–10.
29. Feliciello A, Li Y, Avvedimento EV, Gottesman ME, Rubin CS. A-kinase anchor protein 75 increases the rate and magnitude of cAMP signaling to the nucleus. Curr Biol 1997;7:1011–4.
30. Carlomagno F, Vitagliano D, Guida T, et al. ZD6474, an orally available inhibitor of KDR tyrosine kinase activity, efficiently blocks oncogenic RET kinases. Cancer Res 2002;62:7284–90.
31. Croyle M, Akeno N, Knauf JA, et al. RET/PTC-induced cell growth is mediated in part by epidermal growth factor receptor (EGFR) activation: evidence for molecular and functional interactions between RET and EGFR. Cancer Res 2008;68:4183–91.
32. Piedra J, Martinez D, Castano J, Miravet S, Dunach M, de Herreros AG. Regulation of β-catenin structure and activity by tyrosine phosphorylation. J Biol Chem 2001; 276:20436–43.
33. Rasola A, Fassetta M, De Bacco F, et al. A positive feedback loop between hepatocyte growth factor receptor and β-catenin sustains colorectal cancer cell invasive growth. Oncogene 2007;26:1078–87.
34. Danilkovitch-Miagkova A, Miagkov A, Skeel A, Nakaigawa N, Zbar B, Leonard EJ. Oncogenic mutants of RON and MET receptor tyrosine kinases cause activation of the β-catenin pathway. Mol Cell Biol 2001;21:5857–68.
35. Kanai Y, Ochiai A, Shibata T, et al. c-erbB-2 gene product directly associates with β-catenin and plakoglobin. Biochem Biophys Res Commun 1995; 208:1067–72.
36. Coluccia AM, Vacca A, Dunach M, et al. Bcr-Abl stabilizes β-catenin in chronic myeloid leukemia through its tyrosine phosphorylation. EMBO J 2007;26: 1456–66.
37. D'Amico M, Hulit J, Amanatullah DF, et al. The integrin-linked kinase regulates the cyclin D1 gene through glycogen synthase kinase 3β and cAMP-responsive element-binding protein-dependent pathways. J Biol Chem 2000;275:32649–57.
38. Takemaru KI, Moon RT. The transcriptional coactivator CBP interacts with β-catenin to activate gene expression. J Cell Biol 2000;149:249–54.
39. Mayr BM, Canettieri G, Montminy MR. Distinct effects of cAMP and mitogenic signals on CREB-binding protein recruitment impart specificity to target gene activation via CREB. Proc Natl Acad Sci U S A 2001;98: 10936–41.
40. Pradeep A, Sharma C, Sathyanarayana P, et al. Gastrin-mediated activation of cyclin D1 transcription involves β-catenin and CREB pathways in gastric cancer cells. Oncogene 2004;23:3689–99.
41. Giese K, Kingsley C, Kirshner JR, Grosschedl R. Assembly and function of a TCRα enhancer complex is dependent on LEF-1-induced DNA bending and multiple protein-protein interactions. Genes Dev 1995;9:995–1008.
42. Xu L, Corcoran RB, Welsh JW, Pennica D, Levine AJ. WISP-1 is a Wnt-1- and β-catenin-responsive oncogene. Genes Dev 2000;14:585–95.
43. Eng C. Familial papillary thyroid cancer-many syndromes, too many genes? J Clin Endocrinol Metab 2000;85:1755–7.
44. Cetta F, Chiappetta G, Melillo RM, et al. The ret/ptc1 oncogene is activated in familial adenomatous polyposis-associated thyroid papillary carcinomas. J Clin Endocrinol Metab 1998;83:1003–6.
45. Abbosh PH, Li X, Li L, Gardner TA, Kao C, Nephew KP. A conditionally replicative, Wnt/β-catenin pathway-based adenovirus therapy for anaplastic thyroid cancer. Cancer Gene Ther 2007;14:399–408.
46. Emami KH, Nguyen C, Ma H, et al. A small molecule inhibitor of β-catenin/CREB-binding protein transcription. Proc Natl Acad Sci U S A 2004;101:12682–7.

Attached Manuscript #V

Faraonio R, Salerno P, Passaro F, Sedia C, Iaccio A, **Bellelli R**, Nappi TC, Comegna M, Romano S, Salvatore G, Santoro M, Cimino F.

A set of MiRNA partecipate to the cellular senescence program in human diploid fibroblasts. Cell Death Diff, 2011

Cell Death and Differentiation (2011), 1–9

www.nature.com/cdd

A set of miRNAs participates in the cellular senescence program in human diploid fibroblasts

R Faraonio[1,2], P Salerno[3,6], F Passaro[1,4,2,6], C Sedia[1], A Iaccio[4], R Bellelli[3], TC Nappi[3], M Comegna[1,2], S Romano[1], G Salvatore[5], M Santoro[3] and F Cimino*[,1,4]

Here we show that replicative senescence in normal human diploid IMR90 fibroblasts is accompanied by altered expression of a set of microRNAs (miRNAs) (senescence-associated miRNAs), with 14 and 10 miRNAs being either up or downregulated ($>$2-fold), respectively, in senescent with respect to young cells. The expression of most of these miRNAs was also deregulated upon senescence induced by DNA damage (etoposide) or mild oxidative stress (diethylmaleate). Four downregulated miRNAs were part of miRNA family-17, recently associated to human cell and tissue aging. Moreover, eight upregulated and six downregulated miRNAs mapped in specific chromosomal clusters, suggesting common transcriptional regulation. Upon adoptive overexpression, seven upregulated miRNAs induced the formation of senescence-associated heterochromatin foci and senescence-associated β-galactosidase staining ($P<0.05$), which was accompanied, in the case of five of them, by reduced cell proliferation. Finally, miR-210, miR-376a*, miR-486-5p, miR-494, and miR-542-5p induced double-strand DNA breaks and reactive oxygen species accumulation in transfected cells. In conclusion, we have identified a set of human miRNAs induced during replicative and chemically induced senescence that are able to foster the senescent phenotype by prompting DNA damage.
Cell Death and Differentiation advance online publication, 4 November 2011; doi:10.1038/cdd.2011.143

Replicative or cellular senescence, a state of irreversible arrest of cell division, was first described in cultures of human fibroblasts.[1] Since then, replicative senescence has been described in various mammalian cells.[2] The mechanisms underlying senescence include telomere shortening, upregulation of the CDKN1A (p21WAF1) and CDKN2A (p16INK4a and p14ARF) loci, and accumulation of DNA damage.[3] Telomeres become progressively shorter at every round of cell division and this leads to critically short telomere length sensed as double-strand DNA breaks.[4] DNA damage and DNA-damage response (DDR) could be common events to cellular senescence programs initiated by telomere dysfunction and aberrant oncogene activation.[5]

Senescent cells are marked by lack of DNA replication; expression of senescence-associated β-galactosidase (SA-β-gal); accumulation of discrete nuclear foci that are termed senescence-associated heterochromatin foci (SAHFs); and senescence-associated DNA-damage foci (SDFs). SAHFs are detected by preferential binding of DNA dyes, such as 4′,6-diamidino-2-phenylindole (DAPI), and the presence of certain heterochromatin-associated histone modifications (trimethyl-Lys9 Histone H3). SDFs are nuclear foci containing proteins that are associated to DNA damage (Ser139-phosphorylated histone H2AX -γ-H2AX- and p53-binding protein-1-53BP1).[6]

Senescent cells show striking changes in gene expression, including upregulation of cell-cycle inhibitors (p21WAF1 and p16INK4a) and secreted proteins involved in microenvironment remodeling (IL-6),[7] and downregulation of genes that facilitate cell-cycle progression (c-FOS, cyclin-A, cyclin-B, PCNA)[8] or that are involved in cell-cycle execution (FOXM1, UBE2C, TYMS).[9] Mechanisms underlying the gene expression program that is associated to senescence are still poorly understood.

MicroRNAs (miRNAs) are short (20–24 nt) non-coding RNAs that are involved in post-transcriptional regulation of gene expression. miRNAs are transcribed as part of primary transcripts (pri-miRNAs). The pri-miRNA is cleaved by the Drosha ribonuclease-III to produce an approximately 70-nt stem–loop precursor miRNA (pre-miRNA), which is further cleaved by the cytoplasmic Dicer ribonuclease to generate mature miRNA and antisense miRNA star (miRNA*) products. The mature miRNA is incorporated into an RNA-induced silencing complex (RISC), which recognizes target mRNAs and most commonly results in translational inhibition or destabilization of the target mRNA.[10]

[1]Dipartimento di Biochimica e Biotecnologie Mediche, Università di Napoli Federico II, Napoli, Italy; [2]CEINGE–Biotecnologie Avanzate s.c. a r.l, Napoli, Italy; [3]Istituto di Endocrinologia ed Oncologia Sperimentale (IEOS), C.N.R. c/o Dipartimento di Biologia e Patologia Cellulare e Molecolare, Università di Napoli Federico II, Napoli, Italy; [4]IRCCS Fondazione SDN, Napoli, Italy and [5]Dipartimento di Studi delle Istituzioni e dei Sistemi Territoriali, Università Parthenope, Napoli, Italy
*Corresponding author: F Cimino, Dipartimento di Biochimica e Biotecnologie Mediche, Università di Napoli Federico II, via S Pansini 5, Napoli 80131, Italy.
Tel: +39 081 746 2107; Fax: +39 081 746 3650; E-mail: cimino@dbbm.unina.it
[6]These authors contributed equally to this work.
Keywords: microRNA; cellular senescence; gene expression; DNA damage
Abbreviations: CDK, cyclin-dependent kinase; RISC, RNA-induced silencing microprocessor complex; SAHFs, senescence-associated heterochromatin foci; SDFs, senescence-associated DNA-damage foci; SA-β-gal, senescence-associated β-galactosidase; ATCC, American Type Culture Collection; DMEM, Dulbecco's modified Eagle's medium; PDL, population doubling level; PBS, phosphate-buffered saline; DMSO, dimethyl sulfoxide; DEM, diethylmaleate; BrdU, 5-bromo-2-deoxyuridine; DAPI, 4′,6-diamidino-2-phenylindole; DDR, DNA-damage response; DHE, dihydroethidium; mTOR, mammalian target of rapamycin
Received 21.3.11; revised 27.9.11; accepted 27.9.11; Edited by M Blagosklonny

Being potent regulators of gene expression, we hypothesized that miRNAs were involved in the gene expression program associated to cellular senescence. This hypothesis was supported by recent results obtained by Hackl *et al*.[11] showing that miRNAs of family 17 were downregulated in aged tissues and cells. Moreover, senescence in human lung (WI-38) fibroblasts was accompanied by upregulation of miR-152, miR-410, miR-431, and miR-493, and downregulation of miR-155, miR-20a, miR-25, and miR-15a; knockdown of miR-155 or miR-20a enhanced IR-induced senescence.[12,13]

In this study, we profiled miRNA expression in human senescent fibroblasts (IMR90). We identified 24 miRNAs that were either up- or downregulated in senescent cells. Upon adoptive overexpression, most of the upregulated miRNAs reduced DNA synthesis rate, and induced SA-β-gal staining and SAHFs. Five of them induced a robust DNA damage that likely sustains the senescent phenotype.

Results

Altered expression of a set of miRNAs accompanies replicative senescence in IMR90 fibroblasts. At PDL58, more than 70% IMR90 cells stained positively for SA-β-gal, whereas less than 1% of PDL33 cells stained positively (Supplementary Figure 1). Moreover, PDL58 cells had an expression profile consistent with a senescent phenotype, expressing about three-fold higher levels of p21WAF1 and p16INK4a proteins; higher levels of IL6 mRNA; and reduced levels of cell-cycle-related mRNAs such as cyclin-A, thymidylate synthase (TYMS), cyclin-selective ubiquitin carrier protein (UBE2C), and forkhead box-M1 (FOXM1) with respect to PDL33 cells (Supplementary Figure 1). We profiled miRNA expression in senescent PDL58 with respect to PDL33 IMR90 cells by qRT-PCR. A total of 148 miRNAs were detected ($C_t < 39$ cycles) in at least one of the two samples; 18 miRNAs were upregulated and 51 were downregulated (>2-fold) in senescent *versus* young cells (Supplementary Table 1).

To validate these results, independent preparations of PDL58 and PDL33 IMR90 cells were obtained and the expression of all the highest ranked 18 up- and 14 downregulated miRNAs was investigated in triplicate by qRT-PCR. Results are reported in Table 1. Fourteen (fold changes: 2.7–8.9) and 10 (fold changes: 0.42–0.13) miRNAs were significantly ($P < 0.001$) up- or downregulated in PDL58 *versus* PDL33 cells, respectively (Table 1).

These findings indicate that senescence of IMR90 is associated to altered expression of a set of miRNAs (hereafter referred to as 'senescence-associated miRNAs').

DNA damage and oxidative stress deregulate the expression of senescence-associated miRNAs. Treatment with etoposide,[15] a topoisomerase inhibitor used to induce DNA damage, or DEM,[9] a glutathione depletor able to cause a mild oxidative stress, were applied to chemically induce cellular senescence. When IMR90 cells were exposed to DEM (100 μM) for 10 days or treated with etoposide (20 μM) for 24 h and further cultured for 11 days, 62 and 80% SA-β-gal-positive IMR90 cells, respectively, were detected. This was accompanied by gene expression changes consistent with a senescent phenotype

Table 1 Expression change of senescence-associated miRNAs in IMR90 cells

miRNA	Chromosomal location[a]	Family[a]	Fold changes (PDL58/PDL33)	S.D.	*P*-value
Upregulated					
miR-486-5p	8p11.21	486	8.9	0.009	<0.0001
miR-210	11p15.5	210	7.9	0.9	<0.0001
miR-30e-5p	1p34.2	30	6.5	0.9	<0.0001
miR-376a*	14q32.31	368	5.9	0.7	0.0001
miR-126*	9q34.3	126	5.3	1.4	<0.0001
miR-494	14q32.31	154	4.5	1.6	<0.0001
miR-379	14q32.31	379	4.4	1.1	<0.0001
miR-654	14q32.31	654	4.3	1.4	<0.0001
miR-542-5p	Xq26.3	542	3.8	1	<0.0001
miR-23b	9q22.32	23	3.7	0.6	0.0022
miR-134	14q32.31	134	3.4	1	<0.0001
miR-369-3p	14q32.31	154	3.3	0.4	<0.0001
miR-656	14q32.31	154	3.3	1	<0.0001
miR-485-5p	14q32.31	485	2.7	0.5	<0.0001
Downregulated					
miR-20a	13q31.3	17	0.13	0.01	0.0002
miR-155	21q21.3	155	0.14	0.04	0.0034
miR-17-5p	13q31.3	17	0.15	0.02	0.0060
miR-199b-5p	9q34.11	199	0.21	0.09	0.0002
miR-15b	3q25.33	15	0.23	0.16	0.0008
miR-92[b]	13q31.3; Xq26.2	25	0.27	0.04	0.0001
miR-296-5p	20q13.32	296	0.27	0.2	0.0061
miR-19b[c]	13q 31.3; Xq26.2	19	0.28	0.1	0.0016
miR-93	7q22.1	17	0.35	0.04	<0.0001
miR-106b	7q22.1	17	0.42	0.17	0.01

[a]The information were obtained from miRBase (http://www.mirbase.org/). [b]miR-92 includes two identical sequences (miR-92a-1 and miR-92a-2) encoded by two different loci. [c]miR-19 includes two identical sequences (miR-19b-1 and miR-19b-2) encoded by two different loci.

Table 2 Expression change of senescence-associated miRNAs in IMR90 cells treated with DEM or etoposide

	DEM			Etoposide		
miRNA	**Fold variation[a]**	**S.D.**	***P*-value**	**Fold variation[a]**	**S.D.**	***P*-value**
miR-486-5p	1.55	0.118	0.0018	3.22	0.07	<0.0001
miR-210	1.69	0.12	<0.0001	1.5	0.2	0.0001
miR-30e-5p	3.25	0.57	0.0008	1.82	0.03	<0.0001
miR-376a*	2.87	0.89	<0.0001	1.7	0.27	0.0023
miR-126*	2.35	0.28	0.0004	2.05	0.15	0.0001
miR-494	2.14	0.2	0.0011	0.93	0.04	0.2652
miR-379	1.52	0.06	0.0001	1.39	0.08	0.0070
miR-654	2.29	0.53	0.0046	1.16	0.8	0.5177
miR-542-5p	1.128	0.14	0.5818	1.22	0.04	0.0224
miR-23b	1.94	0.12	0.0002	1.42	0.18	0.0105
miR-134	1.52	0.12	0.0032	1.67	0.002	<0.0001
miR-369-3p	1.44	0.13	0.0036	1.61	0.03	<0.0001
miR-656	1.26	0.06	0.0181	1.21	0.04	0.0137
miR-485-5p	2.33	0.08	0.0001	1.36	0.11	0.0420
miR-20a	0.419	0.002	<0.0001	0.29	0.03	<0.0001
miR-155	0.2	0.002	<0.0001	0.32	0.014	<0.0001
miR-17-5p	0.51	0.01	<0.0001	0.43	0.04	0.0086
miR-199b-5p	0.55	0.06	0.069	0.37	0.02	<0.0001
miR-15b	0.33	0.016	<0.0001	0.33	0.02	0.0013
miR-92	0.43	0.08	0.0018	0.37	0.01	0.0003
miR-296-5p	0.72	0.005	0.0007	0.7	0.02	0.0059
miR-19b	0.39	0.14	0.0125	0.33	0.04	0.0002
miR-93	0.45	0.02	0.0006	0.46	0.06	0.0009
miR-106b	0.84	0.01	<0.0001	0.65	0.07	0.0396

[a]With respect to untreated cells.

(Supplementary Figure 2). RNA was extracted from DEM- and etoposide-treated IMR90 cells, and the expression of the 24 senescence-associated miRNAs was studied in triplicate by qRT-PCR. Results are reported in Table 2. About 90% of the senescence-associated miRNAs were de-regulated (albeit with smaller fold changes than during replicative senescence) upon chemically induced senescence ($P<0.05$). In detail, DEM-mediated senescence was associated with the upregulation (range: 1.26–3.25) of 13 of the 14 (with the exception of miR-542-5p) upregulated senescence-associated miRNAs ($P<0.05$) (Table 2), whereas etoposide-mediated senescence was associated with the upregulation (range: 1.21–3.22) of 12 (with the exception of miR-654 and miR-494) of them ($P<0.05$) (Table 2). Moreover, both DEM-treated (range: 0.84–0.2) as well as etoposide-treated (range: 0.7–0.29) cells showed downregulation of all the 10 downregulated senescence-associated miRNAs ($P<0.05$) (Table 2).

These findings indicate that DNA damage and oxidative stress alter the expression of senescence-associated miRNAs in IMR90 cells, thereby suggesting that DNA damage and oxidative stress, occurring during replicative senescence, may contribute to the altered expression of senescence-associated miRNAs.

A set of miRNAs promotes a senescent phenotype in IMR90 cells. We sought to establish whether upregulation of senescence-associated miRNAs was causally related to senescence. Thus, the nine highest ranked upregulated miRNAs (Table 1) were adoptively upregulated (in the form of synthetic pre-miRNAs) by electroporation in young PDL33 IMR90 cells and their capability of inducing senescence-associated markers was assessed. Negative control was represented by scrambled pre-miRNA-transfected PDL33 IMR90 cells. Positive control was represented by PDL55 (or 58) IMR90 cells. Seven out of the nine miRNAs induced a significant ($P<0.05$) increase of SAHF-positive nuclei (range: 10–24% of the cells) detected by both DAPI staining and 3meH3K9 immunofluorescence with respect to the scrambled control (Figures 1a and b). This was accompanied by a 4- to 18-fold increase of SA-β-gal-positive cells ($P<0.05$) (Figure 1c). miR-654 did not cause any significant increase of SAHF-positive and SA-β-gal-positive cells; instead, we noted a robust cytotoxic effect exerted by this miRNA, assessed as percentage of dead cells upon transfection (data not shown). miR-654 was not studied further.

Senescent cells are arrested in the G_1 phase of the cell cycle. Therefore, we tested whether expression of the highest ranked upregulated miRNAs was also able to reduce BrdU incorporation into newly synthesized DNA. Electroporation of five of them (miR-210, miR-376a*, miR-486-5p, miR-494, and miR-542-5p) in PDL33 IMR90 cells caused a significant ($P<0.001$) reduction (2- to 3-fold) of BrdU incorporation (Figure 2a). Moreover, these five miRNAs also caused a parallel reduction (approximately 30–60%) in cell number ($P>0.05$) (Figure 2b). miR-126* did not exert any detectable effect, and miR-379 and miR-30e-5p caused only negligible reduction of BrdU incorporation and cell proliferation ($P<0.05$) (Figures 2a and b). Negative control was represented by scrambled miRNA-transfected cells (Figures 2a and b).

Altogether, these findings show that seven senescence-induced miRNAs are able to induce SAHF/SA-β-gal positivity, with five of them (miR-210, miR-376a*, miR-486-5p, miR-494, and miR-542-5p) causing a robust reduction of cell proliferation and DNA synthesis rate.

miR-210, miR-376a*, miR-486-5p, miR-494, and miR-542-5p enhance DNA damage. DNA damage and DDR are

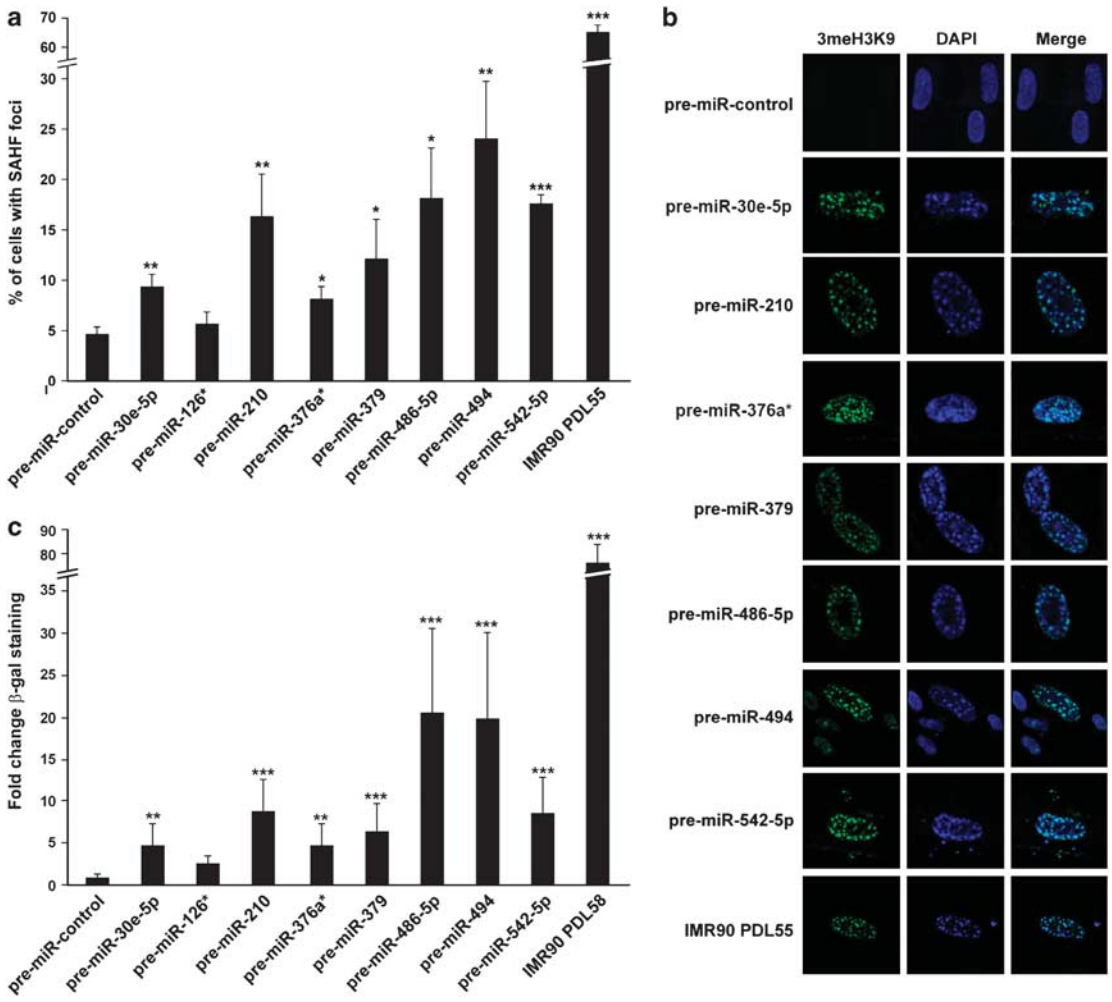

Figure 1 Senescence-associated miRNAs induce SAHFs and SA-β-gal. The nine highest ranked upregulated pre-miRNAs were electroporated in triplicate in PDL33 IMR90 cells. After 7 days cells were fixed and examined by immunofluorescence for α-trimethyl-Lys9 Histone (SAHF) or counterstained with DAPI (**a** and **b**), and stained for SA-β-gal (**c**). (**a** and **b**) Counts of at least 300 cells were averaged and expressed as percent of cells $\pm$ S.D. with SAHF foci. Representative pictures are shown in panel **b**. (**c**) Cells were stained for SA-β-gal. Counts of at least 300 cells were averaged and expressed as fold change $\pm$ S.D. with respect to the scrambled control. Experimental points with $^{*}P<0.05$, $^{**}P<0.01$, or $^{***}P<0.001$ respectively

involved in senescence.[5] Therefore, we asked whether the five senescence-associated miRNAs, that were able to reduce proliferation rate and promote a senescent phenotype, were able to induce DNA damage. To this aim, we used neutral COMET assay to monitor double-strand DNA breaks. Etoposide-treated and scrambled miRNA-transfected cells were used as positive or negative controls, respectively. Tail moments were calculated and percentages of nuclei showing different tail moments were determined. The results shown in Figure 3 demonstrate that all the five miRNAs, but not the scrambled control, caused significant ($P<0.05$) increase in the percentage of cells with tail moment >4, consistent with induction of double-strand DNA breaks (Figure 3).

Finally, we evaluated whether adoptive miRNA expression induced the formation of γH2AX foci in cell nuclei. Senescent cells and etoposide-treated cells were used as positive controls, whereas scrambled miRNA-transfected cells were used as negative controls. Figure 4 shows that miR-210 and miR-494, but not the scrambled control, induced the formation of γH2AX foci in more than 25% of cell nuclei ($P<0.01$). miR-376a*, miR-486-5p, and miR-542-5p increased the number of γH2AX foci-positive nuclei only modestly ($P<0.05$) (Figure 4).

These findings suggest that senescence-associated miRNAs facilitate the establishment of a senescent state by promoting DNA damage and in some cases through increase of a DDR marker.

Role of oxidative stress and the mTOR-signaling pathway in miRNA-induced cellular senescence. Increased intracellular oxygen radicals can elicit DDR and senescence.[5] Therefore, we investigated whether over-expression of senescence-associated miRNAs was able to cause intracellular accumulation of superoxide anion, by flow cytometry upon cell staining using the oxidation-sensitive DHE fluorescent probe. The results reported in Figure 5 demonstrate that overexpression of all five miRNAs (miR-210, miR-376a*, miR-486-5p, miR-494, and miR-542-5p) caused a significant

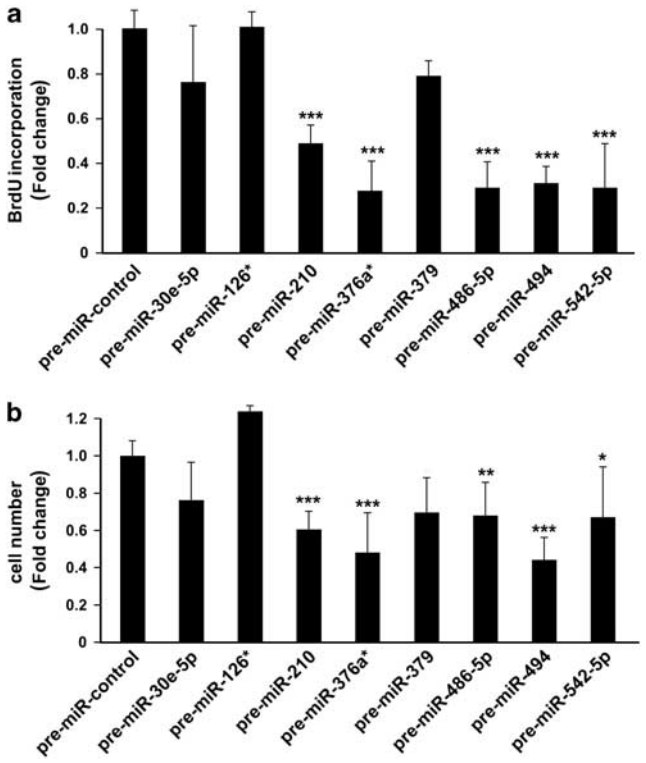

Figure 2 Senescence-associated miRNAs reduce cell proliferation. The nine highest ranked upregulated pre-miRNAs were electroporated in triplicate in PDL33 IMR90 cells. (**a**) After 48 h cells were incubated with BrdU for 24 h and fixed. Coverslips were incubated with an anti-BrdU and secondary fluorescein-conjugated antibody, counterstained with Hoechst-33258, and counted by immunofluorescence. Counts of at least 300 cells were averaged and expressed as fold change ± S.D. with respect to the scrambled control. (**b**) After 96 h cell numbers were counted and expressed as fold change ± S.D. with respect to the scrambled control. Experimental points with $*P<0.05$, $**P<0.01$, or $***P<0.001$ respectively

($P<0.05$) increase in DHE-positive cells with respect to the scrambled control. Of note, miR-210 was previously reported to induce the generation of ROS.[18,19] Furthermore, it appears of interest that miR-494, which caused the highest levels of ROS generation, also caused the highest level of DNA damage as shown by the COMET assay (Figure 3).

The mammalian target of rapamycin (mTOR) pathway was demonstrated to drive senescence in cells treated with several factors, including oxidative agents.[20–22] Thus, initially, we asked whether miRNA transfection caused any change in mTOR pathway activation, by measuring the phosphorylation of the ribosomal S6 protein (S6); S6 is phosphorylated by p70-S6 kinase (p70S6K), which, in turn, is activated by mTOR.[23] IMR90 cells featured high levels of S6 phosphorylation, and adoptive overexpression of any of the five miRNAs (miR-210, miR-376a*, miR-486-5p, miR-494, and miR-542-5p) did not cause detectable change in the levels of phospho-S6 (Supplementary Figure 3). Then, we tested whether inhibition of mTOR by the macrolide antibiotic rapamycin affected cell senescence (SA-β-gal) induced by miRNA transfection. Treatment with rapamycin caused a detectable reduction of SA-β-gal-positive cells upon transfection with the five miRNAs, a reduction that was statistically significant ($P<0.05$) in the case of four of them (Table 3). Rapamycin's effects on SA-β-gal stain were not accompanied by significant reduction of γ-H2AX foci (Table 3).

Altogether, these findings suggest that the senescent phenotype induced by miR-210, miR-376a*, miR-494, and miR-542-5p depends on the activity of the mTOR pathway.

Discussion

Here we have identified a set of 24 miRNAs either up- or downregulated in senescent human diploid fibroblasts.

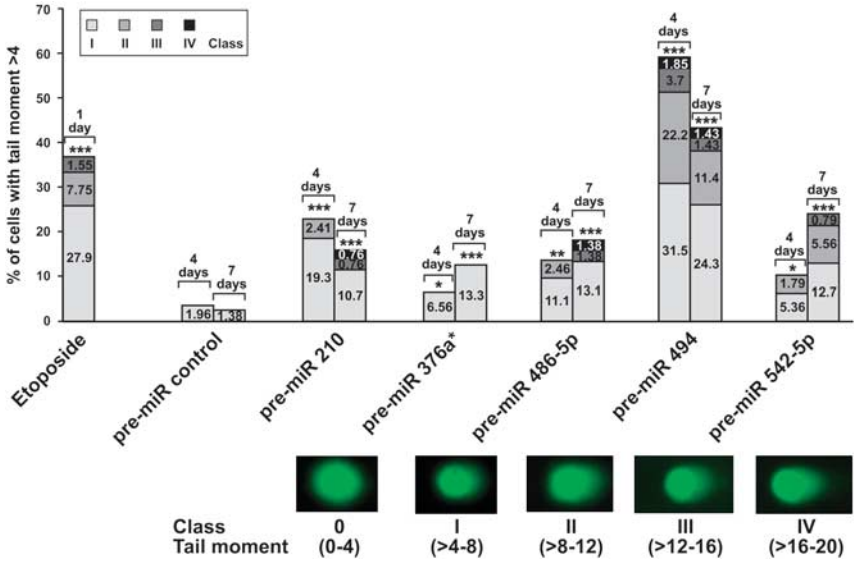

Figure 3 Senescence-associated miRNAs induce DNA damage. The indicated pre-miRNAs were electroporated in PDL33 IMR90 cells. After 4 or 7 days cells were harvested and comet tails were generated by electrophoresis. Slides were stained with SYBER Green and DNA migration was analyzed by fluorescence microscopy. Tail moment was determined and nuclei were divided in classes based on the value of the tail moment (as shown in the representative images of cells transfected with pre-miR-494 at the bottom). The percentage of damaged cells for each class is indicated within the bar graphs. A minimum of 100 cells per experiment were analyzed. Experimental points with $*P<0.05$, $**P<0.01$, or $***P<0.001$ respectively

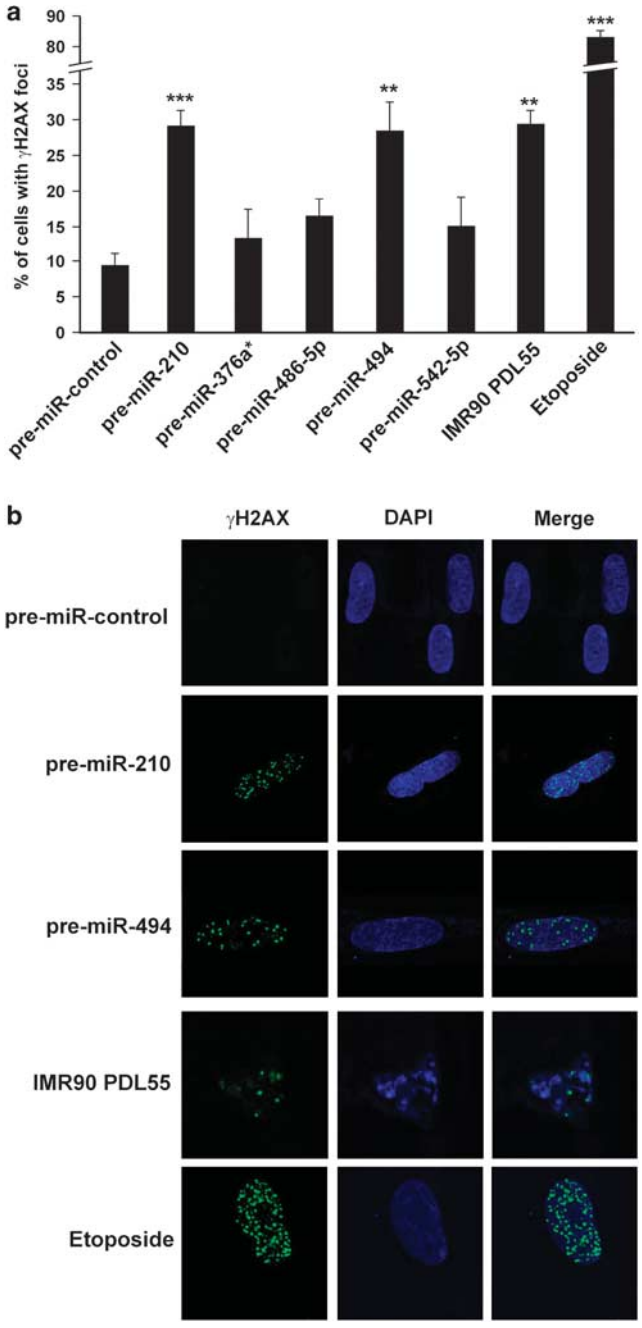

Figure 4 Senescence-associated miRNAs induce γH2AX foci. The indicated pre-miRNAs were electroporated in triplicate in PDL33 IMR90 cells. After 7 days cells were fixed and examined by immunofluorescence for α-H2AX phosphorylated on Ser139 (γH2AX). Coverslips were washed and incubated with an Alexa-488 goat anti-rabbit antibody and counterstained with DAPI. Counts of at least 300 cells were averaged and expressed as percent of cells ± S.D. with γH2AX foci. Representative images are shown in panel **b**. Experimental points in panel (**a**) are indicated with with $^{**}P<0.01$, or $^{***}P<0.001$ respectively

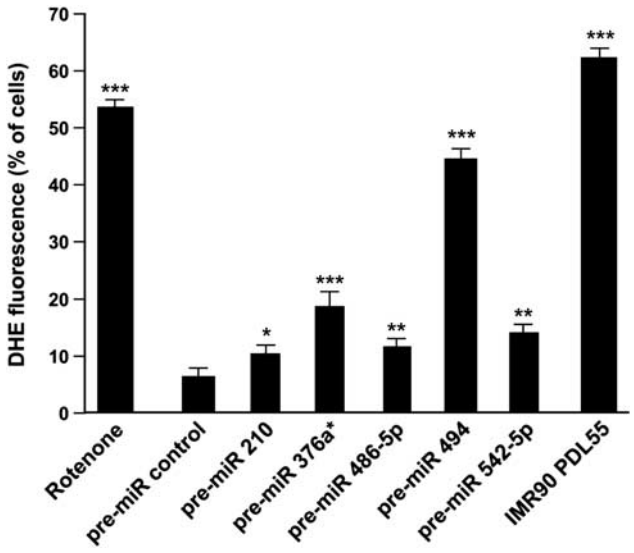

Figure 5 Senescence-associated miRNAs lead to oxidative stress. IMR90 cells (PDL33) were electroporated with the indicated pre-miRNAs. After 72 h cells were incubated with 0.1 μM DHE at 37 °C for 30 min. Intracellular fluorescence was examined by flow cytometry. Fluorescence intensity of 10 000 cells was analyzed in triplicate and expressed as percentage of stained cells ± S.D. As positive controls, PDL33 cells treated with the mitochondrial inhibitor rotenone (5 μM for 2 h) and senescent PDL55 cells were used. Experimental points with $^{*}P<0.05$, $^{**}P<0.01$, or $^{***}P<0.001$ respectively

Table 3 Effects of mTOR inhibition by rapamycin on miRNA-induced senescence and DDR

Pre-miRNA	SA-β-gal staining upon rapamycin (% change)[a]	*P*-value	γH2AX staining upon rapamycin (% change)[b]	*P*-value
Pre-miR-control	−16.2	0.4711	+2.56	0.8520
Pre-miR-210	−43	0.0498	−2.34	0.0808
Pre-miR-376a*	−37.6	0.0052	−2.75	0.2354
Pre-miR-486-5p	−15.3	0.2526	+7.69	0.5734
Pre-miR-494	−46.2	0.0050	−6.59	>0.999
Pre-miR-542-5p	−38.9	0.0262	+6.38	0.9360

[a]Starting 24 h after transfection with the indicated miRNAs, cells were treated for 3 days with 10 nM rapamycin or vehicle, and then stained for SA-β-gal. Counts of at least 300 cells were averaged and expressed as percentage of SA-β-gal-stained cells. Reduction in the percentage of positive cells upon rapamycin treatment is reported. [b]Starting 24 h after transfection with the indicated miRNAs, cells were treated for 3 days with 10 nM rapamycin or vehicle, and then examined by immunofluorescence for γH2AX. Counts of at least 300 cells were averaged and expressed as percent of cells with γH2AX foci. Change in the percentage of positive cells upon rapamycin treatment is reported.

Of note, 8 (chromosome 14q32.31) upregulated and 6 (4 on chromosome 13q31.3 and 2 on chromosome 7q22.1) downregulated miRNAs mapped in specific chromosomal clusters, suggesting that their expression might be co-regulated. We have also shown that the expression of most of the senescence-associated miRNAs was modified in DEM- or etoposide-induced senescence, in the same direction as in replicative senescence. This suggests that oxidative stress and DNA damage are among the factors that mediate senescence-associated miRNA expression changes. However, the effects of DEM and etoposide were smaller than those measured upon replicative senescence, suggest-

ing that either the contribution of other factors or the conditions of chemical treatments were not sufficient to achieve a robust change of miRNA expression.

We have also shown that adoptive expression of five upregulated miRNAs (miR-210, miR-376a*, miR-486-5p, miR-494, and miR-542-5p) induced a senescent phenotype (with SAHFs, SA-β-gal staining, and reduced cell proliferation). Overexpression of these five miRNAs was also associated with double-strand DNA breaks in a neutral COMET assay and, for two of them (miR-210 and miR-494), appearance of a DDR marker (γH2AX foci). Thus, overexpression of the five miRNAs favored DNA damage, and not solely DDR (γH2AX), which can also occur in the absence of DNA damage (pseudo-DDR).[24] Finally, we showed that the mTOR pathway was an essential driver of senescence induced by senescence-associated miRNAs as SA-β-gal staining was significantly reduced by treatment with rapamycin.[20–22] Of note, our preliminary observations, by studying the expression levels of the senescence-inducing miRNAs in human skin broblasts from young (age 17–25) or old (age 89–94) donors, show that the highest expression levels of miR-376a* and miR-494 were found in one old donor cell line, and expression of miR-486-5p was on average two-fold higher in old with respect to young cells.

Overall, these findings suggest a model whereby DNA damage and oxidative stress, which occur during replicative senescence, stimulate the expression of a set of miRNAs, which, in turn, feedback positively to DNA damage and oxidative stress, thereby sustaining the senescent phenotype (Supplementary Figure 4). The mechanisms through which the upregulated miRNAs provoke these effects will deserve further investigation. However, the model is supported by the observation that overexpression of the senescence-associated miRNAs caused an accumulation of superoxide anion and by the fact that some known targets of senescence-associated miRNAs are involved in DNA damage, oxidative stress, cell-cycle control, and apoptosis. For instance, miR-210 was found to activate the generation of ROS by targeting subunits of the electron transport chain (ETC) complexes I and II.[18] Other potential targets of miR-210 in the same pathway included ISCU (iron–sulfur cluster scaffold homolog) and COX10 (cytochrome-*c* oxidase assembly protein), two factors of the mitochondrial electron transport chain and the tricarboxylic acid cycle.[19] In addition, forced expression of miR-210 decreased endogenous levels of RAD52, a key factor in homology-dependent DNA repair (HR).[25] Similarly, miRNA-494 was recently found to be localized to mitochondria, where it may target genes involved in ATP synthesis-coupled electron transport.[26] Of note, miR-210 also suppresses cell-cycle progression by targeting E2F3[27] and fibroblast growth factor receptor-like-1 (FGFRL1).[28] miR-376a* was reported to repress phosphoribosyl pyrophosphate synthetase-1 (PRPS1) involved in DNA/RNA synthesis as well as threonine and tyrosine kinase (TTK) essential for mitosis checkpoint.[29] miR-494 was upregulated in cells exposed to the DNA-damaging agent benzo[a]pyrene (B[a]P) and was found to restrain cell cycle through CDK6 downregulation.[30] Finally, miR-542-5p was upregulated in senescent BJ cells[31] and downregulated in neuroblastoma and other solid tumors.[32]

Though not investigated in our study, it is tempting to speculate that also senescence-downregulated miRNAs contribute to the execution of the senescence program (Supplementary Figure 4). In our study, several miRNAs of the miR-17 family (miR-17-5p, miR-20a, miR-106b, and miR-93) and miR-155 were downregulated both in replicative and chemically induced senescence. Noteworthy, the miR-17 family[33] and miR-155[12] have already been involved in cellular senescence. Hackl *et al.*[11] reported that miRNAs of the miR-17 family were downregulated in replicative senescence and in organismal aging models, their decrease correlating with increased levels of p21WAF1. miRNAs of the miR-17 family (miR-17-92 cluster) were also upregulated in cancer[34–37] and, by targeting p21WAF1, they were able to confer resistance to RAS-induced senescence.[38] On the other hand, miR-155 was downregulated in senescent WI-38 cells, causing increased levels of TP53INP1, a protein acting in the TP53 growth arrest pathway.[12] Another link between miR-155 and cell proliferation comes from recent data showing that WEE1 (WEE1 homolog—*Schizosaccharomyces pombe*), a kinase that blocks cell-cycle progression, is a target of this miRNA.[39]

In conclusion, we have identified a set of miRNAs, which, being modulated by senescence-mediating conditions, and being able to either facilitate DNA damage or regulate the expression of several senescence mediators, may represent critical components of the cellular senescence program.

Materials and Methods

Cell cultures. Normal primary human fibroblasts IMR90 were obtained from American Type Culture Collection (Manassas, VA, USA). IMR90 were grown in Dulbecco's modified Eagle's medium (DMEM) (Invitrogen, Groningen, The Netherlands) supplemented with 10% (v/v) fetal bovine serum and 1% penicillin/streptomycin (Invitrogen). Cultures were maintained at 37 °C in a 5% CO_2-humidified atmosphere. The population doubling level (PDL) was calculated by using the formula $\Delta PDL = \log(n_h/n_i)/\log 2$, where n_i is the initial number of cells and n_h is the final number of cells at each passage. The cells were used at 33 PDL or 58 PDL. More than 70% of PDL58 cells were positive for SA-β-gal. SA-β-gal was assayed according to Dimri *et al.*[14] Briefly, cells were washed twice with PBS, fixed with 2% formaldehyde and 0.2% glutaraldehyde in PBS, and washed twice in PBS. Then, cells were stained overnight in X-gal staining solution (1 mg/ml X-gal, 40 mM citric acid/sodium phosphate (pH 6.0), 5 mM potassium ferricyanide, 5 mM potassium ferrocyanide, 150 mM NaCl, 2 mM $MgCl_2$).

Diethylmaleate (DEM) was purchased from Sigma Chemical Co. (St. Louis, MO, USA) and used at a final concentration of 100 μM in complete medium.[9] Etoposide (VP-16; Calbiochem, La Jolla, CA, USA) was used at 20 μM.[15] Rapamycin was obtained from Merck Chemicals Ltd (Nottingham, UK) and used at 10 nM. Rotenone (Sigma Chemical Co.) was used at 5 μM.

miRNA profiling. Total RNA was isolated using the mirVana MiRNA isolation kit (Ambion, Austin, TX, USA) according to the manufacturer's instructions. The RNA was quantified by Nanodrop (Thermo Scientific, Wilmington, DE, USA) and RNA integrity was analyzed by using the 2100 Bioanalyzer (Agilent Technologies, Waldbronn, Germany). Global miRNA expression analysis was performed by using TaqMan Low Density Arrays (TLDA)/Human microRNA Panel v1.0 (Applied Biosystems, Foster City, CA, USA). This technology detects mature miRNAs from the Sanger miRBase database. Each card/panel contains a primer–probe set for 365 human miRNAs. Briefly, for each sample, 100 ng of total RNA was converted into cDNA by multiplex reverse transcription (RT) using a primer pool from the Taqman array kit (Applied Biosystems), according to the manufacturer's instructions. Then, miRNA levels were measured by quantitative real-time PCR (qRT-PCR) using the 7900HT Sequence Detection System (Applied Biosystems). C_t values were determined by using the automatic threshold in RQ manager v1.1 analysis software (Applied Biosystems). Data were analyzed by using the Sequence Detection System software (v. 2.3) (Applied Biosystems). The endogenous control

RNU48 was used to normalize the relative expression of each miRNA using the $\Delta\Delta C_t$ method (Applied Biosystems User Bulletin No. 2—P/N 4303859).

Real-time PCR. Total RNA was isolated by using the mirVana MiRNA isolation kit (Ambion) according to the manufacturer's instructions. The RNA was quantified by Nanodrop (Thermo Scientific) and RNA integrity was analyzed by the 2100 Bioanalyzer (Agilent Technologies). The TaqMan MiRNA Assay kit (Applied Biosystems) was used to detect the expression of mature miRNAs. Briefly, 100 ng of total RNA was reverse-transcribed (RT) at 16 °C for 30 min, 42 °C for 30 min, and 85 °C for 5 min in a 15-μl reaction volume. 2-μl volume of the RT product was used for PCR in a final volume of 20 μl. The PCR started with an initial denaturation step at 90 °C for 10 min, followed by 40 cycles of 95 °C for 15 s and 60 °C for 1 min. Small nucleolar RNA RNU6 (Applied Biosystems) was used for normalization. PCRs were performed in triplicate and fold changes were calculated by the following formula: $2^{-(\text{sample-1}\Delta C_t - \text{sample-2}\Delta C_t)}$, where ΔC_t is the difference between the amplification fluorescent thresholds of the miRNA of interest and the RNA of RNU6.

Cell electroporation. PDL33 IMR90 cells were electroporated by using Microporator MP100 (EuroClone, Milano, Italy) following the manufacturer's instructions. Briefly, 1×10^6cells were electroporated in 100 μl of suspension buffer (Neon transfection kit; Invitrogen) using 100 nM pre-miRNA (Ambion) according to the manufacturer's protocol adapted to IMR90 cells (pulse voltage: 1400 V for 10 ms, three pulses). Electroporation efficiency was tested by using the Cy3-labeled negative control (Ambion) according to the manufacturer's protocol and was approximately of 75%. After electroporation, cells were seeded and viable cells were counted at 96 h.

BrdU assay. For BrdU (5-bromo-2-deoxyuridine) incorporation assay, electroporated cells were seeded on glass coverslips. Forty-eight hours after transfection, cells were incubated for 24 h with BrdU (10 μM) and fixed. Coverslips were incubated with an anti-BrdU and secondary fluorescein-conjugated antibody. Coverslips were counterstained with Hoechst-33258, rinsed, and mounted in Moviol on glass slides. The fluorescent signal was visualized with an epifluorescent microscope (Axiovert 2; Zeiss, Gottingen, Germany), interfaced with the image analyzer software KS300.

Immunofluorescence. For indirect immunofluorescence, cells were fixed in 4% paraformaldehyde and permeabilized with 0.2% Triton X-100 (5 min on ice), and then incubated with α-H2AX phosphorylated on Ser139 (γH2AX) (R&D Systems, Minneapolis, MN, USA) or α-trimethyl-Lys9 Histone H3 (Lake Placid Biologicals, Lake Placid, NY, USA) for 1 h at room temperature. Coverslips were washed and incubated with an Alexa-488 goat anti-rabbit antibody (Invitrogen) for 30 min at room temperature. After 5 min of DAPI counterstaining, coverslips were mounted and observed with a Zeiss LSM 510 META confocal microscope (Carl Zeiss, Thornwood, NY, USA). At least 300 cells were counted in triplicate experiments.

COMET assay. The neutral comet assay was performed according to the manufacturer's recommendations (Trevigen, Gaithersburg, MD, USA).[16] Slides were incubated for 30 min in lysis buffer and for 40 min in alkaline solution (pH > 13), and comet tails were generated by 15-min electrophoresis in TBE buffer at 20 V, at 4 °C. The slides were stained with SYBER Green and DNA migration was analyzed by fluorescence microscopy (Leica DMS 4000B). Tail moment (TM), defined as the product of the tail length and the fraction of total DNA in the tail (TM = tail length × % of DNA in the tail), was determined by using the software 'Comet Assay II' (Perceptive Instruments, Suffolk, UK). A minimum of 100 cells per experiment were analyzed. All experiments were performed in triplicate.

ROS measurement. Reactive oxygen species (ROS) were measured by using the oxidation-sensitive fluorescent probe dihydroethidium (DHE; Sigma Chemical), according to a published procedure.[17] Briefly, 72 h after miRNA transfection, cells were incubated for 30 min at 37 °C with 0.1 μM DHE, harvested, and resuspended in PBS. To determine fluorescence due to formation of superoxide anion, the cell suspension was subjected to flow-cytometric analysis using a Becton Dickinson FACSCalibur instrument (Becton Dickinson, San Josè, CA, USA), after excitation at 488 nm (FL-2 channel). Results from at least 10 000 cells from each sample were analyzed in triplicate using the CellQuest 3.2.1 software (Becton Dickinson).

Statistical analysis. Statistical analyses were performed by using the GraphPad InStat software program (version 3.06.3, San Diego, CA, USA). All *P*-values were two-sided and differences were significant when $P < 0.05$.

Conflict of Interest

The authors declare no conflict of interest.

Acknowledgements. We thank Professor T Russo for critical reading of the manuscript and Dr. F Merolla for help with statistical analysis. This study was supported by the Ministero dell'Università e della Ricerca Scientifica e Tecnologica (MiUR PRIN 2007, MiUR-PS35-126/IND, MiUR MERIT RBNE08HWLZ_004), Regione Campania LR 5/2003, Associazione Italiana per la Ricerca sul Cancro (AIRC), Italian Ministero della Salute, and Fondazione SDN per la Ricerca e l'Alta Formazione in Diagnostica Nucleare.

1. Hayflick L, Moorhead PS. The serial cultivation of human diploid cell strains. *Exp Cell Res* 1961; **25**: 585–621.
2. Collado M, Serrano M. Senescence in tumours: evidence from mice and humans. *Nat Rev Cancer* 2010; **10**: 51–57.
3. Collado M, Blasco MA, Serrano M. Cellular senescence in cancer and aging. *Cell* 2007; **130**: 223–233.
4. Blasco MA. Telomeres and human disease: ageing, cancer and beyond. *Nat Rev Genet* 2005; **6**: 611–622.
5. d'Adda di Fagagna F. Living on a break: cellular senescence as a DNA-damage response. *Nat Rev Cancer* 2008; **8**: 512–522.
6. Campisi J, d'Adda di Fagagna F. Cellular senescence: when bad things happen to good cells. *Nat Rev Mol Cell Biol* 2007; **8**: 729–740.
7. Coppé JP, Desprez PY, Krtolica A, Campisi J. The senescence-associated secretory phenotype: the dark side of tumor suppression. *Annu Rev Pathol* 2010; **5**: 99–118.
8. Fridman AL, Tainsky MA. Critical pathways in cellular senescence and immortalization revealed by gene expression profiling. *Oncogene* 2008; **27**: 5975–5987.
9. Faraonio R, Pane F, Intrieri M, Russo T, Cimino F. *In vitro* acquired cellular senescence and aging-specific phenotype can be distinguished on the basis of specific mRNA expression. *Cell Death Differ* 2002; **9**: 862–864.
10. Garzon R, Calin GA, Croce CM. MicroRNAs in cancer. *Annu Rev Med* 2009; **60**: 167–179.
11. Hackl M, Brunner S, Fortschegger K, Schreiner C, Micutkova L, Mück C *et al.* miR-17, miR-19b, miR-20a and miR-106a are downregulated in human aging. *Aging Cell* 2010; **9**: 291–296.
12. Wang Y, Scheiber MN, Neumann C, Calin GA, Zhou D. MicroRNA regulation of ionizing radiation-induced premature senescence. *Int J Radiat Oncol Biol Phys* 2010; **81**: 839–848.
13. Grillari J, Hackl M, Grillari-Voglauer R. miR-17-92 cluster: ups and downs in cancer and aging. *Biogerontology* 2010; **11**: 501–506.
14. Dimri GP, Lee X, Basile G, Acosta M, Scott G, Roskelley C *et al.* A biomarker that identifies senescent human cells in culture and in aging skin *in vivo*. *Proc Natl Acad Sci USA* 1995; **92**: 9363–9367.
15. Te Poele RH, Okorokov AL, Jardine L, Cummings J, Joel SP. DNA damage is able to induce senescence in tumor cells *in vitro* and *in vivo*. *Cancer Res* 2002; **62**: 1876–1883.
16. Minopoli G, Stante M, Napolitano F, Telese F, Aloia L, De Felice M *et al.* Essential roles for Fe65 Alzheimer amyloid precursor-binding protein, in the cellular response to DNA damage. *J Biol Chem* 2007; **282**: 831–835.
17. Trifunovic A, Hansson A, Wredenberg A, Rovio AT, Dufour E, Khvorostov I *et al.* Somatic mtDNA mutations cause aging phenotypes without affecting reactive oxygen species production. *Proc Natl Acad Sci USA* 2005; **102**: 17993–17998.
18. Puisségur MP, Mazure NM, Bertero T, Pradelli L, Grosso S, Robbe-Sermesant K *et al.* miR-210 is overexpressed in late stages of lung cancer and mediates mitochondrial alterations associated with modulation of HIF-1 activity. *Cell Death Differ* 2011; **18**: 465–478.
19. Chen Z, Li Y, Zhang H, Huang P, Luthra R. Hypoxia-regulated microRNA-210 modulates mitochondrial function and decreases ISCU and COX10 expression. *Oncogene* 2010; **29**: 4362–4368.
20. Leontieva OV, Blagosklonny MV. DNA damaging agents and p53 do not cause senescence in quiescent cells, while consecutive re-activation of mTOR is associated with conversion to senescence. *Aging (Albany NY)* 2010; **2**: 924–935.
21. Korotchkina LG, Leontieva OV, Bukreeva EI, Demidenko ZN, Gudkov AV, Blagosklonny MV. The choice between p53-induced senescence and quiescence is determined in part by the mTOR pathway. *Aging (Albany NY)* 2010; **2**: 344–352.
22. Demidenko ZN, Shtutman M, Blagosklonny MV. Pharmacologic inhibition of MEK and PI-3K converges on the mTOR/S6 pathway to decelerate cellular senescence. *Cell Cycle* 2009; **8**: 1896–1900.
23. Hay N, Sonenberg N. Upstream and downstream of mTOR. *Genes Dev* 2004; **18**: 1926–1945.

24. Pospelova TV, Demidenko ZN, Bukreeva EI, Pospelov VA, Gudkov AV, Blagosklonny MV. Pseudo-DNA damage response in senescent cells. *Cell Cycle* 2009; **8**: 4112–4118.
25. Crosby ME, Kulshreshtha R, Ivan M, Glazer PM. MicroRNA regulation of DNA repair gene expression in hypoxic stress. *Cancer Res* 2009; **69**: 1221–1229.
26. Bandiera S, Ruberg S, Girard M, Cagnard N, Hanein S, Chretien D *et al.* Nuclear outsourcing of RNA interference components to human mitochondria. *PLoS One* 2011; **6**: e20746.
27. Biswas S, Roy S, Banerjee J, Hussain SR, Khanna S, Meenakshisundaram G *et al.* Hypoxia inducible microRNA 210 attenuates keratinocyte proliferation and impairs closure in a murine model of ischemic wounds. *Proc Natl Acad Sci USA* 2010; **107**: 6976–6981.
28. Tsuchiya S, Fujiwara T, Sato F, Shimada Y, Tanaka E, Sakai Y *et al.* MicroRNA-210 regulates cancer cell proliferation through targeting fibroblast growth factor receptor-like 1 (FGFRL1). *J Biol Chem* 2011; **286**: 420–428.
29. Kawahara Y, Zinshteyn B, Sethupathy P, Iizasa H, Hatzigeorgiou AG, Nishikura K. Redirection of silencing targets by adenosine-to-inosine editing of miRNAs. *Science* 2007; **315**: 1137–1140.
30. Duan H, Jiang Y, Zhang H, Wu Y. MiR-320 and miR-494 affect cell cycles of primary murine bronchial epithelial cells exposed to benzo[a]pyrene. *Toxicol In Vitro* 2010; **24**: 928–935.
31. Bonifacio LN, Jarstfer MB. MiRNA profile associated with replicative senescence, extended cell culture, and ectopic telomerase expression in human foreskin fibroblasts. *PLoS One* 2010; **5**: e12519.
32. Schulte JH, Marschall T, Martin M, Rosenstiel P, Mestdagh P, Schlierf S *et al.* Deep sequencing reveals differential expression of microRNAs in favorable versus unfavorable neuroblastoma. *Nucleic Acids Res* 2010; **38**: 5919–5928.
33. Mendell JT. miRiad roles for the miR-17-92 cluster in development and disease. *Cell* 2008; **133**: 217–222.
34. He L, Thomson JM, Hemann MT, Hernando-Monge E, Mu D, Goodson S *et al.* A microRNA polycistron as a potential human oncogene. *Nature* 2005; **435**: 828–833.
35. Volinia S, Calin GA, Liu CG, Ambs S, Cimmino A, Petrocca F *et al.* A microRNA expression signature of human solid tumors defines cancer gene targets. *Proc Natl Acad Sci USA* 2006; **103**: 2257–2261.
36. O'Donnell KA, Wentzel EA, Zeller KI, Dang CV, Mendell JT. c-Myc-regulated microRNAs modulate E2F1 expression. *Nature* 2005; **435**: 839–843.
37. Grillari J, Grillari-Voglauer R. Novel modulators of senescence, aging, and longevity: small non-coding RNAs enter the stage. *Exp Gerontol* 2010; **45**: 302–311.
38. Hong L, Lai M, Chen M, Xie C, Liao R, Kang YJ *et al.* The miR-17-92 cluster of microRNAs confers tumorigenicity by inhibiting oncogene-induced senescence. *Cancer Res* 2010; **70**: 8547–8557.
39. Tili E, Michaille JJ, Wernicke D, Alder H, Costinean S, Volinia S *et al.* Mutator activity induced by microRNA-155 (miR-155) links inflammation and cancer. *Proc Natl Acad Sci USA* 2011; **108**: 4908–4913.

Supplementary Information accompanies the paper on Cell Death and Differentiation website (http://www.nature.com/cdd)